Aus dem Department für Augenheilkunde Tübingen
Universitäts-Augenklinik

Lipid-DNA Nanopartikel als neuartige Medikamententräger für die Behandlung retinaler Erkrankungen

Inaugural-Dissertation
Zur Erlangung des Doktorgrades
der Medizin

der Medizinischen Fakultät

der Eberhard Karls Universität zu Tübingen

vorgelegt von
Simmang, David

2019

Dekan:	Professor Dr. med. I. B. Autenrieth
1. Berichterstatter:	Professor Dr. med. M. Spitzer
2. Berichterstatter:	Privatdozent Dr. med. G. Willmann
Tag der Disputation:	10.11.2019

Table of content

List of abbreviations

- µg Microgram
- µL Microliter
- µm Micrometer
- µM Micromolar
- AMD Age-related macular degeneration
- CME Cystoid macular edema
- CNV Choroidal neovascularization
- d Days
- DAPI 4´6´-diamidino-2-phenylindole
- DME Diabetic macula edema
- DPBS Dulbecco's phosphate-buffered saline
- DR Diabetic retinopathy
- EDTA (Ethylenedinitrilo)tetraacetic acid
- EMA European Medicines Agency
- FDA Food and Drug Administration
- GCL Ganglion cell layer
- h Hours
- HCL Hydrochloric acid
- INL Inner nuclear layer
- IPL Inner plexiform layer
- $MgCl_2$ Magnesium chloride
- min Minutes
- NaCl Sodium chloride
- NP Nanoparticle
- ONL Outer nuclear layer
- OPL Outer plexiform layer
- PLA Polylactic-acid
- PLGA Polylactic-coglycolic-acid
- PRL Photoreceptor layer
- RPE Retinal pigment epithelium
- RVO Retinal vein occlusion

- TAE Tris-acetate-EDTA
- TBS Tris buffered saline
- Tris base 2-Amino-2-(hydroxymethyl)-1,3-propanediol
- TUNEL TdT-mediated dUTP-biotin nick end labeling
- VEGF Vascular endothelial growth factor

1. Introduction

1.1. Anatomy of the eye

The eye is the main sensory system for the perception of our environment. This complex function is made possible by a highly diverse organ consisting of various specified tissues. The following short introduction into the anatomy of the human eye is supposed to recapitulate the necessary information to understand the experiments conducted in this thesis.

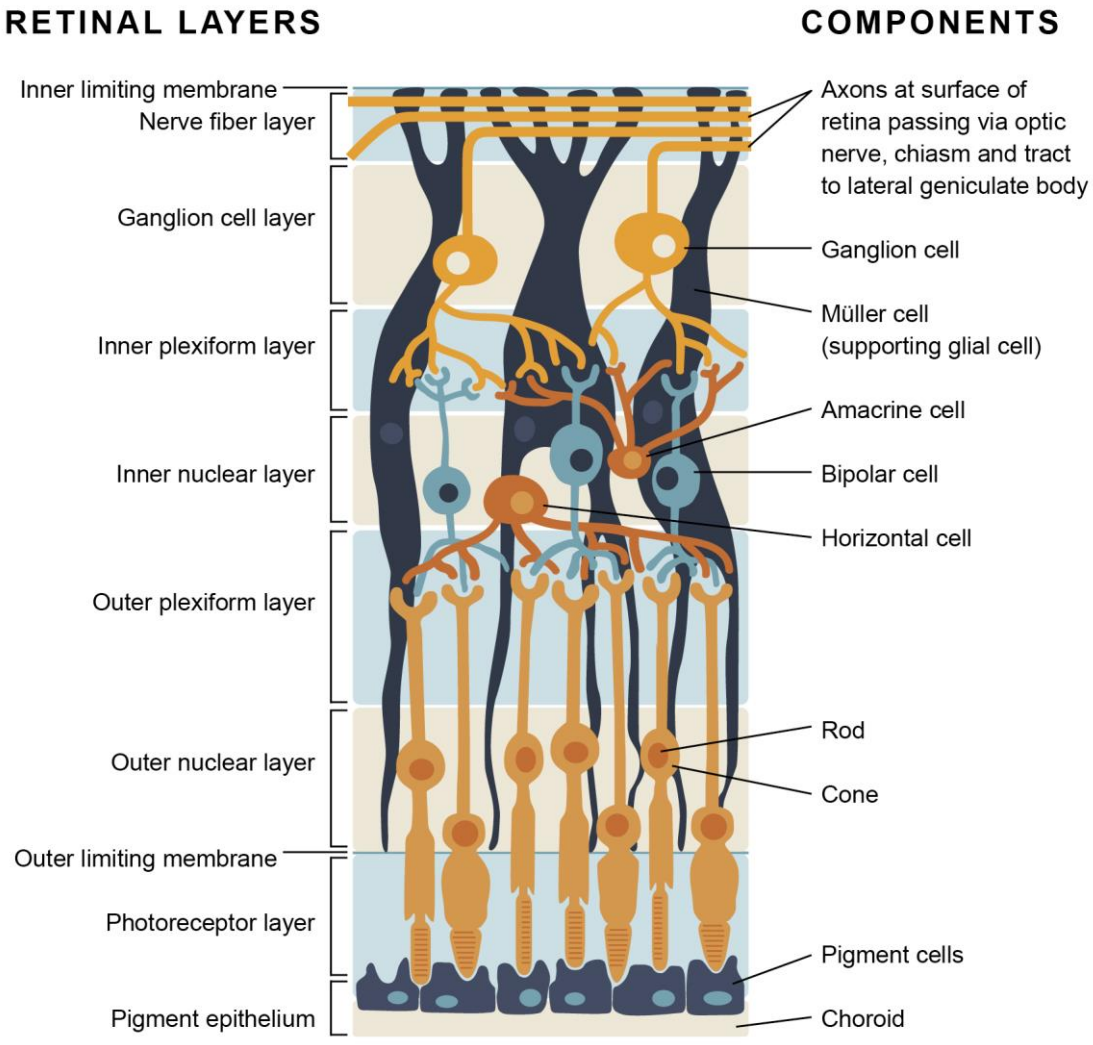

Figure 1 Schematic representation of the layers in the retina and their components; with kind permission of Hain, B.

Although the Retina is only 0.1-0.5 mm thick, it is composed of many different layers (Figure 1). The most outer stratum and closest to the choroid is the retinal

pigment epithelium (RPE). Cells found in the RPE layer play an important role in a multitude of processes, including absorption of redundant light, several transport and buffering phenomena and the secretion of signaling molecules. Aside from that they are responsible for the phagocytosis of photoreceptor segment membranes and contribute to the immune privileged status of the eye. The next stratum towards the vitreous body is the photoreceptor layer (PRL). Here light signals are translated by rods and cones into electric pulses. Even further towards the interior, the outer limiting membrane separates the outer from the inner segments of the photoreceptor cells. In the following outer nuclear layer (ONL) the somata of these cells are found. Their axons reach into the outer plexiform layer (OPL) and make contact with the horizontal, bipolar and amacrine cells. This collection of cells is responsible for initial processing and modification of the signals. Their cell bodies are found towards the interior of the eye, in the inner nuclear layer (INL). In this layer also the Müller cells are situated. They provide structure and metabolites to the surrounding cells. In the following inner plexiform layer (IPL) all mediating cells pass on their information to the ganglion cells. Their somata are located in the ganglion cell layer (GCL) and their axons proceed parallel to the surface of the retina as the nerve fiber layer towards the optical nerve. On the inside of this layer the inner limiting membrane forms a barrier between the vitreous and the retina[1].

There are two locations in the retina that deserve special mentioning due to their particularly specific role. The first is the point where all the nerve fibers of the ganglion cells leave the eye, the optic disc. As there are solely axons in the position, no photoreceptors are found and no visual information is obtained from this point. Then, 15° temporal of the optic disc the *macula lutea* forms an oval pit in the retina. In this area a high density of cones is found in the photoreceptor layer. In its center the *fovea centralis retinae* is localized, which is specialized for sharp central vision and characterized by the absence of blood vessels.

When studying the anatomy of the eye and the retina in specific, imaging through microscopy can be used for precise observation of the earlier described layers. Here, especially fluorescence microscopy offers great possibilities as dyes with

different colors can be used to monitor a multitude of structures or markers at the same time. Staining of the cell nucleus by 4',6-diamidino-2-phenylindol (DAPI) is used to localize the different cells in the retina and distinguish the different layers (Figure 2). After treatment with DAPI the cell nucleus is visible under the microscope in a blue filter, as this color is the emission peak for the fluorescence of the dye. Then, coming from the vitreous body and going out of the eye the found layers of the retina are: ganglion cell layer (GCL), inner plexiform layer (IPL), inner nuclear layer (INL), outer plexiform layer (OPL), outer nuclear layer (ONL), photoreceptor layer (PRL) and choroid. Neither of the limiting membranes can be clearly identified due to exclusive nucleus staining. The sclera forms the outward boundaries of the bulbus, visible as a relatively consistent order of blue nuclei outside of the retina. Embedded into loose connective tissue, the sclera itself is embedded safely in the orbita.

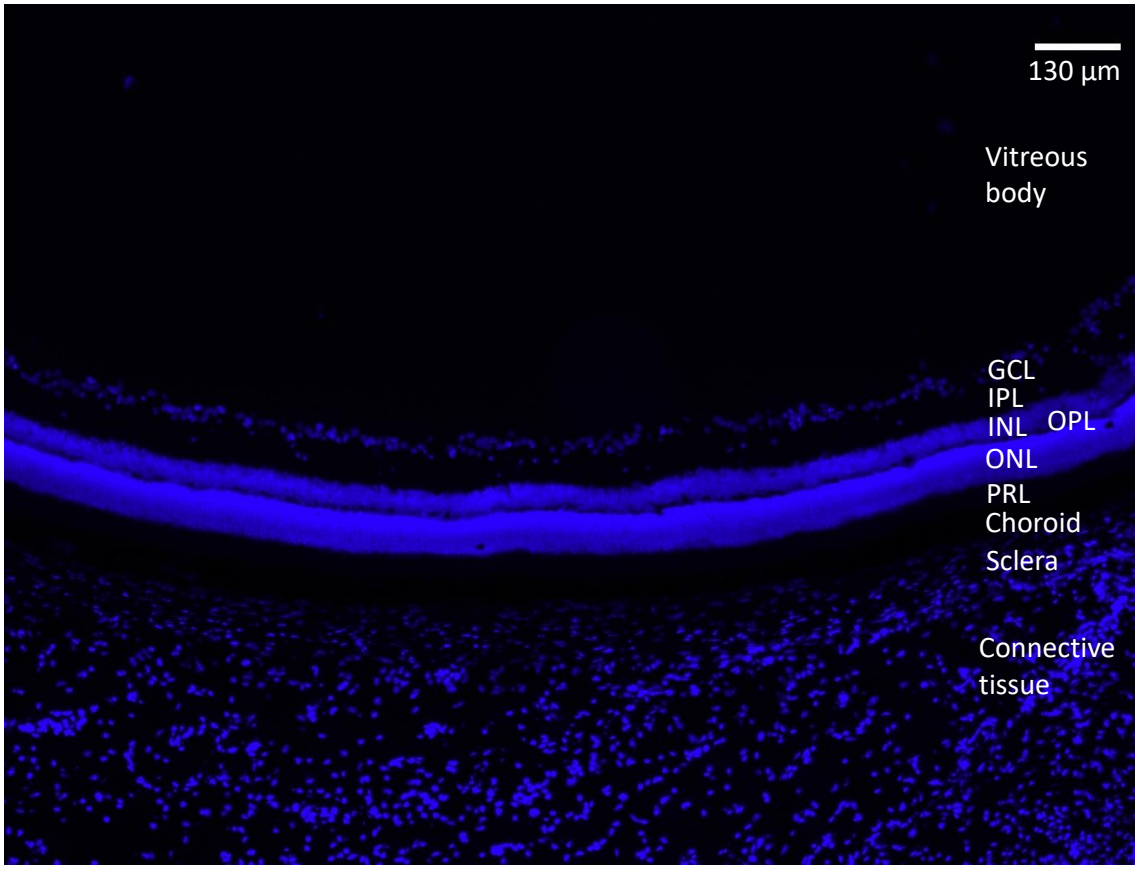

Figure 2 Layers of retina, sclera and connective tissue of a native ex-vivo pig eye. Designation of different layers added: coming from the vitreous body and going out of the eye the found layers of the retina are: ganglion cell layer (GCL), inner plexiform layer (IPL), inner nuclear layer (INL), outer plexiform layer (OPL), outer nuclear layer (ONL), photoreceptor layer (PRL), choroid, sclera and connective tissue.

1.2. Diseases of the posterior segment

In this paragraph three of the most frequently diagnosed retinal diseases are presented. These include age-related macular degeneration, diabetic retinopathy and retinal vein occlusion. They all have in common that one of their main treatment options involve intravitreal injections.

1.2.1. Age-related macular degeneration

Age-related macular degeneration (AMD) is the most frequent cause of loss of eyesight after the 60th year of age in western countries. In all found cases about 15 % of the patients have the exudative form, which is accompanied by choroidal neovascularization (CNV)[2]. Cases of visual impairment and blindness as a consequence of this ailment are estimated to increase from 620,000 in 2010 up to 1.6 million in 2050[3]. The prevalence of this disease is 1.2 % amongst the 43 - 86 year old people, with the majority of the patients being after their 75th life year[4,5]. Additionally, no difference is found between men and women regarding the prevalence. However, Caucasians are proven to hold a higher risk for the occurrence of AMD than other ethnicities[6].

In exudative AMD, pathological angiogenesis leads to visual impairment due to restructuring in the region of the macula. At the onset of the disease, deposits of the outer segments of the photoreceptors are accumulating in the pigment epithelium and change the composition of the proteins over lifetime, thereby forming senile plaques. This in turn leads to increased thickness of the Bruch's membrane and as a consequence results in a higher diffusion resistance towards the choroidal epithelium. In exudative AMD it is assumed that a cascade initiated by this process that leads to the release of inflammatory markers, oxygen radical formations and numerous growth factors, such as the vascular endothelial growth factor (VEGF). These can be released by numerous ocular cells and fulfill a variety of functions such as stimulation of endothelial growth, promotion of vascular permeability and dissociation of tight junction components. As a result, small vessels that originate from the choroidal capillaries penetrate through lesions of the Bruch's membrane and grow into the sub-retinal space and partially

under the retinal pigment epithelium. The originating vessels show pathologically degenerated cell structures, due to their immaturity which in turn causes leakage of exudates and blood constituents into the extravasal space[7]. Subsequently edema and cellular remodeling processes alter the surrounding areas and can be observed in the typical picture of exudative AMD during indirect funduscopy. The progression of this bilaterally occurring disease leads to decreased visual acuity, blurred vision, scotoma and ultimately to the loss of sight.

For treatment, therapeutic strategies should be implemented as soon as possible in order to maintain a high visual acuity. For the majority of all exudative AMD cases the treatment option of choice consists of inhibition of the neovascularization via intravitreal injection of anti-VEGF medication. Momentarily the most commonly applied drugs are antibodies or antibody fragments that bind VEGF and thereby reduce the neovascularization. Examples here are aflibercept, ranibizumab or off-label bevacizumab[7]. These anti-VEGF treatments are currently the only therapeutic agents able to stabilize or improve vision in patients suffering from neovascular ocular ailments[8]. In the ANCHOR and MARINA studies it was successfully shown, that approximately 90 % of the patients that were treated with the anti-VEGF agent ranibizumab remained at a relatively consistent level regarding their visual acuity after twelve months of treatment. Reversely, this means that approximately 10 % were unable to stay on a stabile level concerning their visual acuity on anti-VEGF treatment whereas 30 % of the patients even increased their visual acuity under ranibizumab treatment[9,10]. Unfortunately, until now there is no treatment for the late stage of non-exudative AMD that is responsible for a slowly progressing macular atrophy, which is called geographic atrophy.

1.2.2. Diabetic retinopathy

Diabetic retinopathy (DR) is the most common cause for visual impairment or loss of sight in the industrial countries in working-age individuals. Around 4.1 million people in the U.S. suffer from diabetic retinopathy of which approximately 900,000 developed a sight-threatening stage of the disease[11]. After disease duration of minimum 15 years more than 80% of the type one diabetes patients

and over 60% of the type two diabetes patients suffer from DR. Subsequently, approximately 24% with type one and 6% with type two diabetes develop proliferative DR[12].

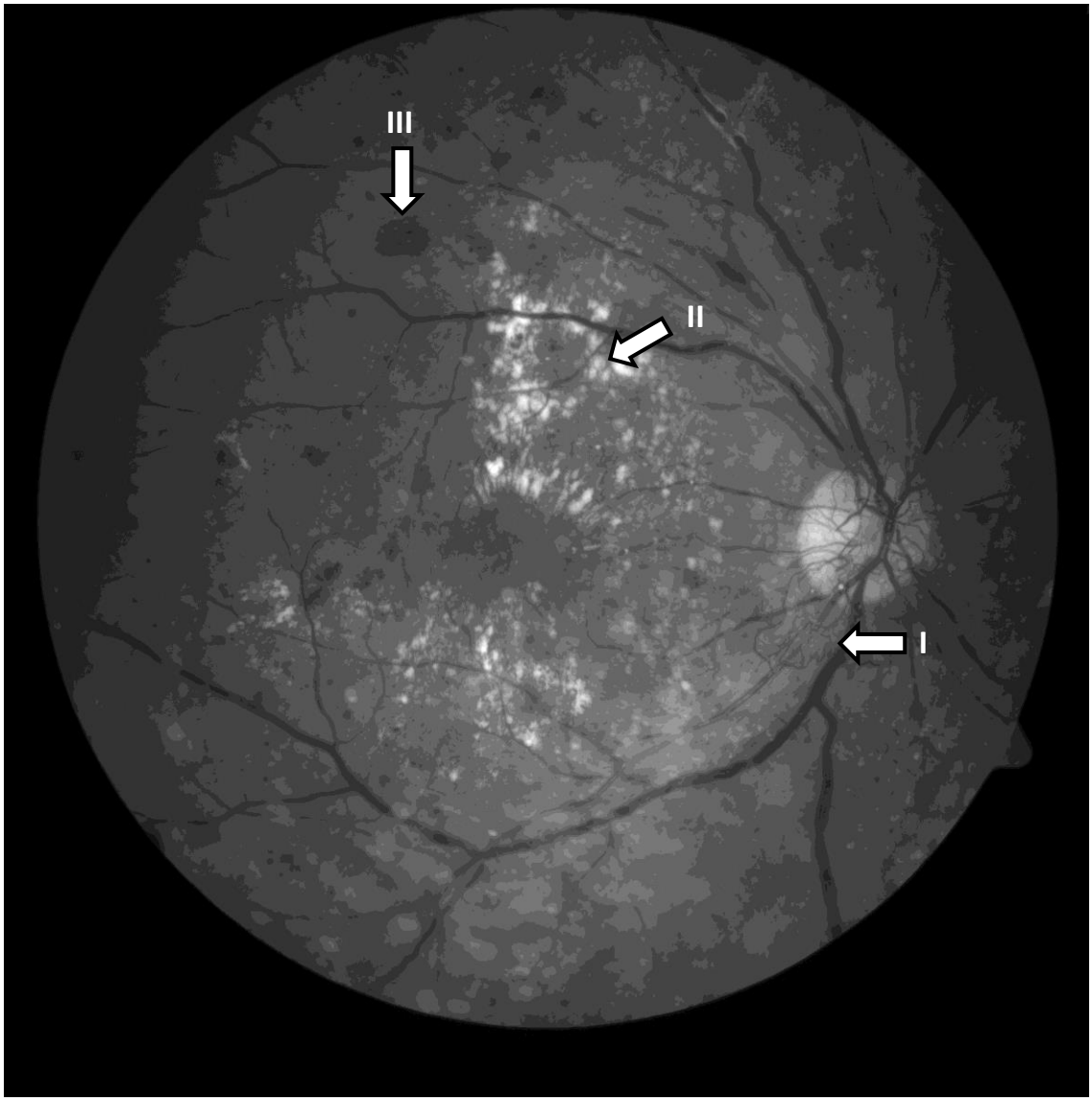

Figure 3 Fluorescence angiography of a patient suffering from DR to depict the blood vessels of the ocular fundus, displaying typical pathologies of DR: I: neovascularization around the papilla; II: leakage of macromolecules (hard exudates); III: retinal bleedings; modified picture, obtained from Spitzer M., Images of the Universitäts-Augenklinik Tübingen.[13]

From the pathophysiological perspective, DR is a micro vasculopathy of the retinal capillaries caused by a diabetic metabolic situation. Due to the local environment, capillary occlusion and deranged vascular wall permeability are observed, causing ischemia. All these factors together result in the release of

proangiogenic cytokines and sight-threatening changes in the retinal tissue (Figure 3). This has various consequences such as micro aneurysms, exudates, bleedings, edema, necrosis and neovascularization. Here, damage to the basal membrane and the vascular endothelium can be identified as the main factors for developing DR. Subsequently, the blood retina barrier breaks down and leakage of macromolecules and fluids accumulate in the intracellular space which may lead to diabetic macula edema (DME). As a consequence of the micro aneurysm and the bulges of the vascular walls, cytokines such as VEGF are released and may lead to pathological neoangiogenesis in order to compensate the insufficient supply of oxygen[14]. In this, the hyaloid membrane of the vitreous body functions as scaffold for the neovascularization.

First line therapy of DR concerns systematic treatment of the causal reasons for this ailment. First to mention is the strict adjustment of the blood glucose levels. Another important parameter to take into consideration is reduction of the blood pressure. Local therapy often consists of laser treatment or administration of intravitreal injections that resolve the swelling of the leaking blood vessels. Initially monthly injections are necessary or post-laser checkups every three months[15,16]. However, it must be noted that recent studies have shown that intravitreal injection therapy with anti-VEGF antibodies or antibody fragments seems to be more effective than laser treatment[15,17,18].

1.2.3. Retinal vein occlusion

Retinal vein occlusion (RVO) is the second most common retinal vascular disease of the eye after DR. The prevalence of retinal vein occlusion ranges from 0.3 to 1.6 %. The blue mountain eye study examined the incidence of RVO in people above the age of 49 and found that after a period of five years 0.8 % of all monitored subjects were suffering from this vascular ailment whereas after ten years this had increased to 1.7 %[19]. Most patients suffering from this disease are diagnosed between their 60th and 70th year of life although there are also younger reported cases.

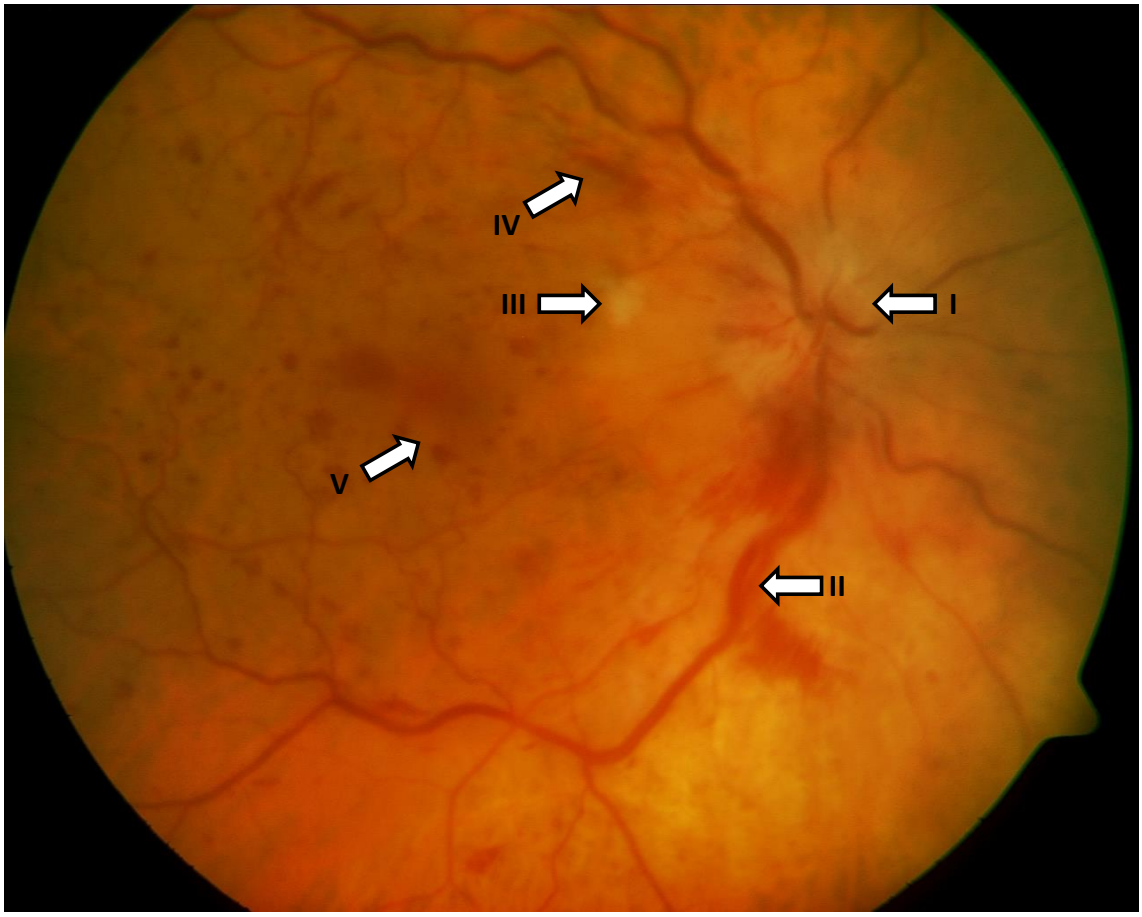

Figure 4 Fundus photography of a patient suffering from RVO highlighting typical disease pathologies: I: papilledema; II: dilatation and increased tortuosity of the retinal veins; III: ischemia; IV: streaky retinal bleedings; V: cystoid macular edema; modified picture, obtained from Spitzer M., Images of the Universitäts-Augenklinik Tübingen.[13]

In the development of RVO, thrombotic changes in the vascular system cause intraluminal constriction of vessels, which results in an increase in pressure of the local venous system[20]. The diminished or absent drainage of the retinal veins, combined with the elevated pressure, leads to leakage of blood components into the retinal tissue. In the region around the central retinal vein this may lead to the typical extracellular cystoid macular edema (CME). Additionally, as a consequence of the restricted perfusion, local ischemia occurs (Figure 4). This is followed by the expression of permeability increasing cytokines (e.g. VEGF). Depending on the severity of the occlusion and the resulting ischemia, the induced edema which in severe ischemia may later be followed by neovascularization differs in intensity. Therefore, the symptoms observed in RVO are dependent on the extent of the occlusion and especially on its localization. Due to possible hemorrhages and edemas in the retinal tissue, symptoms of RVO

range from reduced vision acuity to a total loss of sight. In general, a branch retinal vein occlusion (BRVO) is approximately three times more likely to occur than the closure of the central vein (CRVO). Fortunately, less severe symptoms are associated with the former. Occlusions of the retinal veins itself are rarely to be remedied causally, e.g. thrombolysis is considered to be not effective for RVOs.

Currently, in RVO therapy mainly the neovascular effects of the retinal vein occlusion and macula edema are treated[21-23]. Hence, intravitreal injection of anti-VEGF medication is the treatment of choice.

1.3. Drug delivery to the posterior segment today

Successful delivery of pharmaceuticals to the posterior segment of the eye still remains a challenging task in the treatment of retinal diseases, despite advanced understanding of anatomical barriers and transport mechanisms. The main task of ocular drug delivery is to overcome these protective obstacles to achieve therapeutically relevant concentrations of therapeutic agents in the target tissues. In general, systemic and local treatments can be distinguished. In the field of ophthalmology the local application of medication is highly favored. There are two important reasons for this and both are related to the immune privileged status of the eye. Similar to the brain, the retina is separated from the circulating blood by a selective blood-retina barrier[24]. In here, tight junctions fulfill a special role in two different layers of tissue. The cells of the retinal pigment epithelium are connected by a belt of tight junctions at the basal pole. These contact sites form channels between the cells but also heavily restrict diffusion. They form the first component in the blood-retina barrier. The second part consists of the endothelial lining of the intraretinal blood vessels also showing tight junctions with similar characteristics as to those found in the RPE. These two components work in synergy and heavily limit the diffusion of compounds from the blood to the retina. As a result, systemically utilized drug substances will hardly be able to reach their target tissue. It has previously been shown that after systemic administration of a drug, less than 2 % reaches the vitreous body[25]. The second major reason why

local drug application is preferred is because systemic adverse effects can be precluded. For administration of drugs to the eye the following routes are mostly used:

- Topical application
- Intravitreal injections
- Periocular injections

Their advantages and disadvantages will be discussed below.

1.3.1. Topical application

For topical treatment eye drops offer an elegant method for therapy of anterior segment diseases due to their ease of application and good tolerability. However, only very low amounts of active substance can be found in the posterior segment of the eye after using this application form. Approximately only 0.1 ‰ of the drug detected in tear fluids penetrates deep enough to reach the retina and the choroid[26]. The main reasons for this are firstly, the corneal clearance, consisting of lacrimation and tear transition[25] and secondly, that to reach the posterior segment the medication first has to diffuse through the cornea. The cornea is composed of several layers that serve to prevent this. Additionally, after passing the cornea the medication needs to circumvent lymphatic clearance[27]. Due to the very low efficiency of delivery, eye drops only play a minor role in the treatment of posterior segment diseases. For example, prevention and treatment of the cystoid macular edema (CME) can be performed via eye drops. Nevertheless, the benefit and efficiency of this intervention is still discussed[28].

In order to improve eye drops, efforts have been made to develop contact lens systems which contain certain medication or increase the uptake of medication into the eye. Recently, molecular imprinted polymeric gels have been tested successfully for contact lens mediated enhanced drug delivery[29,30]. In addition, conjugation of nanoparticles or liposomes with contact lens is a novel approach that is currently investigated[31]. However, most of these recent findings mainly prove local efficacy and do not show sufficiently high drug levels at the retina.

Therefore, drug delivery to the posterior segment through eye drops remains difficult.

1.3.2. Intravitreal injections

In order to obtain a sufficiently high concentration of medication at the retina, pars plana intravitreal injections are currently the most efficient application technique. It is the method of choice for intraocular administration of antibiotics[32], corticosteroids[33], chemotherapeutic agents[34] and anti-VEGF medication[35,36]. When performing an intravitreal injection, a thin needle perforates the limbus and enters the vitreous between the *corpus ciliare* and the retina. After injection of the drug, a concentration equilibrium is first established, after which a loss of the medication occurs[37]. The blood retina barrier works in favor of the approach, as loss through the blood circulation is prevented[24]. Unfortunately, after injection the drug molecules are still eliminated rapidly via the circulating aqueous humour, leading to the excretion through the canal of Schlemm. Another route of removal is the retina itself, where the medication is removed from the eye utilizing active transport mechanisms[38]. The half-life period of substances in the vitreous body is mainly depending on its molecular weight, but also on the status of the vitreous space (e.g. shorter drug half-life in vitrectomized eyes). Most drugs with low molecular weights only possess a short half-life in the range of several hours[39]. Therefore, often very high doses are necessary to be able to keep a clinically relevant concentration in the posterior segment over a significant amount of time. However, high doses increase the chance of side effects. Inevitably, this leads to the need of numerous re-injections. Serious side effects such as retinal detachment, hemorrhage[40], increased intraocular pressure[41], endophthalmitis[42] or cataracts[43] though rarely occurring endanger successful outcome of the therapy and affect patient comfort. For example, after intravitreal application of VEGF such side effects have been observed in 0.1-0.2 % of the treated patients[44]. Nevertheless, intravitreal injections are currently the preferred route of administration for many indications, including AMD.

Recently, depot or slow-release systems have been developed that enhance the problematically short half-life observed after intravitreal injection. Currently in use

are implants composed of polymers with slow release characteristics for the encapsulated drugs[45]. In here one can distinguish between biodegradable and non-biodegradable devices. Examples are Ozurdex® (Dexamethason), Vitrasert® (Ganciclovir) and Retisert® (Fluocinolone Acetonide), which are all approved for clinical employment. The implant devices can be injected into the vitreous or be positioned in the pars plana tissue itself. Advantages of these drug delivery vehicles are numerous. First and foremost, the desired drug concentration can be held on a consistent level over a longer period of time providing the necessary medication dosage. Second, a lower incidence of local complications such as infections or lens damage is expected due to reduced frequency of injections[46]. Finally, they often also offer more consistent drug release. Nevertheless, it has to be noted that the devices that are not bio-degradable may require surgical removal. In the future different locations for placement of the implants might be leading to even more beneficial dosing. For example, choroidal, conjunctival and scleral tissue might be future targets, but also subcutaneous implants could be useful in future therapy for retinal diseases[47].

1.3.3. Periocular injections

Among periocular injections one can distinguish between retrobulbar, peri-bulbar, subtenon and subconjunctival injections. Administration via this route may offer a chance to enhance drug delivery to the posterior segment[48]. Recently, it has been shown that the subconjunctival application leads to 54 times higher medication levels compared to systemic injections, showing the significant advantage of this technique over systemic application[49]. Another benefit of this application method is that these injections are far less invasive than intraocular injections, thereby reducing the risk of complications. After periocular application, the medication reaches the target structures of the posterior segment via transscleral or transcorneal diffusion and through local blood circulation[50]. The sclera covers the vast majority of the overall surface of the bulbus and therefore offers a large absorption area. Additionally, it is more permeable to drug molecules than the conjunctival and corneal tissue, which is advantageous for delivery purposes[51]. Similar to the diffusion from the eye, the passage capacity of molecules is mainly defined by their molecular weight. As such, small

molecular compounds are favored over larger antibodies for periocular injections. Currently, predominantly lipophilic, long lasting corticosteroids are applied with this technique. Therefore, diseases treated with this modus are first and foremost posterior uveitis or other inflammatory vessel or retinal diseases. Possible side effects that are observed after applying this therapeutic approach are an increased intraocular pressure, hyphema, strabismus and corneal decompensation[25]. In order to attain higher intraocular drug concentrations over a longer period of time, episcleral depots can be employed. These function in a similar manner as the intravitreally injected depots described above.

1.4. DNA based nanoparticles

Nanoparticles can be formulated out of various different materials and have recently been receiving more and more attention in the field of drug delivery due to their versatile nature. They may vary in size from 10 to 100 nm and in contrast to macroscopic objects, these submicron vehicles exhibit special properties due to their high surface area and the large influence of Brownian motion. In combination with potential targeting mechanisms these submicron properties are especially desired in tissues where physiological barriers hinder establishing therapeutically relevant concentrations of agents – such as in the posterior segment of the eye. Manufacturing them out of DNA provides many advantages over other materials. For example, the size and structure of liposomes and microspheres are often greatly differing, which can hinder efficient therapy. The self-recognition properties of DNA constitute molecules uniform in size and functionality. They can be designed into desired shapes with control over spatial orientation, thereby assuring the required characteristics. Additionally, nucleic acid nanoparticles have not yet been investigated for the use of intravitreal drug delivery devices thus far.

In this work nanoparticles constructed from different amphiphilic oligonucleotides are employed to investigate their potential in ocular drug delivery. The DNA sequences differ in their respective total length, number of hydrophobic modifications and sequence. To incorporate non-water-soluble entities,

dodecyne-modified deoxyuracil are coupled onto the growing oligonucleotide chain at the terminal end during DNA synthesis (Figure 5-I). Microphase separation enables the amphiphiles to self-assemble into micellar structures when introduced into an aqueous medium (Figure 5-II). Inside the formed micelles a lipid core is located consisting of the alkyl tales of the modified deoxyuridine nucleotides, which are shrouded by single stranded DNA in the corona. The micellar construct as described above will from hereon be referred to as nanoparticles (NPs). Hybridization with complementary oligonucleotides offers the possibility of facile binding of a therapeutic agent or a fluorophore for imaging purposes to these NPs (Figure 5-III).

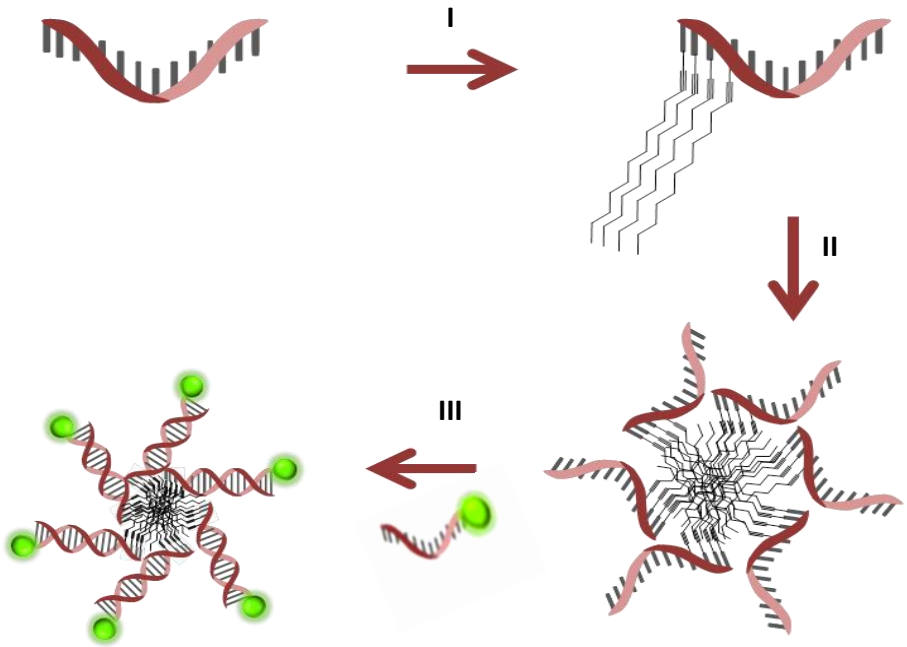

Figure 5 Schematic representation of the different steps of NP-assembly: I: incorporation of dodecyne-modified deoxyuracils at the terminus of the oligonucleotide chain; II: self-assembly of the amphiphilic DNA into micellar structures (NP) in aqueous medium; III: hybridization of the NP with complementary oligonucleotides functionalized with a covalently bound fluorophore; modified image, obtained from Vries, J.W.d., DNA Nanoparticles as Ocular Drug Delivery Platform.[52]

The formed NPs have an approximate diameter of 12 nanometer (nm). However, this parameter can be modulated by altering the sequence length of the amphiphilic oligonucleotides. The micellar structures consist of an average of 25 lipid-DNA oligonucleotides[53].

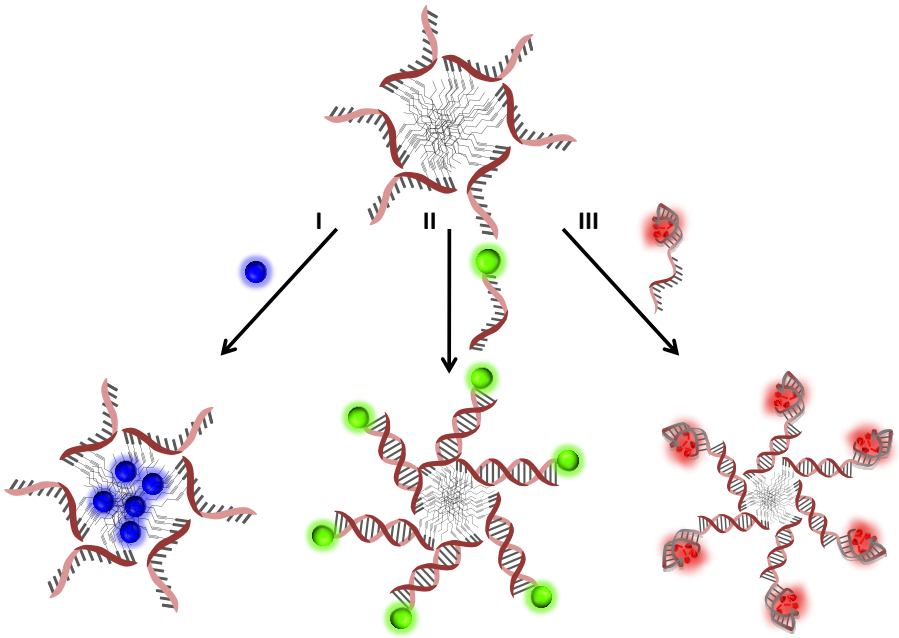

Figure 6 Schematic representation of different options of NP loading. I: loading of the NP via hydrophobic interactions inside the lipid-tail core; II: hybridization with the complementary DNA that is covalently functionalized with the molecule of interest; III: adaptive binding of an agent utilizing an aptameric sequence; modified image, obtained from Vries, J.W.d., DNA Nanoparticles as Ocular Drug Delivery Platform.[52]

For loading of actives, these NPs offer diverse options (Figure 6). Firstly, lipophilic interactions can be used to load hydrophobic medication in the core of the NP. Aside from that covalent binding of therapeutic agents to the complementary strand provides a convenient option. However, this involves chemical modification of the target compound, which may lead to an inactive or even toxic drug. A third and more elegant method is the loading of NPs via an aptamer hybridized to the single stranded corona, enabling the drug delivery of almost any drug. Aptamers are oligonucleotides which fold around a target molecule to form an adaptive binding. The target is kept in place by electrostatic interactions, hydrogen bonds and base stacking.

The safety of the used NP platform has been tested in different ocular cell lines in previous experiments with no toxic effects detectable. Additionally, in-vivo studies have also been performed with single and multiple exposures at various concentrations of NPs. Apoptosis screening was undertaken using TdT-mediated dUTP-biotin nick end labeling (TUNEL) staining showing no increased cellular damage under the influence of the applied NPs[52].

All the presented options for modification, loading and the promising properties due to their small size led to the hypothesis that these DNA based NPs can be employed as a versatile drug delivery platform for ocular therapy of posterior segment diseases.

1.5. Thesis motivation and overview

Eyesight is the main medium of perception of our environment. As a consequence our eyes are embedded and protected by numerous different tissues and barriers, extraordinary in anatomy and physiology. Therefore, efficient drug delivery to the posterior segment of the eye remains a challenging task until today and is a major obstacle in the field of ophthalmology that needs to be overcome. Incorporating DNA nanostructures for drug delivery combines the potential of submicron attributes with the versatility of nucleic acid. This combination employed in the field of ophthalmology will certainly lead to more opportunities for research in treatment development. The ability to design base sequences in order to utilize certain attributes of DNA holds manifold options and potentials for therapies in the future.

The purpose of the work was to investigate the behavior of novel lipid-modified DNA nanoparticles (NPs) injected into the vitreous body and periocular tissue. First the intravitreal application of lipid DNA NPs as a novel type of drug delivery platform was investigated. Here, the defined NPs were introduced in the approximate center of the vitreous body of ex-vivo porcine eyes. Afterwards, the behavior in regard to diffusion and retention of the vehicles was investigated utilizing a fluorophotometer. The next step in the examination of the utilized NPs was to define the ocular adhesion areas and variations in adhesion duration under ex-vivo conditions under the fluorescence microscope. After studying the diffusion and retention of the NPs in an ex-vivo setting, the same parameters were examined in-vivo. Therefore, a rat eye model was employed and the same defined drug delivery vehicles were injected into the posterior segment. The analysis of adhesion areas and variations in adhesion duration of the different NPs was performed as described above. Finally, the lipid DNA NPs were applied through subconjunctival injections into the periocular tissue. This was done in order to evaluate this administration technique in regard to its depot function and local distribution of the carrier. The adhesion areas and duration of presence were tested in the same in-vivo model as used before.

2. Materials and Methods

2.1. Reagents and consumables

- 0.9 % NaCl, Fresenius Kabi Deutschland GmbH
- 2-Amino-2-(hydroxymethyl)-1,3-propanediol (Tris base), Roche
- 4',6-diamidino-2-phenylindole (DAPI), Invitrogen # D1306
- Atipamezole 5.0 mg/ml, Albrecht GmbH
- Atto-488 labelled complementary DNA at HPLC grade purity, Biomers.net
- Conjuncain: Conjuncain®, EDO®, (4.0 mg/mL Oxybuprocainhydrochlorid), Bausch and Lomb GmbH, Berlin, Germany
- Cover glasses 24x50 mm, R. Langenbrinck Labor- & Medizintechnik
- Dulbecco's phosphate-buffered saline (DPBS), GIBCO®
- Eppendorf tubes, Eppendorf®
- (Ethylenedinitrilo)tetraacetic acid (EDTA), Sigma-Aldrich # 1233508 USP
- Fentanyl 50 µg/ml, Albrecht GmbH
- Flumazenil Kabi 0.1 mg/ml, Fresenius Kabi Deutschland GmbH
- FluorSave, Calbiochem
- Gentamicin, Gentamicin-POS® (5.0 mg/mL Gentamicinsulfate), Ursapharm GmbH
- Glacial acetic acid, Sigma # A6283
- Glass slides "Superfrost plus", R. Langenbrinck Labor- & Medizintechnik
- Hydrochloric acid solution (HCL), Sigma # 30723
- Magnesium chloride ($MgCl_2$), Sigma # M8266
- Medetomidin 1.0 mg/ml, Albrecht GmbH
- Methanol, AnalaR® NORMAPUR® # UN 1230
- Midazolam 5.0 mg/ml, Hameln Pharmaceutical GmbH
- Mydriatic agent, University Pharmacy Tübingen, (9 mL containing: Phenylephrin-HCL (225 mg), Tropicamid (45 mg), Povidon 25 (270 mg), Aqua ad. inj. (8.36 g))
- Naloxon 0.4 mg/ml, Hameln Pharma Plus GmbH
- Pipetting tips (20 µl, 100 µl, 1000 µl), Greiner bio-one

- Sodium chloride (NaCl), Sigma # S7653
- Tissue-Tek O.C.T., Sakura Finetek
- Ultra-pure water (Resistivity ≥ 18.2 MΩ), Merck millipore

2.2. Equipment

- 10 µL Syringe, Model 1701 RN SYR, Small Removable NDL, 32 gauge, 2 in, point style 3, Hamilton
- 50 µL Syringe, Model 1705 RN SYR, Small Removable NDL, 22 gauge, 2 in, point style 2, Hamilton
- Cryostat, Leica CM 1900, Leica Microsystems GmbH
- Fluorotron Master™, Ocumetrics
- Magnetic stirrer COMBIMAG RCT, IKA
- Micro-pipettes , Eppendorf®
- Microscope, Axioplan 2 Imaging, including Openlab software (Improvision), Zeiss
- Ophthalmology surgical retroskop opmi cs-xy S4, Zeiss
- Thermocycler UnoCycler VWR 732-1200, VWR International GmbH

2.3. Buffers

Preparation of TAE stock

First, 14.6 g EDTA and 242 g tris base were dissolved in 800 mL of ultra-pure water while stirring. Afterwards, acetic acid was added to adjust the pH of the solution to 8.0. Finally, ultra-pure water was added to obtain a total volume of 1 L.

Preparation of NP buffer stock

400 µL of NP stock buffer was prepared by adding 100 µL of TAE stock (described above), 300 µL of $MgCl_2$ (1 M) and 100 µL of NaCl (5 M) into an Eppendorf tube.

Preparation of 1x TBS buffer

For preparation of the TBS buffer 87.66 g NaCl and 60.57 g tris base were dissolved in 800 mL of ultra-pure water, using a magnetic stirrer until a clear solution was obtained. Afterwards, 25 % HCl was titrated to adjust the pH to 7.4.

Ultra-pure water was added until reaching a total amount of 1 L of the 10x solution. For further use a dilution of 1:10 in ultra-pure water was performed.

2.4. Methods

2.4.1. Preparation of NPs

NPs were prepared in Eppendorf tubes in NP buffer by combining the desired amount of ultrapure water, NP buffer stock (described in section 2.3), the lipid oligonucleotide of interest and its fluorescently labeled complementary sequence bearing an Atto-488 dye on the 5' end. For the NP stock buffer 2 µL was added to 98 µL final solution to obtain a final concentration of 8 mM Tris-Acetate, 1 mM EDTA, 20 mM NaCl and 12 mM $MgCl_2$, pH 8.0. The NPs were prepared at a concentration of 20 µM. For functionalization equimolar amounts of complementary DNA strand were used. Finally, NPs were formed and hybridized using a thermal gradient. In a thermocycler the NP solutions were heated up and kept at (90 °C for the duration of 30 minutes). Afterwards, they were cooled down by 1°C every two minutes until room temperature was reached. NPs were stored in the dark at room temperature until further use.

2.4.2. Fluorophotometric measurements

In order to measure the fluorescence in the vitreous of the utilized eyes an ocular fluorophotometer was employed (Fluorotron Master™, Ocumetrics, Mountain View, CA). Before measurements were performed, the eye of interest was aligned with the lens of the system and the optical axis of the Fluorotron Master™. A blue laser is emitted through the optics of the fluorophotometer which leads to excitation of the fluorophore molecules. These in turn emit fluorescent green light that is recognized by the incorporated photodetector and measured at the point of intersection. The fluorescence was recorded in 0.25 mm sections along the determined optical axis by a program which converts the reading to the corresponding concentration. Thereby, a profile is generated that shows the fluorescence intensity as a function of the distance from the retina.

2.4.3. Evaluation of results obtained from fluorophotometric measurements

To investigate the diffusion behavior of different NPs, it is important to note that the integrated fluorescence intensity obtained from the fluorophotometric measurements requires normalization. In order to detect the NPs, they were functionalized with the fluorescent dye Atto-488, which was attached via covalent binding to the complementarily strand. This strand was then hybridized to the NPs, thereby obtaining the fluorescently labeled vehicle. Binding of this dye to the DNA requires chemical modification of the structure of this molecule which leads to alteration of its fluorescence strength. The magnitude of those changes is dependent on the sequence of the DNA it is coupled to. As the NPs constitute unique sequences (different length and different amounts of lipid modified bases), the dye exhibits specific intensities for each NP. This means that the fluorescence intensity measured for one NP cannot be directly compared to the next, or to the free dye. In order to make the found results for the NPs comparable, for each an individual starting value was defined which represents 100 %. All the following measurements of the specific NP structure were divided by this first value, generating a relative value which can be compared between the different NPs.

For normalization two different starting values were utilized. The first normalization was performed by measuring the respective NP in solution within a cuvette before injection using the cuvette holder of the fluorophotometer. This value gives information about the total injected amount and which fraction is detected. It will from hereon be given as the “solution” measurement. The second one was measured directly after injection, which is displayed in the later figures as the “instant” time point. This value gives insight in the time dependent distribution of the NPs in the vitreous body. Both normalization methods were utilized in order to compare the NPs.

For all eyes investigated, the mean value and standard deviation were calculated for each time point using Excel 2010. The statistical significance was calculated utilizing JMP 13. Here, analysis of variance (ANOVA) and Dunnett’s post-hoc tests were performed. The small molecule control (Atto-488) data served as

“control”. Significances are displayed in the graphs of the discussion as: * for the value of P ≤ 0.05, ** for the value of P ≤ 0.01 and *** for the value of P ≤ 0.001. In the interest of clarity the statistical evaluation is incorporated in the Discussion (4.1.1).

For the ex-vivo experiments the investigated time points were before injection and after 0, 5, 15, 30 minutes as well as after 4, 8 and 24 hours of incubation (n=6-8) (see section 2.4.5). In-vivo measurements were also performed before injection and 0, 1, 3 and 5 days post injection (n=6) (see section 2.4.6).

2.4.4. Intravitreal injection of lipid-modified DNA NPs into ex-vivo pig eyes

Porcine eyes, freshly obtained from the local abattoir were kept at a temperature of 4 °C and treated within 4h after delivery. Before administration of NPs or control, the eyes were shortly washed with ultra-pure water and left to adjust to room temperature. For NP administration, the eyes were placed on the bottom of a petri dish and fixated with one hand. Afterwards, the *pars plana* was penetrated approximately 4 mm posterior to the limbus of the eye using a needle of 30 gauge. Then, 40 µL of NP solution (20 µM) was injected into the center of the vitreous body under microscopic observation (Ophthalmology surgical retroskop opmi cs-xy S4, Zeiss). The porcine eyes were then incubated for the designated time points in PBS buffer.

For fluorophotometric evaluation, measurements were performed as described in 2.4.2, before injection and after 0, 5, 15, 30 minutes as well as after 4, 8 and 24 hours of incubation(n=6-8).

For microscopy, the porcine eyes (n=3) were embedded in Tissue-Tek and subsequently frozen in liquid nitrogen after 5, 15, 30 minutes, 1 or 2 hours of incubation. Afterwards, cryosections were prepared, stained and imaged as described in 2.4.7.

2.4.5. Intravitreal injection of lipid-modified DNA NPs into in-vivo rat eyes

Adult Lister Hooded Rats were obtained from Charles River (Germany) and treated according to the German animal protection law (Research permission AK 3/11 and 1/15 to Sven Schnichels). Before treatment the animals were anesthetized by peritoneal injection of a three components anesthesia (0.1 mL/10 g bodyweight). For this, 5 mL of the anesthesia was prepared using 0.5 mL Fentanyl (0.005 mg/kg), 2.0 mL Midazolam (2.0 mg/kg), 0.75 mL Medetomidin (0.15 mg/kg) and 1.75 mL of 0.9 % NaCl. Afterwards, the eyes were dropped with Conjuncain (4.0 mg/mL Oxybuprocainhydrochlorid, Bausch and Lomb GmbH, Berlin, Germany) further ensuring local anesthesia, and a mydriatic agent (University Pharmacy Tübingen, - 9 mL containing: Phenylephrin-HCL (225 mg), Tropicamid (45 mg), Povidon 25 (270 mg)) in order to increase visualization during microscopic observation of the position of the injection needle. For intravitreal application 10 µL of NP solution (20 µM) were injected into vitreous body, approximately 3 mm posterior to the limbus using a 30 gauge needle.
After the surgery, an antidote was employed subcutaneously to terminate the anesthesia (0.3 mL/10 g bodyweight). For the preparation of 15 mL of the antidote, 1.5 mL naloxon (0.12 mg/kg), 10 mL flumazenil (0.2 mg/kg) and 0.75 mL atipamezol (0.75 mg/kg) were added to 2.75 mL of 0.9 % NaCl. Finally, gentamycin ointment was applied onto the injection site to prevent infection. For the following fluorophotometric measurements and fluorescence imaging different time points were investigated.

For fluorophotometric evaluation, measurements were performed pre injection and 0, 1, 3 and 5 days post injection as described in 2.4.2. In order to do so, the living rats was anaesthetized as described above and the eyes (n=6) were dilated using mydriatic agent. The anesthesia was terminated by injection of the antidote.

For microscopy the rats were euthanized with carbon dioxide inhalation after the designated time periods of 0, 5, 1, 3 and 5 days. The treated eyes (n=6) were enucleated, frozen in Tissue-Tec and further processed as described in 2.4.7.

2.4.6. Injection of lipid-modified DNA NPs into periocular tissue of in-vivo rat eyes

For these experiments Adult Lister Hooded Rats were treated similar as those described in 2.4.5. Also the anesthesia was prepared and performed as described above. In order to additionally ensure local anesthesia, conjuncain (4.0 mg/mL Oxybuprocainhydrochlorid, Bausch and Lomb GmbH, Berlin, Germany) was dropped topically at the site of the injection. Administration of 40 µL NP solution (20 µM) into the periocular tissue was performed subconjunctivally. A 30 gauge needle was inserted 5 mm into the conjunctival tissue approximately 10 mm temporolateral from the most lateral point of the limbus under microscopic observation. Antidote prepared as described above and administered at 0.3 mL/10 g bodyweight was administered subcutaneously to end the anesthesia after surgery. In addition gentamycin eye drops were applied locally. The rats were euthanized with carbon dioxide inhalation after the designated time points of 30 minutes, 2, 4 and 24 hours as well as three days. The treated eyes including the surrounding subconjunctival tissue were then excised, frozen in Tissue-Tec and further processed as described in 2.4.7. Throughout the different time points in this experiment the analyzed eyes always equaled n=2, except for the time periods of one and three days where for U4T-18 and U6T-12 n=6 eyes were examined.

2.4.7. Fluorescent microscopy and imaging

Frozen sections of Tissue-Tek O.C.T. (Sakura Finetek) embedded porcine and rat eyes were longitudinally cut (12 µm) on a cryostat (Leica CM 1900), thaw-mounted onto glass slides (Superfrost plus, R. Langenbrinck Labor- & Medizintechnik) and stored at -30 °C until further use. For visualization each section was fixed with 300 µL methanol (ten minutes) and afterwards washed with 1x TBS solution (3 x 3 minutes). In a next step the nuclei were counterstained with 100 µL 0.4 µg/mL DAPI (five minutes), before being washed with 1x TBS buffer (3 x 3 minutes) once more. After drying, the stained slides were covered in FluorSave (Calbiochem) and furnished with cover glasses (R. Langenbrinck Labor- & Medizintechnik). Finally, the prepared sections were imaged using a fluorescent microscope (Axioplan 2, Zeiss with Openlab software, Improvision).

The nucleus stain was imaged employing a small band DAPI filter (wavelength of emission maximum: ~461 nm), whereas the fluorescent dye conjugated to the NP was captured utilizing a FITC small band filter (wavelength of emission maximum: ~495/519 nm). The obtained layers were combined to visualize the location of the dye with respect to the tissue of the posterior segment. In order to comprehend sizes a scale was introduced into the pictures indicating 130 µm of length. This scale was inserted using Microsoft Paint for Windows 10. The Openlab software gives information about how many pixels in which magnification add up to which size. For the 50 times magnification that was used for the imaging in this thesis, the amount of 100 pixels resembles 130 µm.

3. Results

To investigate the suitability of DNA based NPs as a treatment modality for diseases of the posterior segment their half-life time and adhesion capacity to specific ocular tissues were tested. To gain initial insight in these properties, a variety of NPs were first injected in ex-vivo porcine eyes and their diffusion and adherence was monitored by fluorescence photometry and microscopy, respectively. Afterwards, this experimental setup was translated into in-vivo rats. The same parameters were investigated after intravitreal injection of several NPs that showed superior properties in the ex-vivo setup. Finally, to explore the use of this platform for delivery using a periocular administration route, they were also employed in sub-conjunctival injections.

In order to gain insight in how the structural properties of these NPs relate to their adhesion capabilities, several NPs were designed. The sequences details of lipid-modified oligonucleotides that were employed are displayed in Figure 7.

Name	Sequence(5'→ 3')	Lipid modified Bases # (%)
U4T-12	UUUUGCGGATTC	4(33)
U4T-18	UUUUGCGGATTCGTCTGC	4(22)
U6T-12	UUUUUUGGATTC	6(50)
U6T-18	UUUUUUGCGGATTCGTCT	6(33)
U6T-20	UUUUUUGCGGATTCGTCTGC	6(30)

Figure 7 Sequence and details of lipid-modified oligonucleotides used for NP preparation.

As can be seen, the name of the respective NP already partially reveals the characteristics of the oligonucleotide. First, the letter "U" indicates the use of the lipid modified nucleotide. Next, the number following the U gives the total amount of modified deoxyuridine nucleotides in the sequence. The letter "T" in the name reveals that the modified bases are located on the terminus of the oligonucleotide, starting from 5'-end. Finally, the number in the end gives the total amount of nucleotides in the sequence.

In the following experiments, the NPs were formed by preparing the oligonucleotide of interest together with the complementary sequence, both at a concentration of 20 µM. Afterwards they were thermally cycled in order to form uniformly sized NPs that can directly be employed for intravitreal or sub-conjunctival injections. As a first step the diffusion behavior of the different NPs was investigated in an ex-vivo setup.

3.1. Intravitreal injection of lipid-modified DNA NPs into ex-vivo pig eyes

3.1.1. Examination of diffusion of DNA NPs within an ex-vivo vitreous body

Different NPs were injected into the vitreous of the ex-vivo pig eyes and the fluorescence signals were quantified inside the eye using an ocular fluorophotometer. As described in 2.4.2 this device is able to measure the intensity as a function of depth by sequentially focusing on points along the optical axis (from retina to cornea) in the ocular cavity. It then combines these signals into a fluorescence profile which is directly proportional to the concentration of the used NP. In Figure 8 an example of the data obtained from a typical fluorescence measurement is displayed. The first measurement was made directly after injection of the NP. Afterwards, the signal was measured at 5, 15, 30 minutes (min) and 2 hours (h).

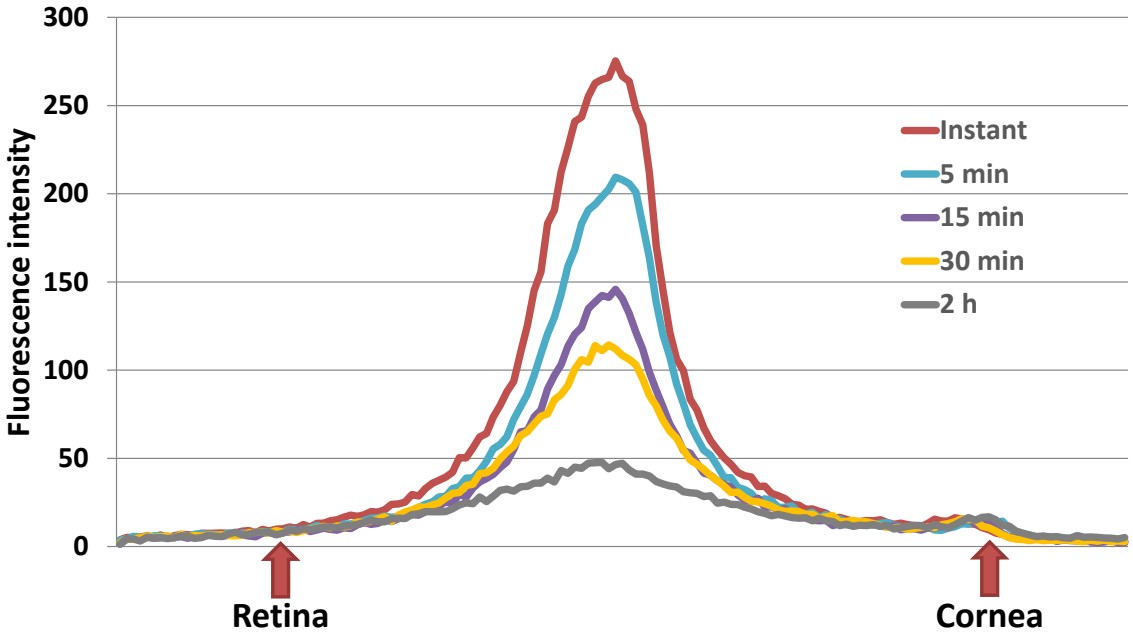

Figure 8 Fluorescence intensity (y axis) measured at different time points after intravitreal injection of U4T-18 NPs along the optical axis (x axis) in ex-vivo porcine eyes. The decreasing intensity over time indicates diffusion of the NPs into the vitreous body

As can be seen, directly after injection of the NPs the highest signal was obtained in the vitreous body (Instant). The maximum fluorescence intensity here was approximately 270 units. As the fluorescence intensity is strongly dependent on the device and setup in which it is measured, no SI units could be given. However, throughout this thesis the experimental setup was kept constant. Therefore, values found for the different NPs could be compared amongst each other. In Figure 8 also a steady decrease of the signal was observed over time, indicating diffusion of the carrier from the ocular cavity.

To quantify and compare the amount of NP present, the fluorescence intensity in the vitreous body at a given time point was integrated and normalized as explained in 2.4.3 for all eyes (n=6-8).

As small molecular control to the NPs, the free Atto-488 was used. The integrated intensity of the control dye was compared with the initial intensity (solution) in order to obtain more insight in the total amount of molecules present in the vitreous body (Figure 9).

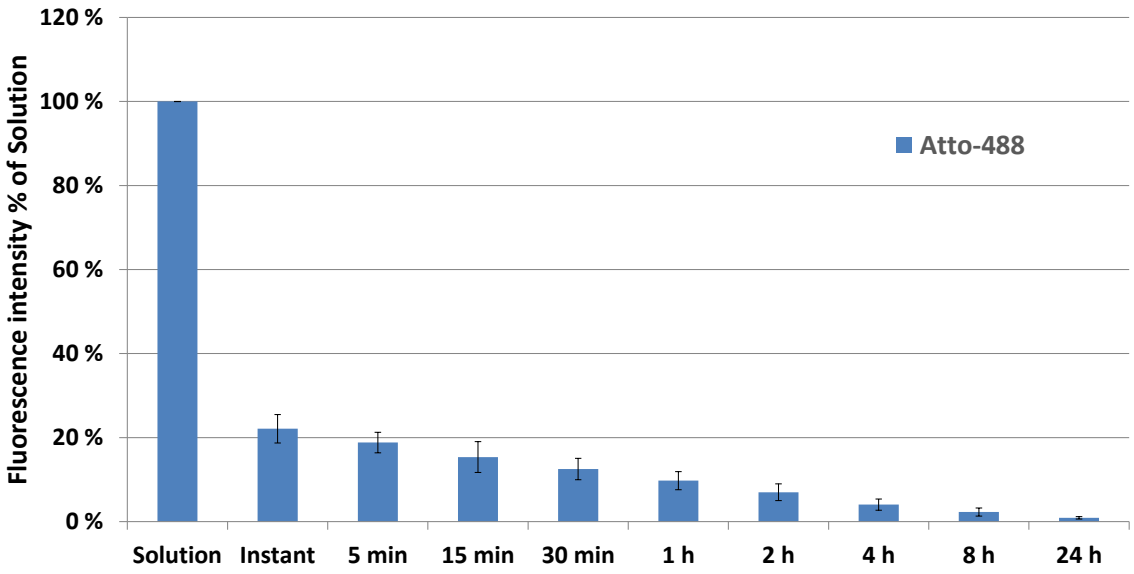

Figure 9 Integrated fluorescence intensity normalized to the solution measurement (y axis) at different time points after injection of Atto-488 control dye (x axis) into the vitreous body in ex-vivo porcine eyes (n=6), standard deviation added. The sudden drop from the solution measurement to the instant time point can presumably be explained by the dilution of the dye by the vitreous fluid. The normalization to the solution value shows that the control rapidly diffused into the vitreous body.

As expected, the intensity of fluorescence decreased over time with an initial sudden drop. The intensity of fluorescence detected in the eye right after injection was only 22 % of the solution value. Furthermore, after five minutes the measured value already dropped down to 19 %, whereas after two hours the detected intensity of fluorescence was only 7 %.

In order to be able to directly compare this data with different NPs, normalization was also performed to the initial measurement taken directly after injections (Figure 10). To relate the measured fluorescence after injection to the situation before treatment, the native fluorescence of the employed porcine eyes was also incorporated into the graph (prescan).

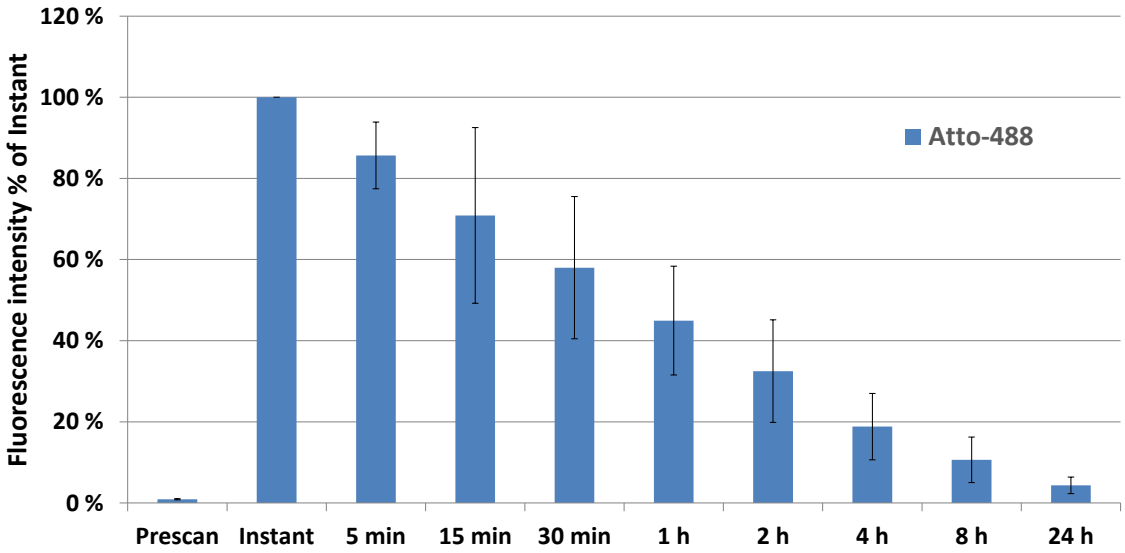

Figure 10 Integrated fluorescence intensity normalized to the instant measurement (y axis) at different time points after injection of Atto-488 control dye (x axis) into the vitreous body in ex-vivo porcine eyes (n=6), standard deviation added. The strong decrease of detected fluorescence over time indicates rapid diffusion of the control into the vitreous body.

After one hour the fluorescence intensity was detected to be at 58 % of the instant fluorescence, whereas after eight hours the detected intensity of fluorescence was only around 11 %. Finally, after 24 hours the intensity has dropped to 4 %. It must be noted here that the peak detected after this period of time was only marginally above the prescan measurement (1%). This data indicates a very rapid diffusion of the control compound from the injection point into the vitreous body.

After measurement of the small molecular control, the comparison with the different NPs could be made. The first lipid-DNA NP that was investigated was U4T-12. This NP sequence consists a total of twelve nucleotides, of which four contain a lipophilic modification. For the experiment porcine eyes were prepared and injected in the same fashion as described in in 2.4 and the fluorescence was measured at different time points after injection. Afterwards the fluorescence signal was normalized to the fluorescence intensity of the U4T-12 solution before injecting (Figure 11).

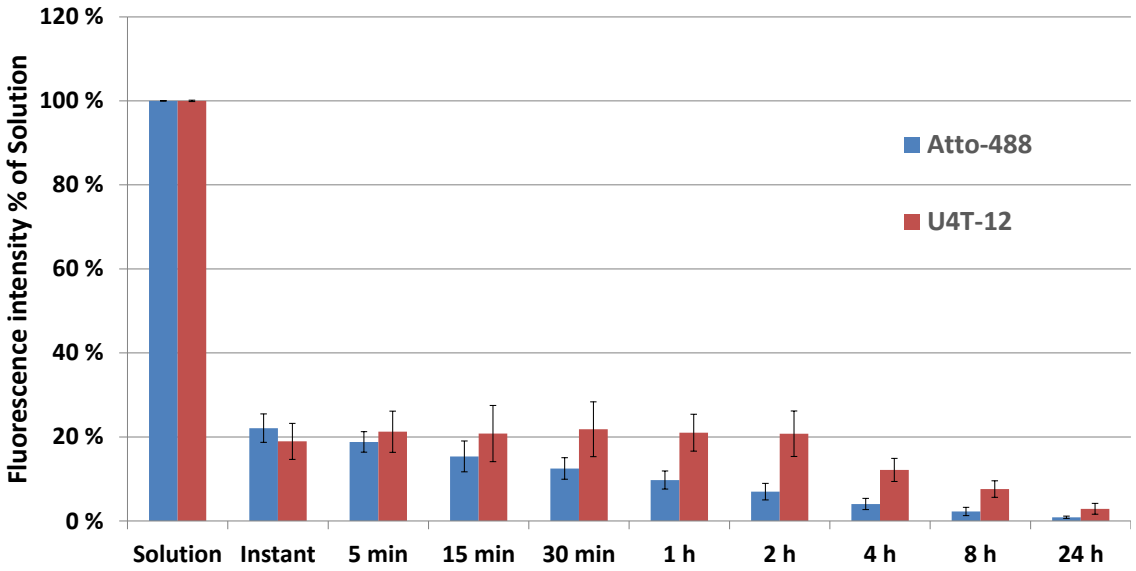

Figure 11 Integrated fluorescence intensity normalized to the solution measurement at different time points after injection of the U4T-12 NPs (red) into the vitreous body in ex-vivo porcine eyes (n=6-8), standard deviation added. For comparison the data for the control Atto-488 is also given (blue). Normalization to solution showed a lower fluorescence for U4T-12 directly after injection, but higher mean values at all time points after 15 min compared to the control dye, indicating efficient long-term retention.

Normalization to the solution indicated clear differences between the NP and the control. Directly after injection the found average intensity for the NPs (19 %) was slightly lower than for the Atto-488 solution (22 %). Strikingly, the fluorescence intensity of U4T-12 NPs increased from the measurements taken directly after injection to 30 minutes after that (22%). In contrast to the control, the NPs were detected at higher levels after the first five minutes and for the rest of the duration of the experiment.

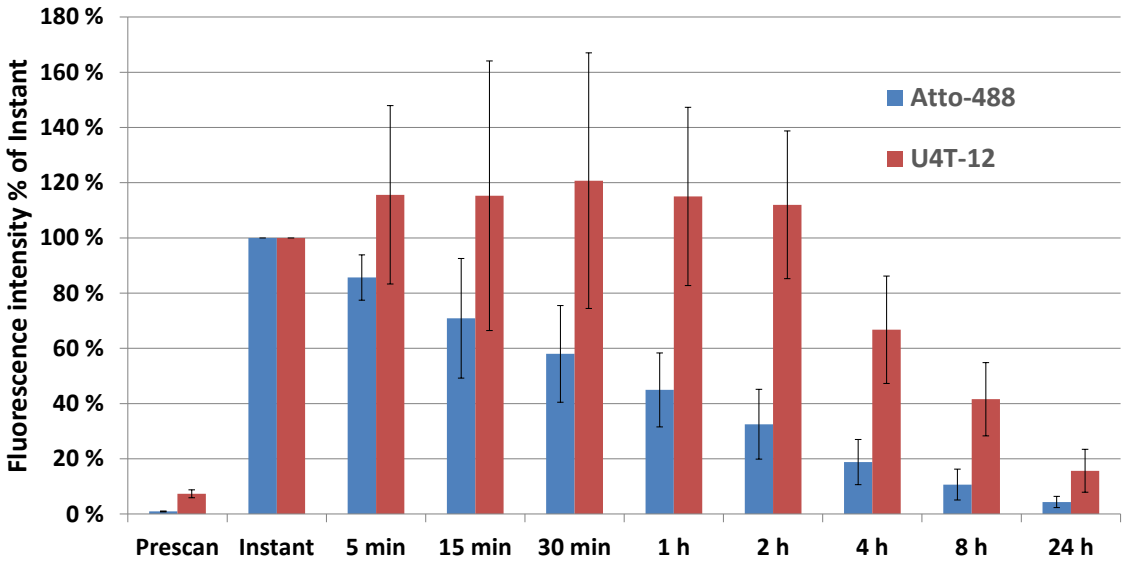

Figure 12 Integrated fluorescence intensity normalized to the instant measurement at different time points after injection of the U4T-12 NPs (red) into the vitreous body in ex-vivo porcine eyes (n=6-8), standard deviation added. For comparison the data for the control Atto-488 is also given (blue). U4T-12 displayed higher mean values at all observed time points compared to the control dye indicating excellent retention.

The obtained data was also normalized to the signal determined directly after injection (Figure 12). Similar to the observation in Figure 11, the integrated fluorescence intensity for the U4T-12 NPs increased after the first measurement to a maximum of 121 % after 30 minutes. Relatively consistent fluorescence intensity was observed until the two hours measurement (112 %). A sharp decrease followed and after 24 hours approximately 20 % of the initial fluorescence remained.

Afterwards, the properties of U4T-18 NPs were investigated. Analogous to the first studied NP, it was comprised of four modified nucleotides, but contained a larger segment of conventional bases. The preparation and analysis were undertaken as described in 2.4. First, the fluorescence signal was normalized to the solution value (Figure 13).

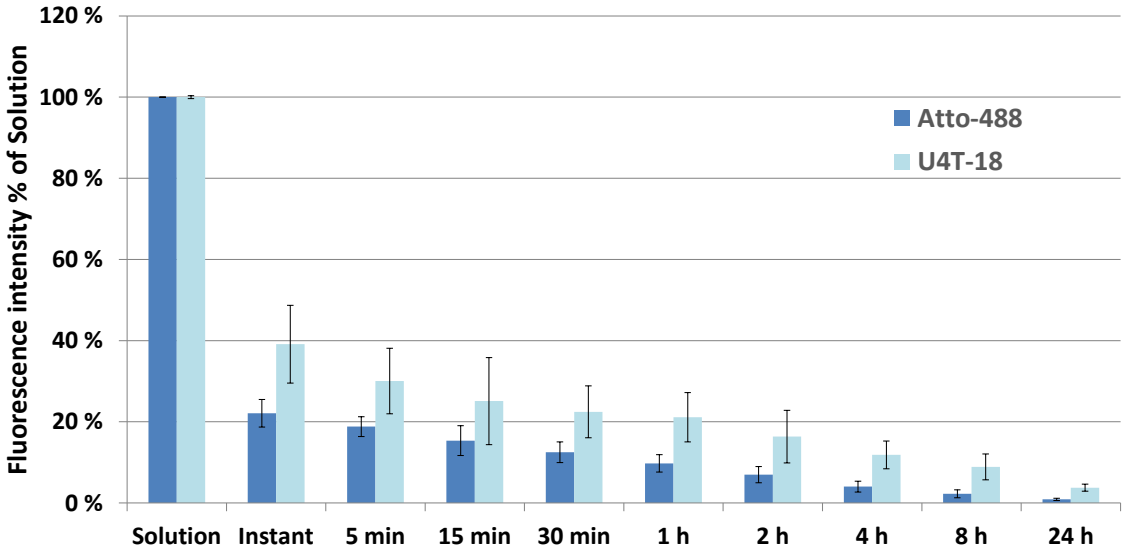

Figure 13 Integrated fluorescence intensity normalized to the solution measurement at different time points after injection of the U4T-18 NPs (light blue) into the vitreous body in ex-vivo porcine eyes (n=6-8), standard deviation added. For comparison the data for the control Atto-488 is also given (blue). When lipid modified DNA-normalized to solution U4T-18 NPs showed higher mean values at all time points compared to the control dye indicating good retention.

U4T-18 NPs (39 %) started at almost double the percentage of the solution value compared to the control (22 %) at the instant time point. Afterwards it decreased steadily and in a similar fashion. U4T-18 NPs showed higher levels of fluorescence than the control at any given time point and did not drop below the 10 % mark within the first four hours after injection.

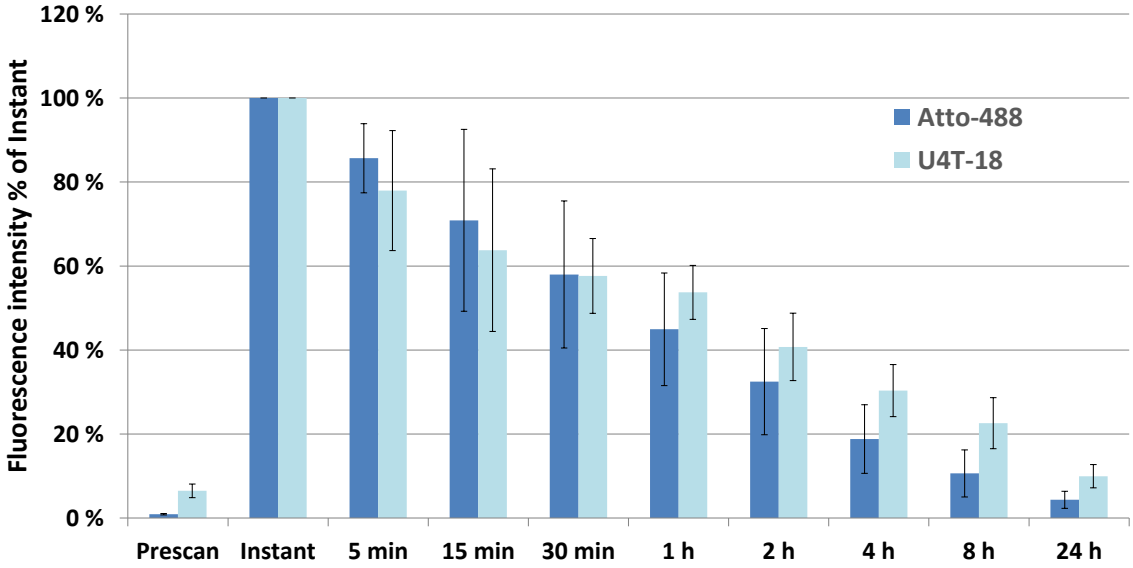

Figure 14 Integrated fluorescence intensity normalized to the instant measurement at different time points after injection of the U4T-18 NPs (light blue) into the vitreous body in ex-vivo porcine eyes (n=6-8), standard deviation added. For comparison the data for the

control Atto-488 is also given (blue). U4T-18 displayed higher mean values at all time points after 15 minutes compared to the control dye indicating proper retention properties.

Also for U4T-18 the obtained data was compared to the instant value that was detected directly after injection (Figure 14).The decrease in fluorescence intensity found for the U4T-18 solution was constant after the instant time point. The measured NP fluorescence stayed below the control the first 30 minutes after injection. For all other time points U4T-18 was found to hold higher values than the control which dropped to 8 % after eight hours whereas the NPs stayed above the 20 % mark.

After evaluating the diffusion properties of two NPs bearing four modified deoxyuracils, three NPs containing six modified nucleotides were evaluated. First, the fluorescence of U6T-12 NPs was investigated, which contained a total of twelve bases of which only 50 % were unmodified. All steps of this process were undertaken as described in in 2.4 and initially normalized to the solution value (Figure 15).

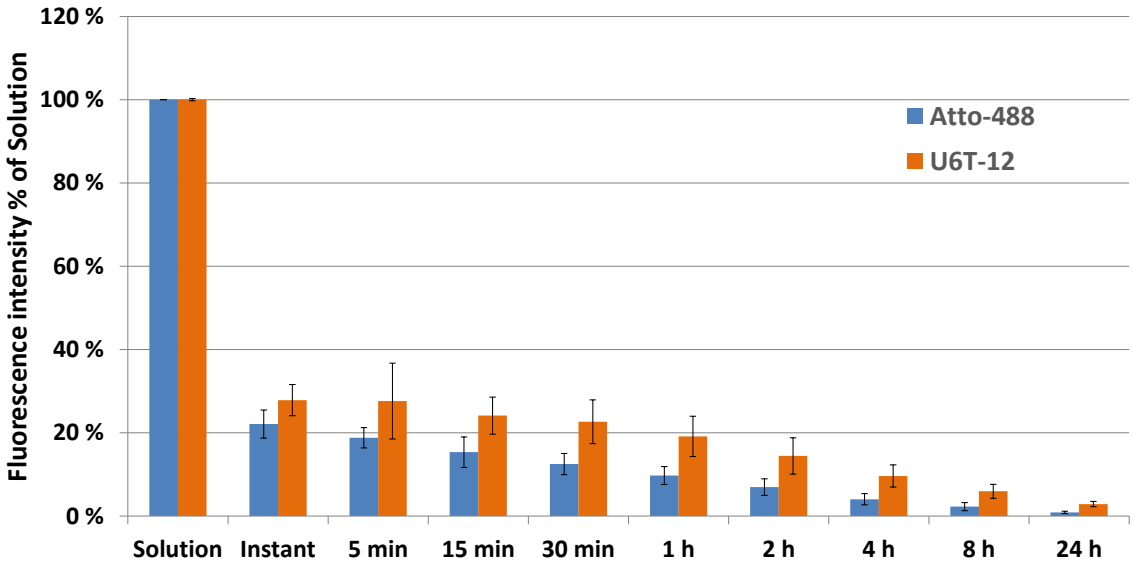

Figure 15 Integrated fluorescence intensity normalized to the solution measurement at different time points after injection of the U6T-12 NPs (orange) into the vitreous body in ex-vivo porcine eyes (n=6-7), standard deviation added. For comparison the data for the control Atto-488 is also given (blue). Directly after injections the values for U6T-12 NPs were slightly lower than the control. Other than that, this NP showed higher mean values at all time points, demonstrating good long-term retention.

All time points showed a higher fluorescence for U6T-12 than for the control. The amount of integrated fluorescence for U6T-12 detected instantly after injection was 28% and remained constant until after the five minutes measurement. A steady decrease followed and after the eight hours measurement the integrated fluorescence dropped below 10 %.

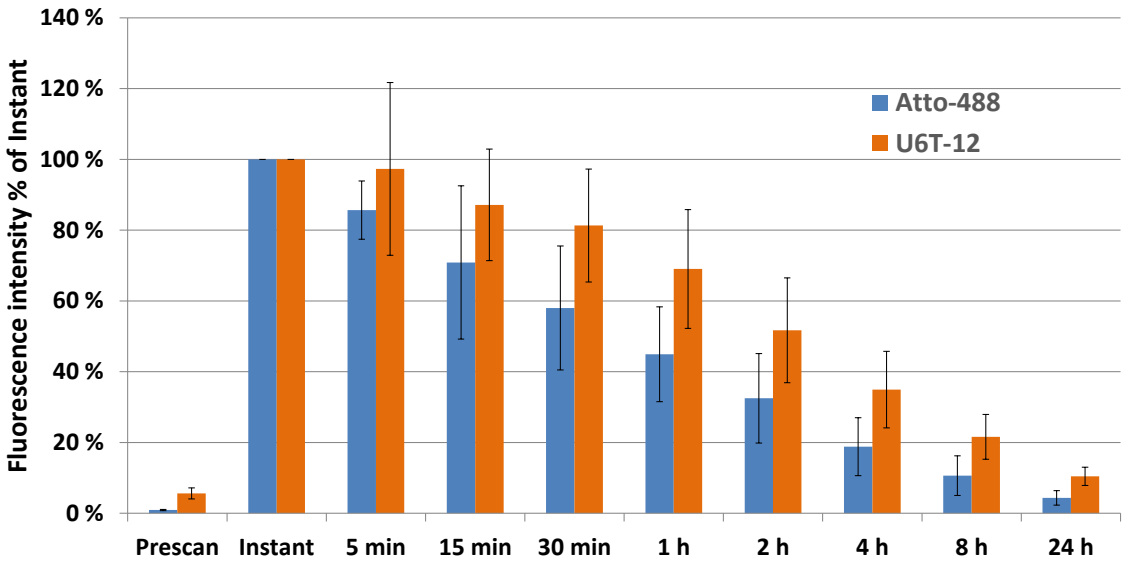

Figure 16 Integrated fluorescence intensity normalized to the instant measurement at different time points after injection of the U6T-12 NPs (orange) into the vitreous body in ex-vivo porcine eyes (n=6-7), standard deviation added. For comparison the data for the control Atto-488 is also given (blue). The fluorescence intensity for U6T-12 was higher than the initial time point at 5 minutes after injection and slowly decreased afterwards, indicating good retention properties.

Afterwards the fluorescence measurements for U6T-12 were normalized to the determined instant value (Figure 15). The fluorescence intensity for the U6T-12 NPs showed a steady decreasing trend with higher values than the control at any given stage. At the instant time point the detected value remained at 97% of the instant measurement. U6T-12 stayed at a remarkably high level above 80% of integrated fluorescence intensity before it dropped to 69% after one hour. Even two hours after injection, the detected intensity remained above 50 % and was found at 52 % of integrated instant fluorescence.

The next NP to be investigated was U6T-18. Similar to U4T-18 it consisted of a total of 18 nucleotides. However, in this case six were modified with an alkyl

chain. The integrated fluorescence intensity was firstly normalized to the solution value (Figure 17).

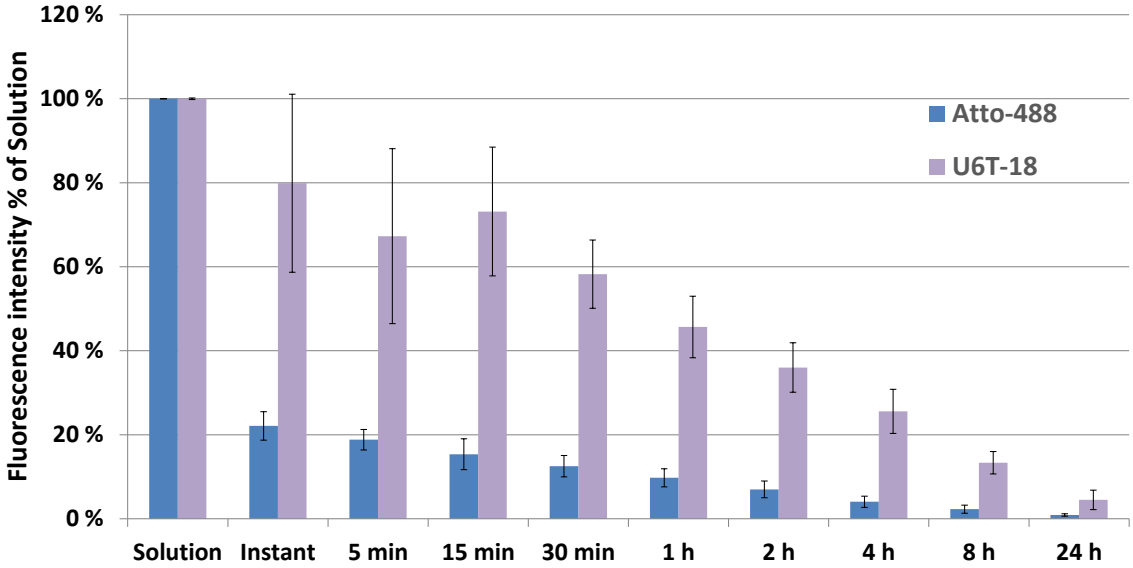

Figure 17 Integrated fluorescence intensity normalized to the solution measurement at different time points after injection of the U6T-18 NPs (purple) into the vitreous body in ex-vivo porcine eyes (n=6), standard deviation added. For comparison the data for the control Atto-488 is also given (blue). The fluorescence intensity of U6T-18 NPs higher than the control dye at all observed time points and almost reaches solution levels. This suggests outstanding retention properties.

Remarkably, the found fluorescence intensities of U6T-18 NPs are the highest ones observed for all solution normalized values of the investigated NPs. The integrated fluorescence intensity of 15 minutes (73%) exceeds the one of five minutes (67%) but stays below the instant value (80%). This value was the highest one found for all NPs. In addition, only the intensity of U6T-18 NPs remained decisively over 20 % at the four hour measurement (26%) due to its slow decrease. Also, it must be noted that for this NPs the relative intensity always stayed above those measured for the control.

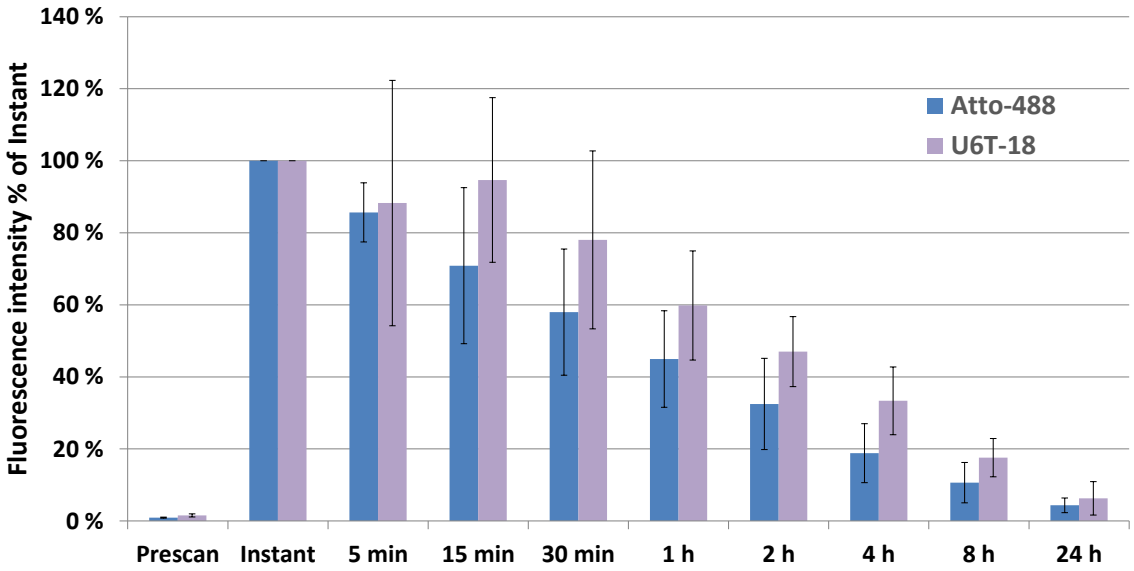

Figure 18 Integrated fluorescence intensity normalized to the instant measurement at different time points after injection of the U6T-18 NPs (purple) into the vitreous body in ex-vivo porcine eyes (n=6), standard deviation added. For comparison the data for the control Atto-488 is also given (blue). The U6T-18 NPs exhibited higher fluorescence at all observed time points compared to the control dye, showing good retention.

As before, the obtained data were also compared to the instant value (Figure 18). Also here the integrated fluorescence intensity of 15 minutes (95%) exceeded the one of five minutes (88%). Afterwards, the fluorescence intensity decreased in a constant manner over time, but always remained at a notably higher level than the control. Two hours after injection, the detected intensity remained just under 50 % of the initial value and was found at 49 %. After four hours it dropped to 33 %.

The longest and last NP to be investigated was U6T-20, containing a total of 20 nucleotides of which six were modified with lipid tails. At first, the integrated values were normalized to the fluorescence intensity of the solution before injecting (Figure 19).

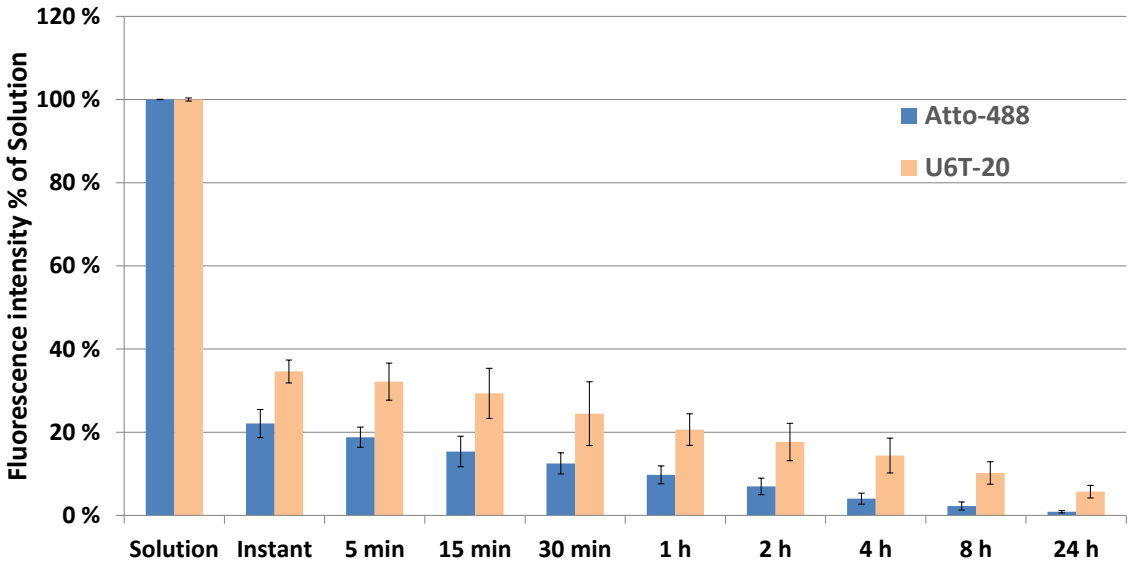

Figure 19 Integrated fluorescence intensity normalized to the solution measurement at different time points after injection of the U6T-20 NPs (beige) into the vitreous body in ex-vivo porcine eyes (n=6), standard deviation added. For comparison the data for the control Atto-488 is also given (blue). The U6T-20 NPs demonstrated higher fluorescence values at all time points when compared to the control dye. This indicates that these NPS possesses efficient retention properties.

Right after injection the amount of U6T-20 (35 %) was notably higher than the control (22 %). This NP showed a similar steady decrease to U4T-18 and remained at higher levels of fluorescence than the control. U6T-20 did not drop below the 10 % mark within the first eight hours after injection.

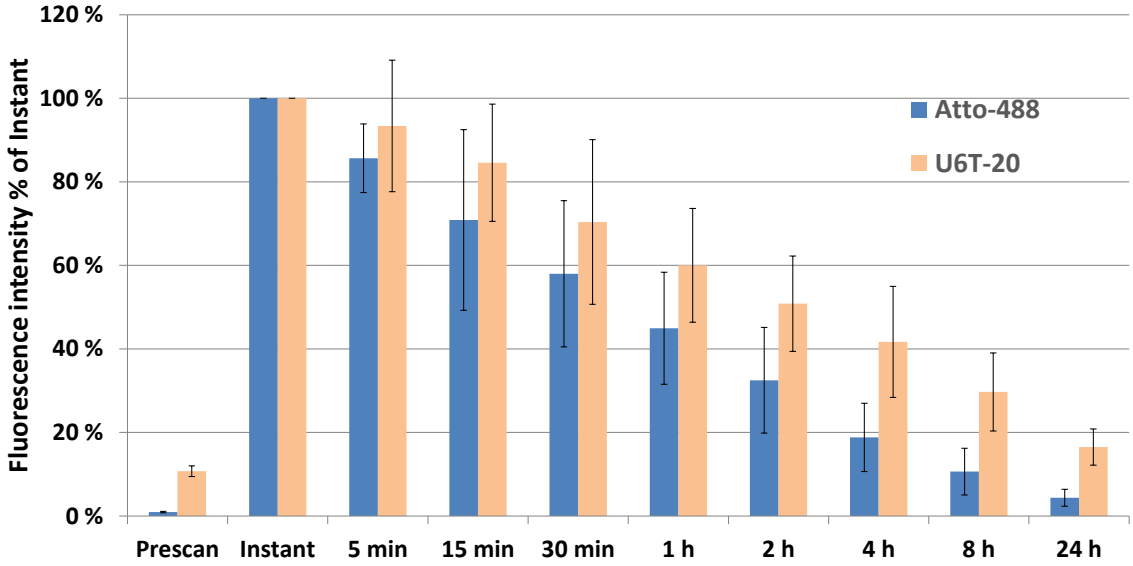

Figure 20 Integrated fluorescence intensity normalized to the instant measurement at different time points after injection of the U6T-20 NPs (beige) into the vitreous body in ex-vivo porcine eyes (n=6), standard deviation added. For comparison the data for the control Atto-488 is also given (blue). The U6T-20 NPs showed a slow decrease of the intensity over time compared to the control dye, implying efficient retention properties.

Also for the last NP the obtained data was normalized to the instant value (Figure 20). The measured intensity of U6T-20 decreased constantly over time after injection. However, after the five minute time point it had only lost 7 % in fluorescence intensity and at 15 minutes it remained at 85 %. While the initial time period doubled from hereon (30 minutes, 1, 2, 4 hours) the value of measured fluorescence intensity decreased by approximately 10% every time. The 24 hour value was the highest one found out of all investigated NPs when normalized to the instant time point (17%).

In the fluorophotometric analysis U4T-12 and U6T-18 showed superior performance in regard to their diffusion and half life time. First of all, when normalized to the instant fluorescence, U4T-12 convinced with high relative values, a strong plateau phase and a late decrease in integrated fluorescence. Secondly U6T-18 displayed one of the highest levels of intensity and a steady decrease over time especially in the solution measurements. These results made U4T-12 and U6T-18 suitable candidates for further experiments in an in-vivo setup.

3.1.2. Examination of adhesion sites and variations in adhesion duration of DNA NPs in an ex-vivo setup

As a next step in the investigation of the use of DNA NPs for drug delivery to the posterior segment the adhesion of these vehicles to ocular tissue has been investigated by fluorescence microscopy. Before introducing the results, a good understanding of the observed structures in the retina is needed. As outlined in the introduction, after DAPI staining the cells can be observed in blue when imaging the sections. For visualization the employed NPs were functionalized with a green fluorescent dye, similar as described in the previous section. A typical example of a NP positive picture after intravitreal injection is given in Figure 21. In the figure the different cell layers that are found in the retina are named and the NPs are clearly visible in green. This allows analysis of their

adhesion sites. As can be seen, the NPs appear as a thin layer of green fluorescence on the GCL of the retina.

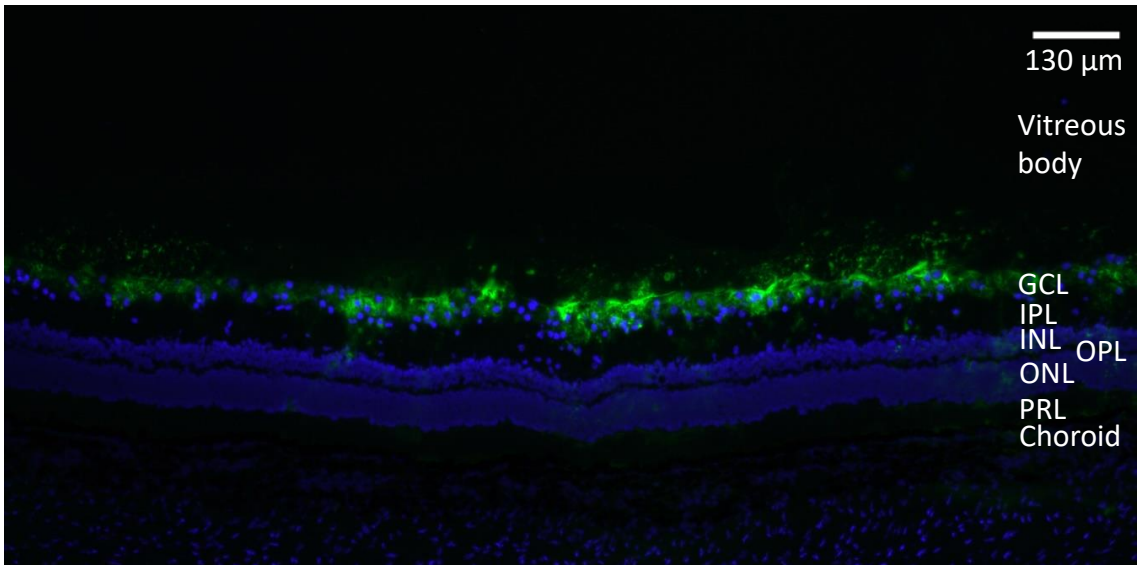

Figure 21 Fluorescent image of the retina of an ex-vivo porcine eye that has been injected with U6T-20 NPs. The designations of the different retinal layers were visualized. Coming from the vitreous body and going out of the eye these layers are: ganglion cell layer (GCL), inner plexiform layer (IPL), inner nuclear layer (INL), outer plexiform layer (ONL), outer nuclear layer (OPL), photoreceptor layer (PRL) and the choroid.

In order to obtain representative pictures for the conditions multiple sections were stained for each eye and several selection criteria were used. One of these naturally included the overall quality of the section and the integrity of the retina. Another important criterion was the inherent fluorescence of the tissue. To gauge the extent of autofluorescence of the observed tissue, a third filter was employed. As no specific staining was performed with a dye for this filter, any fluorescence observed here must have been due to autofluorescence. Samples that exhibited a large amount of autofluorescence were omitted in the evaluation.

First the control dye was injected into the porcine vitreous body in order to prove that any observed adhesion of the NPs to the intraocular tissue is due to their structure. Therefore pig eyes were injected with 40 µL of 20 µM Atto-488 solution. After defined incubation times of 5, 15, 30 minutes, 1 and 2 hours in PBS they were prepared as cryosections and stained with DAPI. The sections were then investigated under the fluorescence microscope (Figure 22).

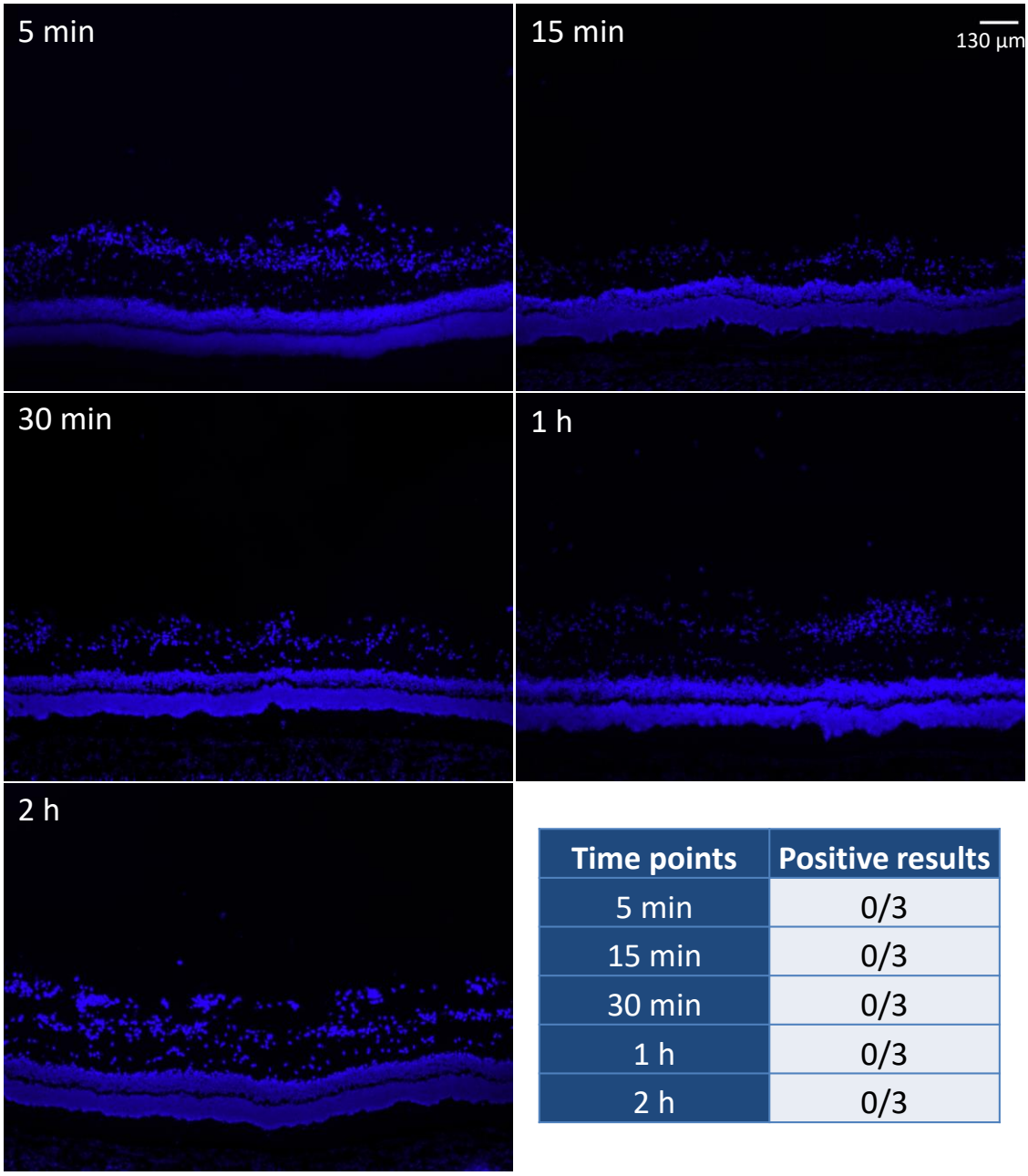

Time points	Positive results
5 min	0/3
15 min	0/3
30 min	0/3
1 h	0/3
2 h	0/3

Figure 22 Representative fluorescent images of retinas of ex-vivo porcine eyes after injection with the Atto-488 control and incubation for designated time points. No signs of fluorescence were observed. Bottom right: table with number of control positive eyes at different time points, confirming the absence of the control dye.

As expected, the eyes injected with the control did not show any positive results regarding adhesion of the fluorescent dye towards the retinal tissue in any of the analyzed time points. Also, in no other tissues or the vitreous body itself fluorescence was found in any of the cryosections. Hence, it can be concluded that the small molecular dye did not exhibit any affinity to the retinal tissue.

In the next step to investigate the affinity of the NPs to ocular structures, the same experiment was performed with different NP vehicles. First, U4T-12 was injected in ex-vivo porcine eyes as explained in 2.4.4 and the adhesion was analyzed by fluorescence imaging (Figure 23).

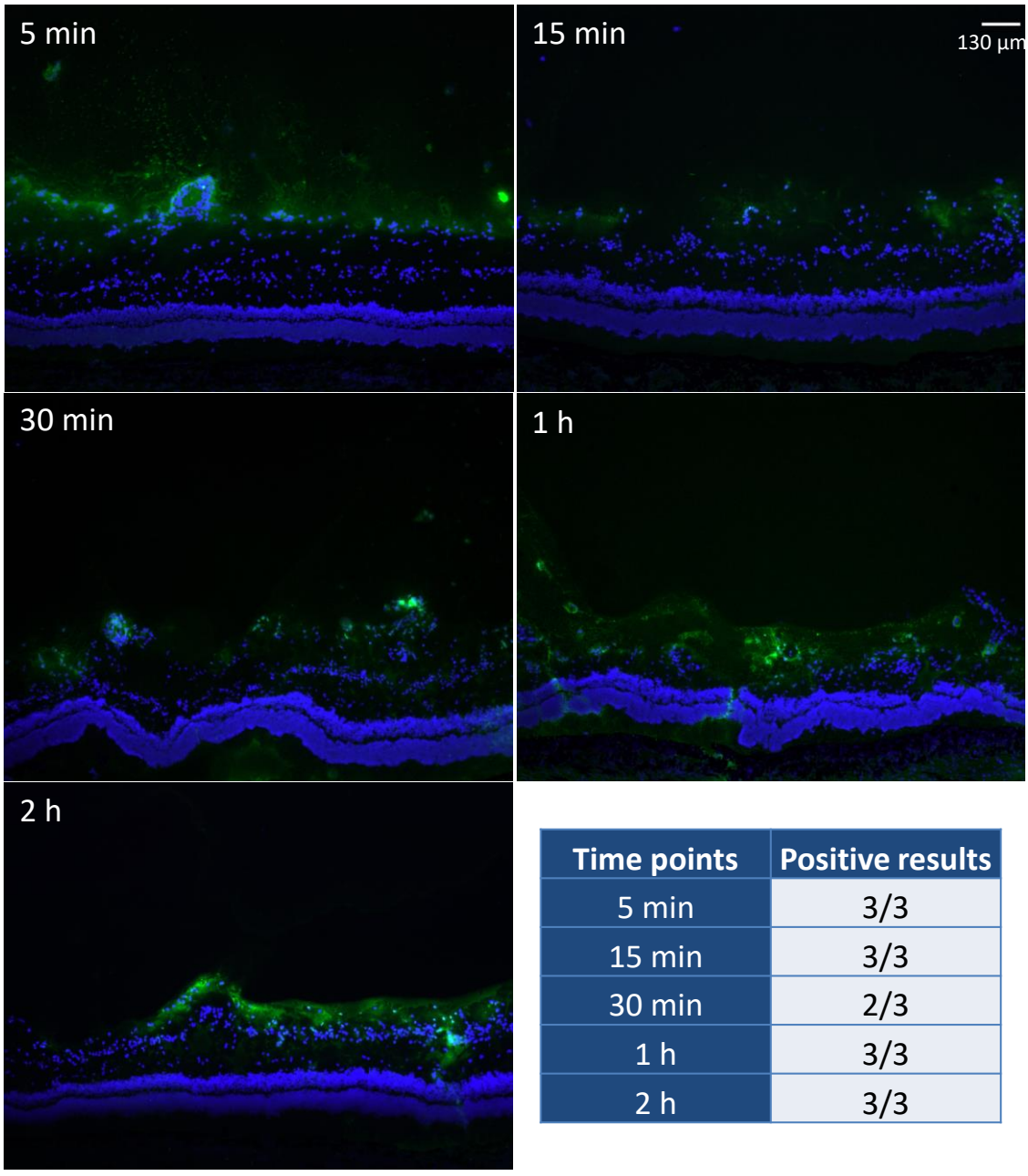

Time points	Positive results
5 min	3/3
15 min	3/3
30 min	2/3
1 h	3/3
2 h	3/3

Figure 23 Representative fluorescent images of retina of ex-vivo porcine eyes, injected with U4T-12 NPs and incubated for designated time points. Bottom right: table with number of control positive eyes at different time points. The amounts of displayed NPs in the pictures and the results from the table indicated excellent adhesion towards the retinal tissues.

The U4T-12 NPs can clearly be identified as their green fluorescence is highly visible in the obtained images. The NPs formed a considerable layer on the inner parts of the retina, mainly on the inside of the GCL, on the border to the vitreous body. At five minutes post injection, NPs could already be observed in the cellular structures. The green fluorescence was mainly found surrounding the DAPI stained nuclei on those cells which were facing towards the vitreous body. The total depth of the layer of NPs found in the vitreous was approximately 300 micrometer (µm). Strikingly, NPs could be observed that were not directly bound to the cells, but rather located in the vitreous body itself. This has not been the case for the control dye. Also, the NPs were fully covering the retina displayed on this picture with the most pronounced adhesion site in the region of the outer GCL nuclei.

For later time points a more distinct line of the fluorescent NPs was visible with a dense pattern of the NPs located at the GCL. Additionally, at the later time points the green fluorescence was found in more basal parts of the retina. This was very well visible at one and two hours post injection. For example, at the two hours' time point high coverage of the retina was found with an average penetration depth of the NP layer of around 120 µm. It was obvious that the NPs reached below the GCL and had contact with the INL.

In almost all investigated eyes the NPs were found to adhere to the cellular layers of the retina. Only one eye was found 30 minutes after injection where the NPs were not detected. However, later time points again showed good adhesion to the retinal structures again.

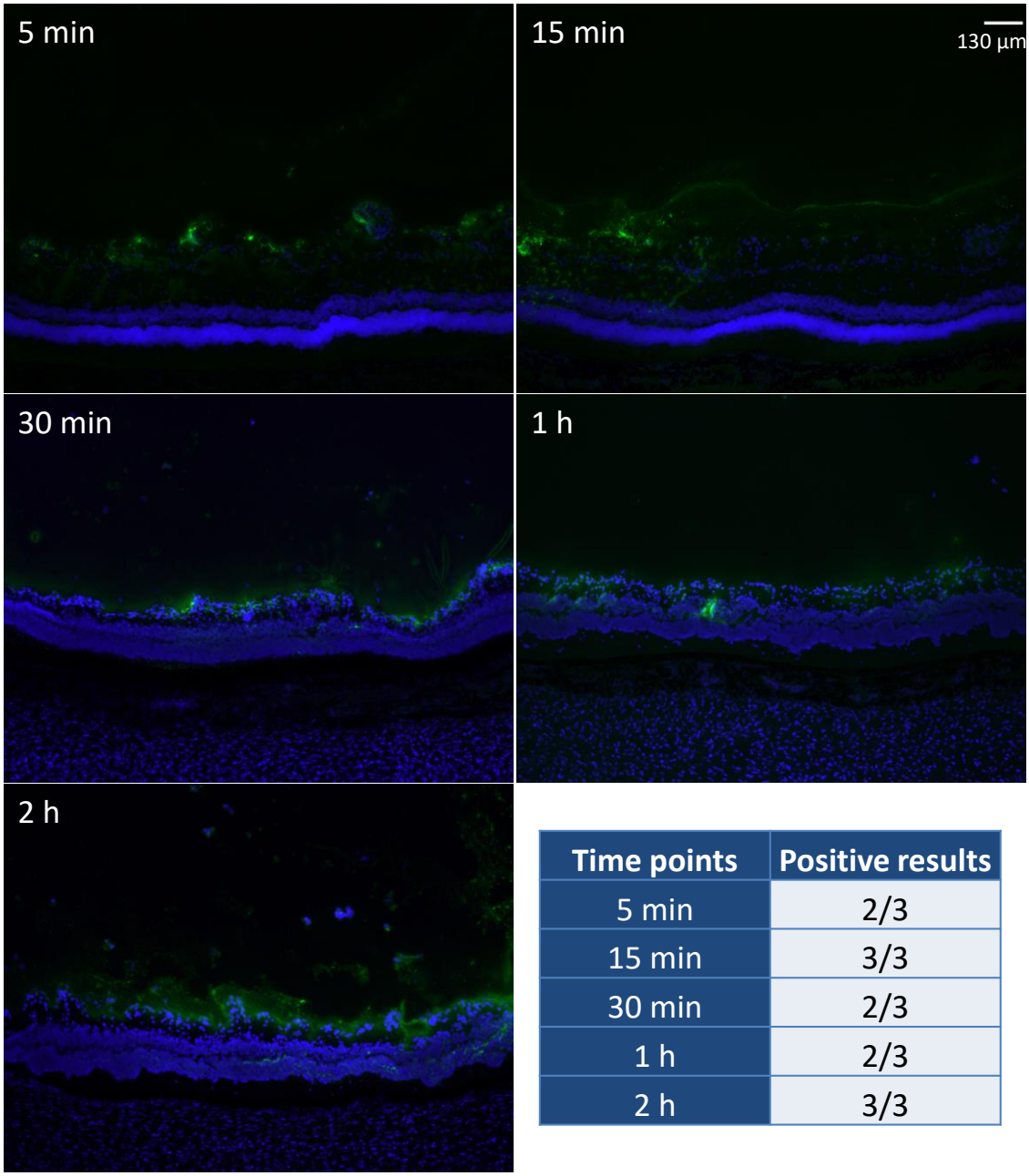

Time points	Positive results
5 min	2/3
15 min	3/3
30 min	2/3
1 h	2/3
2 h	3/3

Figure 24 Representative fluorescent images of retina of ex-vivo porcine eyes, injected with U4T-18 NPs and incubated for designated time points. Bottom right: table with number of control positive eyes at different time points. The clearly visible NPs in the pictures and the results from the table indicated good adhesion towards the different tissues in the retina.

Similar to the fluorophotometric study, the U4T-18 NPs were injected next (Figure 24). U4T-18 covered the entire width of the retina shown in the five minutes micrograph. However, the fluorescence observed was not as strong as found for U4T-12 and mainly formed by multiple spots. These were connected by smaller lines of NPs adhesion to the retina that penetrated less than 30 µm deep. With

longer incubation periods, the presence of the NPs appeared to migrate from around the GCL to the more basal structures. Strikingly, the layer of fluorescence formed broad lateral borders in the two hours picture. However, compared to the U4T-12 NPs, these vehicles displayed a fainter fluorescence. Also, the mean depth of the found green stratum seemed lower than for the first investigated NP.

At three out of five time points 2/3 injected eyes were NP positive. The time points of two hours and 15 minutes displayed the only 100% positive findings which were two less than in the U4T-12 analysis. This underlined the trend observed in the images, regarding the characteristics of the found fluorescence.

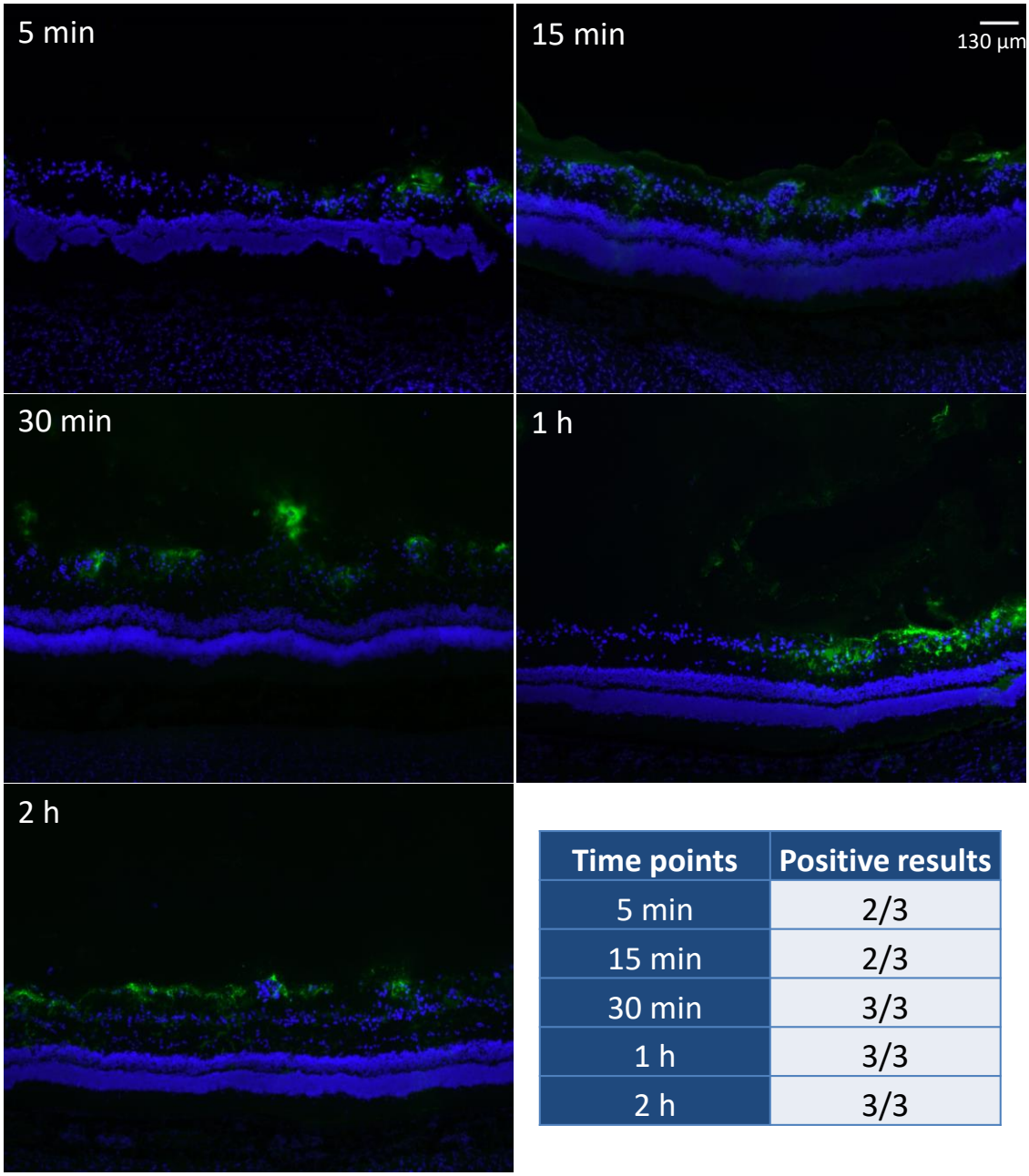

Time points	Positive results
5 min	2/3
15 min	2/3
30 min	3/3
1 h	3/3
2 h	3/3

Figure 25 Representative fluorescent images of retina of ex-vivo porcine eyes, injected with U6T-12 NPs and incubated for designated time points. Bottom right: table with number of control positive eyes at different time points. The observed NPs in the pictures combined with the positive results from the table showed the outstanding adhesion of this NP towards the retinal tissues.

As first NP with six modified nucleotides, U6T-12 was investigated (Figure 25).

The injected U6T-12 NPs demonstrated positive findings in all given time points that were investigated. They were especially located in the GCL, a characteristic which has been observed also for the previous NPs. However, in contrast to the previous NPs, U6T-12 showed less intense fluorescence and also covered less

area. For example, in the 5 minutes image only one location with NPs could be identified that exhibited a high local intensity and a diameter of approximately 100 µm. After 15 minutes of incubation the green fluorescing NPs covered the entire inside of the GCL but the lining was not as intense as for the earlier investigated NPs and below 100 µm in depth. Unlike those early time points, the ones from 30 minutes and onwards showed stronger fluorescence intensities over almost the entire GCL. After 30 minutes of incubation, six sites of NPs partially covered the GCL, which displayed local gaps. Those aggregations had a maximum diameter of 130 µm. After one hour the NPs were covering approximately 50 % of the retina and were also localized in the vitreous body. Despite forming a ribbon shaped pattern throughout the picture, the NPs were still locally stronger concentrated and did not distribute evenly over the retina. After two hours of incubation the ribbon like structures were not apparent but the NP covering on the GCL was distinct and to be found on the entire inside of the GCL. In summary, U6T-12 showed rather weak fluorescence with incomplete coverings in the majority of the given images. A total of 13/15 positive results were found whereas for the incubation times of 5 and 15 minutes only 2/3 eyes were positive.

Similar as for the NPs U4T-12 and U4T-18, also NPs having six lipid-modified bases and more conventional nucleotides were investigated. Therefore, first U6T-18 was analyzed in regard to adherence towards the retinal tissues (Figure 26). It should be mentioned here that for the fluorophotometric results, the U6T-18 NPs showed promising results regarding their retention in the vitreous body. Preparation and injection were undertaken as described in 2.4.4.

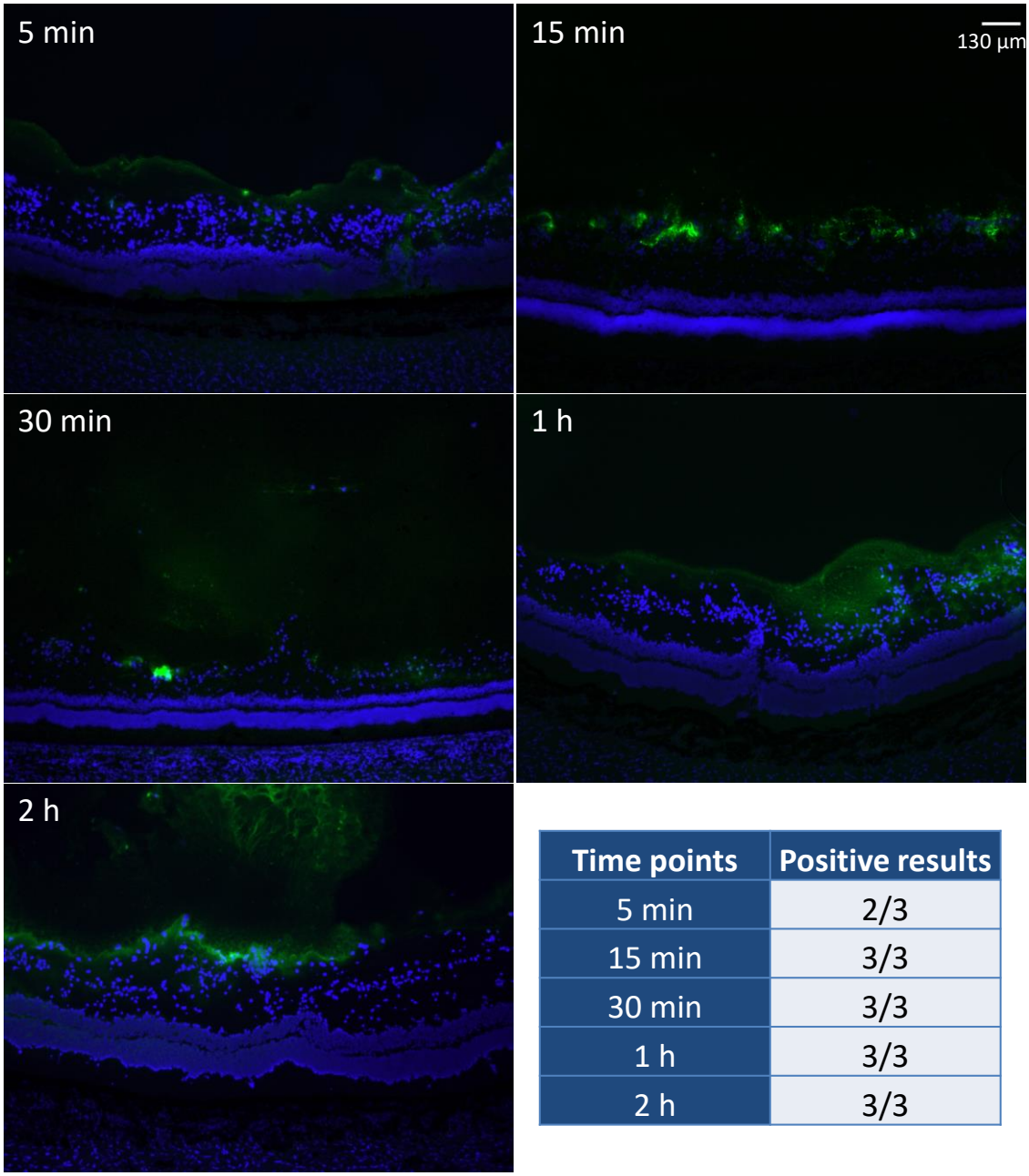

Time points	Positive results
5 min	2/3
15 min	3/3
30 min	3/3
1 h	3/3
2 h	3/3

Figure 26 Representative fluorescent images of retina of ex-vivo porcine eyes, injected with U6T-18 NPs and incubated for designated time points. Bottom right: table with number of control positive eyes at different time points. The amounts of displayed NPs in the images and the results from the table indicated excellent adhesion towards the tissues of the retina.

In the U6T-18 series the fluorescently labelled NPs were found covering the retina throughout the incubation time points with predominant adherence on the inside of the GCL. Already five minutes after injection the fluorescent NPs were covering the entire GCL, albeit with a lower intensity than found for the U6T-12 NPs. In contrast, no gaps were observed. In the 15 minutes image the NPs were found

as multiple spots sized below 80 µm in diameter but displaying a strong intensity. The significant difference to previously investigated NPs was the presence of NP fluorescence in the vitreous body, even after longer incubation periods. In the 30 minutes picture the NPs present in the vitreous appeared as of weak intensity with two highly intense but local accumulations of less than 100 µm in the GCL. After one hour of incubation the coating was much more intensive with an average depth of 80 µm and covering approximately 90 % of the retina. In the last time point of this series the retention properties of U6T-18 became particularly obvious. The imaged fluorescence formed an accumulation which ran in strings through the network of the vitreous and measured over 200 µm. The GCL was coated in a distinct line of NPs over its entire width. Recapitulating the findings for U6T-18 one must note the predominance of NP which was still to be found in the vitreous body after two hours, stressing the retention qualities of this NP. However, U6T-18 also formed a constant coating displaying rather intense fluorescence on the GCL and therefore appeared more favorable in regard to adherence properties than for example U4T-18 or U6T-12 NPs.

These findings are also in good agreement with the observed results found in the fluorophotometric measurements. Additionally, the summarizing table underlined this with 14/15 eyes found to be positive. This was the same amount of positive results that had also been found for the U4T-12 NPs.

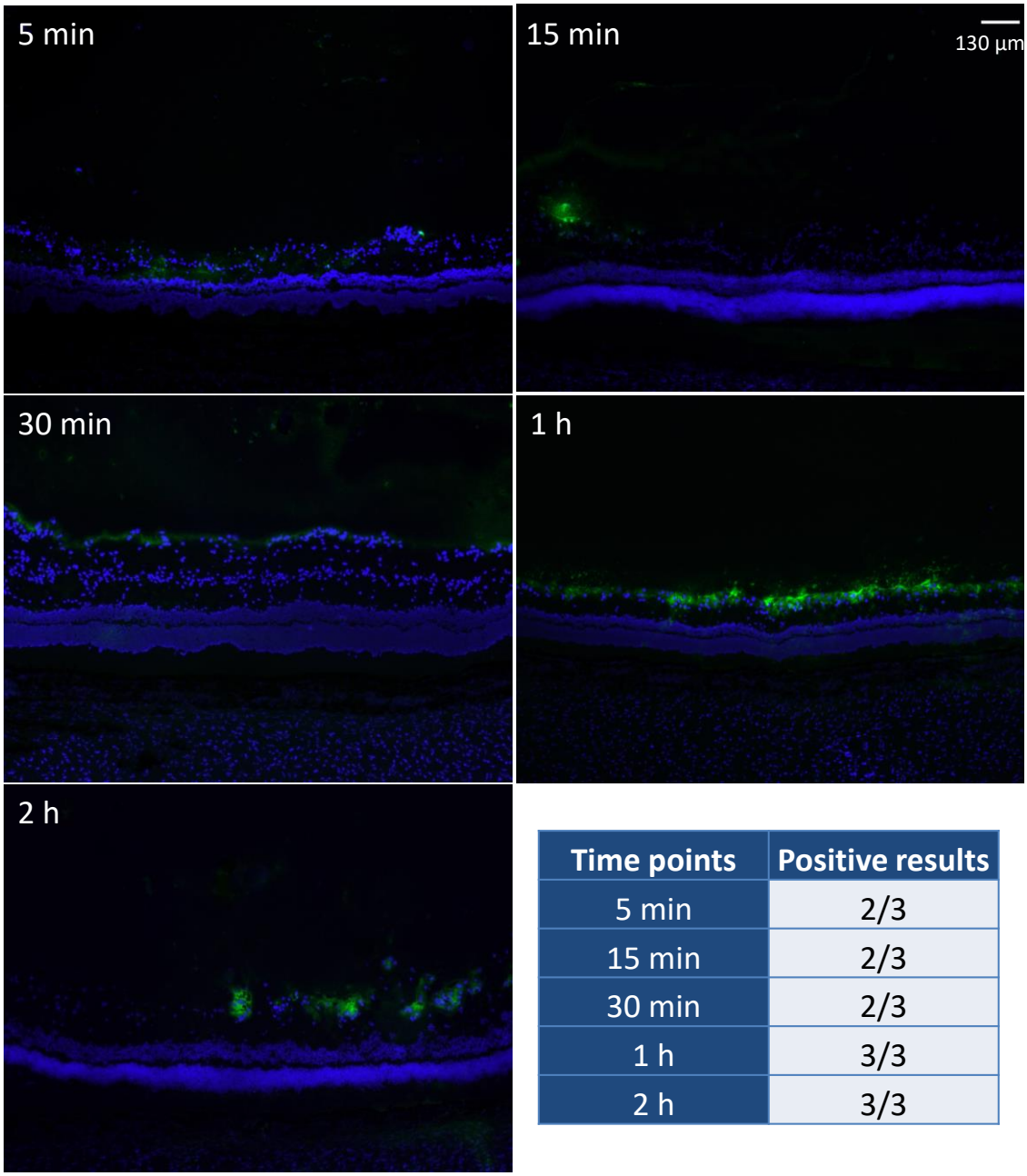

Time points	Positive results
5 min	2/3
15 min	2/3
30 min	2/3
1 h	3/3
2 h	3/3

Figure 27 Representative fluorescent images of retina of ex-vivo porcine eyes, injected with U6T-20 NPs and incubated for designated time points. Bottom right: table with number of control positive eyes at different time points. The NPs in the pictures and the results from the table indicated effective adhesion towards the retina.

The U6T-20 NPs were last investigated for adherence and distribution in the ocular tissue. Porcine eyes were prepared and injected as described in 2.4.4.

For U6T-20, fluorescence was found in all given time points but in lower intensity compared to previously investigated NPs. After five minutes just three fluorescent spots could be identified in the GCL. After 15 minutes the fluorescence became

stronger but was mainly found as a single spot of approximately 130 µm diameters. At 30 minutes of incubation the fluorescence began to form a uniform layer on the inside of the GCL, but exhibited a faint fluorescence compared to previously found results. In contrast, the one hour result displayed a much stronger and dense coating, which was not comparable to the other findings for U6T-20. Here, the entire GCL was covered by a green stratum of NPs. In the last image of the series the fluorescence was concentrated at four locations with a width and depth below 100 µm. In comparison to the fluorescence find after one hour, the figure at two hours suggested a lower covering of the GCL. In summary, this last NP appeared less promising than the previously investigated NPs. This was primarily due to weak intensity of fluorescence and non-existent coverage in the majority of the eyes.

The table supported what has been observed in the images. With only 12/15 the positive findings in the eyes injected with U6T-20 were as frequent as in the ones injected with U4T-18 solution. Strikingly, the early time points (5, 15 and 30 minutes) lacked positive results. Those were also the ones where the fluorescence in the images appeared weaker.

The fluorescence imaging of U4T-12 and U6T-18 showed excellent coverage of NPs in regard to the retinal tissue. Both were found to be the only NPs out of this ex-vivo setup displaying 14/15 positive eyes. Indicating superior performance, U4T-12 and U6T-18 NPs have been chosen for further in-vivo experiments.

3.2. Intravitreal injection of lipid-modified DNA NPs into in-vivo rat eyes

After exploring the diffusion through the vitreous body and the adhesion potential of the DNA-NPs, in-vivo injections were administered using the two best performing NPs selected from the ex-vivo investigations. To this extent one NP from the group containing four lipid modified nucleotides and one from the group containing six lipid modified nucleotides were selected. Here U4T-12 and U6T-

18 were chosen due to their prolonged retention after injection and excellent adhesion to the ocular structures. The in-vivo experiments were performed by injecting the NPs in rat eyes. Again, the free Atto-488 served as control. Similar to the ex-vivo part, the retention and adhesion was first investigated by ocular fluorophotometry and afterwards through fluorescence microscopy.

3.2.1. Examination of diffusion of DNA NPs within an in-vivo vitreous body

In order to analyze the diffusion behavior of the NPs the in-vivo rat eyes were scanned using a fluorophotometer. However, unlike previously performed, the graphs were not integrated. This because the in-vivo rat eye model made the implementation of a constant measurement axis over several days impossible. As a result, no reliable data could be obtained from a single animal over several days. Therefore it was decided to select representative scans of the injected Atto-488 control solution, U4T-12 and U6T-18 NPS in order to highlight the different diffusion manners of the control solution versus NPs.

The graph presented in Figure 28 gives an indication of the diffusion of the small molecular control in the vitreous and aqueous humor of the rat eye. The autofluorescence observed in the eye is illustrated by the “pre injection” graph which was obtained directly before injection. Several characteristic local peaks could be found which indicate the position of the retina and the cornea. For orientation purposes the approximate position of retina and cornea were highlighted in the figure. A smaller peak can be found between these two which may be observed due to auto fluorescence in the area of iris and lens.

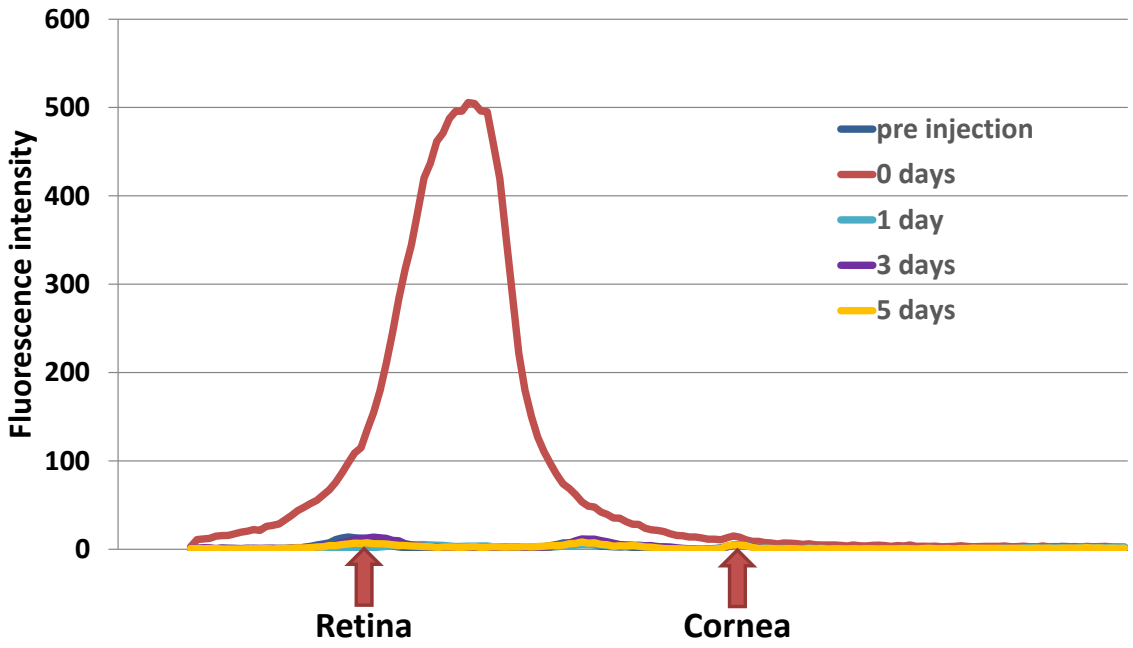

Figure 28 Fluorescence intensity (y axis) measured at different time points after intravitreal injection of Atto-488 along the optical axis (x axis) in an in-vivo rat eye. The fast decrease in intensity over time indicated rapid diffusion of the dye into the vitreous body.

As expected, a strong peak was detected right after injection of the control solution. The position of this peak indicated the location of the maximum concentration of the dye inside the vitreous. All the following measurements did not differ discernible from the pre injection measurement, indicating rapid clearance of the control dye out of the optical axis of the eye. This was also in good agreement with the results observed earlier in the ex-vivo experiments.

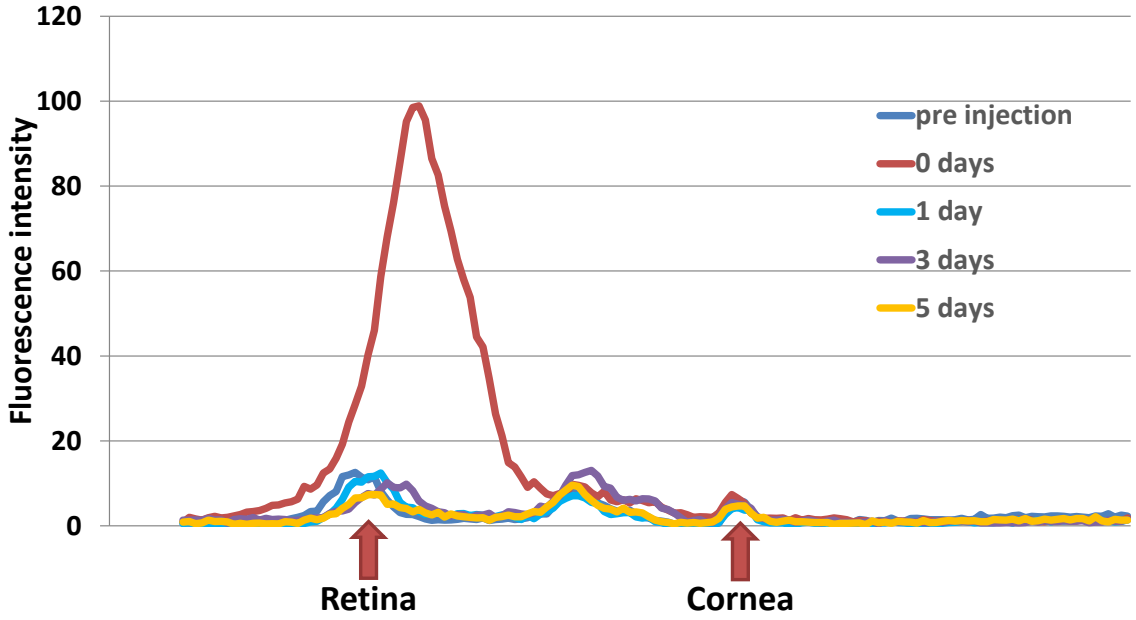

Figure 29 Fluorescence intensity (y axis) measured at different time points after intravitreal injection of U4T-12 NPs along the optical axis (x axis) in an in-vivo rat eye. The stark decrease in intensity on the first day can presumably be explained by difficulties in aligning the measured eye with the fluorophotometer.

Next the diffusion characteristics for the intravitreally injected U4T-12 NPs are investigated) (Figure 29). Compared to the detected fluorescence found for Atto-488, the displayed figure indicated approximately one fifth of the intensity for the U4T-12 “0 days” measurement. This lower value can be explained by the conjugation of the dye to the complementary DNA, as was described in section 3.1.1. The position of the peak was similar to the one previously observed for the control in the vitreous. However, measurements for the later time points did not display any positive peaks exceeding the levels of fluorescence found in the eye before injection. This finding was most likely due to changes in positioning of the eye between measurements and hence related to problems in aligning the optical axis of the eye to the optical axis of the fluorophorometer.

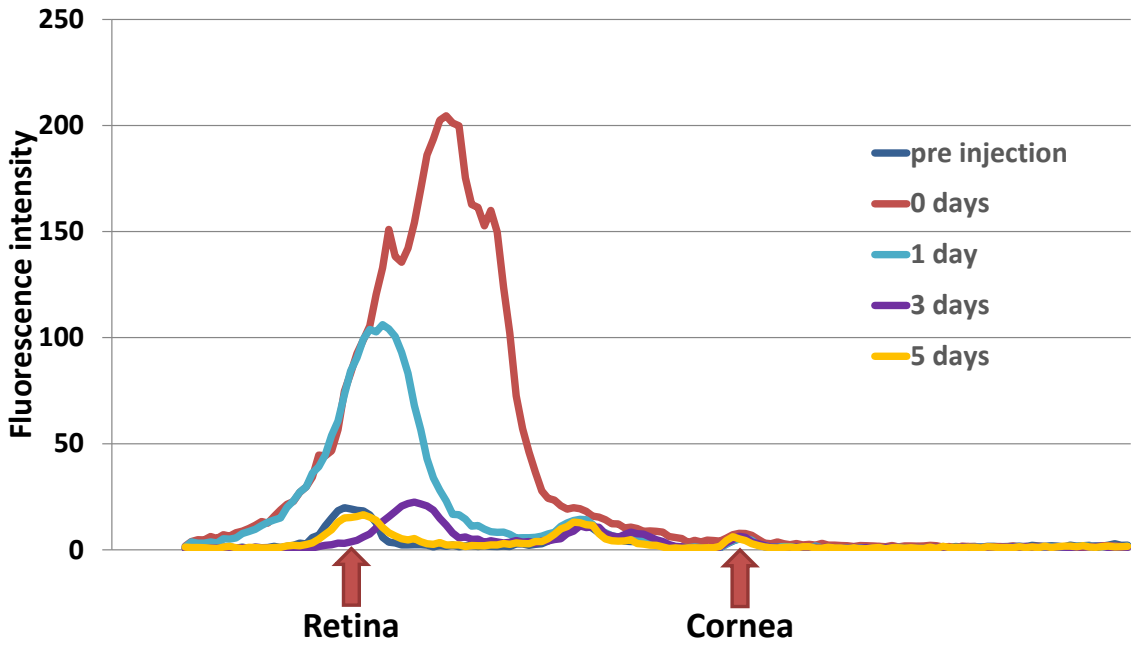

Figure 30 Fluorescence intensity (y axis) measured at different time points after intravitreal injection of U6T-18 NPs along the optical axis (x axis) in an in-vivo rat eye. A drop in the intensity over time was observed, which stressed the retention properties of the NPs.

In Figure 30 the diffusion characteristics for the intravitreally injected U6T-18 NP are presented. As can be seen in the figure above, the detected fluorescence right after injection of the U6T-18 showed a different profile both in height and shape of the peak when compared to the control. The found fluorescence intensity was less than half the amount of Atto-488, which again could be attributed to the conjugation of the dye to the complementary DNA. Secondly the main peak exhibited shoulder peaks on both sides. Nevertheless, the location of the peak was the same as the “0 days” peak found for Atto-488. Remarkably, one day after injection the peak had changed position and intensity. The peak height was half of the original amount and it had relocated more towards the retina. After three days a slightly higher fluorescence was found than before injection. Here the observed peak had shifted slightly towards the cornea. This observation presumably was due to aligning problems of the rat eye with the measured optical axis. Finally, five days after injection no difference to the initial state could be detected.

After confirming the prolonged presence of at least one of the NPs in the intraocular space, their adherence to the ocular structures was investigated by fluorescence microscopy.

3.2.2. Examination of adhesion sites and variations in adhesion duration of DNA NPs in an in-vivo setup

In a similar fashion as in the ex-vivo experiments, the control was first investigated. Rats were injected with 10 µL of the Atto-488 control (20 µM) into the vitreous. The rats were sacrificed after ½, 1, 3 or 5 days. The eyes were enucleated, frozen and prepared as cryosections before performing nucleus staining with DAPI. Fluorescence imaging was used in order to define the adhesion sites and the presence of the control (Figure 31).

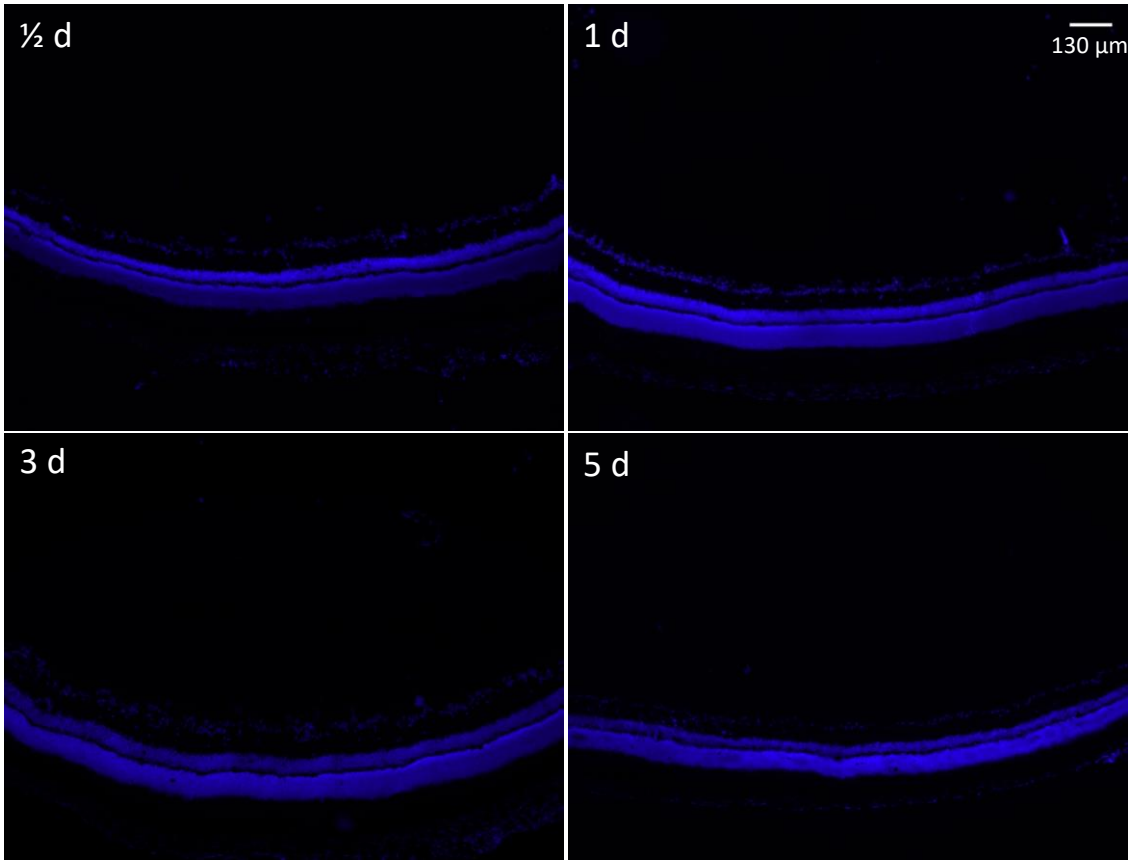

Time points (d)	Positive results
½	0/6
1	0/6
3	0/6
5	0/6

Figure 31 Representative fluorescent images of the retina of rat eyes injected with Atto-488 at different time points. Bottom: table of positive results found in the eyes at different time points. In agreement with earlier experiments, no adhesion of Atto-488 towards the retina was found.

As expected, the eyes injected with the control were found to be negative in all investigated time points regarding the adhesion of the fluorescent dye towards the retinal tissue (Figure 31). Also no fluorescence was found in the vitreous body of any the analyzed eyes or in any of the prepared cryosections. It can be concluded that the small molecular dye did not exhibit any affinity to the retinal tissue, as was already observed in the ex-vivo experiments.

After confirming that the control dye did not exhibit any affinity to the ocular structures, the adhesion behavior of the lipid-modified DNA NPs could be

investigated. First U4T-12 NPs were injected by administration of 10 µL of 20 µM solution into the vitreous body. Afterwards the rats were sacrificed at the same defined time points and processed as described previously (Figure 32).

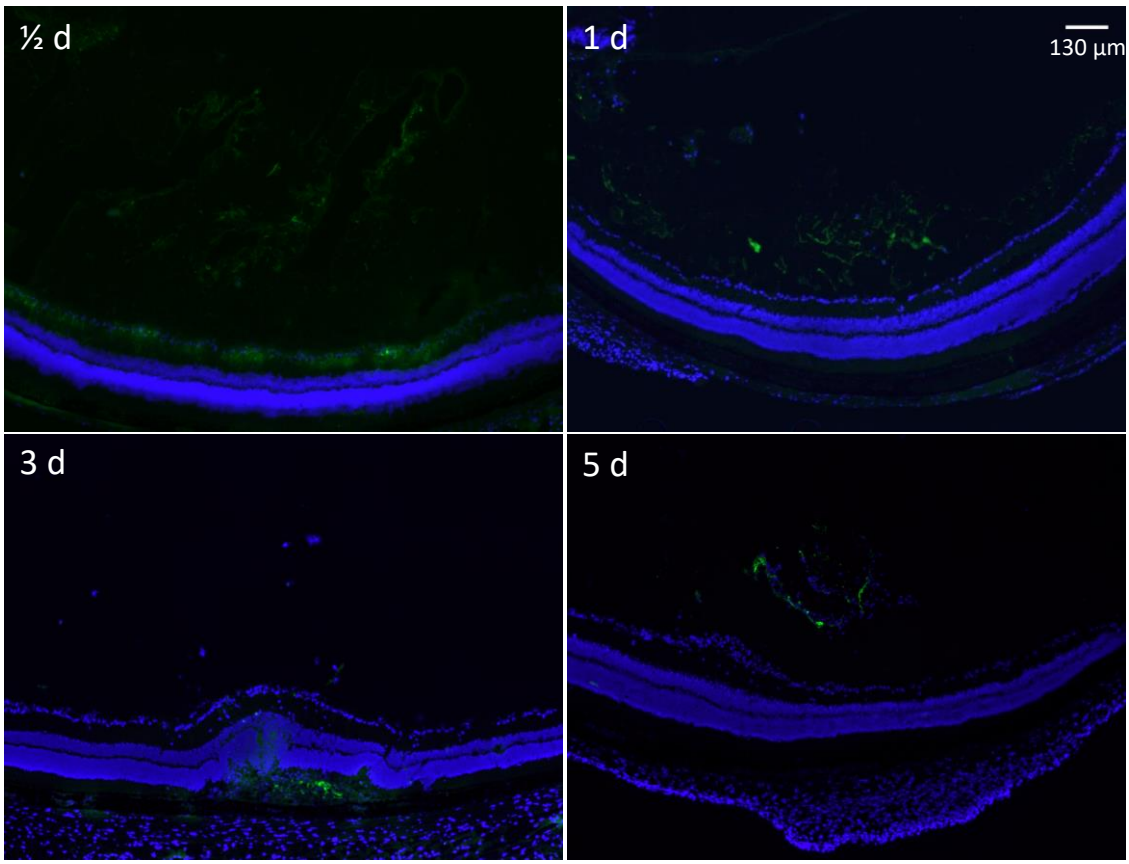

Time points (d)	Positive results
½	5/6
1	4/6
3	3/6
5	1/6

Figure 32 Representative fluorescent images of the retina of rat eyes injected with U4T-12 at different time points. Bottom: table of positive results found in the eyes at different time points. The pictures and the table displayed excellent adhesion of U4T-12 towards the retinal tissues and their retention in this matrix.

Already half a day after injection the U4T-12 NPs showed a strong presence in the vitreous and exhibited a thick layer of NP on the inside of the retina. The fluorescent NPs in the vitreous body showed filamentous arrangements, which represented the network structure of the vitreous. The fluorescing stratum on the retina itself was mainly located around the nuclei of the entire GCL, measuring

approximately 100 µm in dept. At one day post injection, the NPs were mostly located 50 µm inside from the retina in the vitreous body. However, no layer of fluorescence was found in the GCL. Instead, the NPs formed a reticular structure exhibiting a high fluorescence, indicating high local concentrations. At the widest location it measured approximately 200 µm in depth. Also, in the majority of the intravitreal space the presence of NPs could be observed. In the picture taken three days after NP application the injection site could be seen. At this location a couple of cells had been dislocated into the vitreous and the injection canal was partially still observable. Noticeably the majority of the pictured fluorescence was to be found outside the ONL approximately at the position of the injection site. A depot of NPs of approximately 300 µm wide and 130 µm deep had accumulated here. Signs of fluorescing NPs were stretching out into the INL, characterized by a dense layer of nuclei. The fluorescence findings at this three days' time point were not as area-wide as the ones before. Additionally, they were limited to the site of injection and no NPs were found in the GCL. In the five days image, a number of cells were observed in the vitreous, about 200 µm from the retina. They were surrounded by fine isolated fibers of NP. Outside of this location no presence of NPs was obvious. The enveloped fluorescing molecules appeared to form a thin layer on the surfaces of the cells.

In summary, half a day after injection the NPs formed an intensive coating with an average depth of 100 µm on the inside of the retina. After one day however no coating was present but filamentous structures formed an aggregate of locally 200 µm in diameter just outside of the retinal tissue in the vitreous body stretching over 2/3 of the displayed width. Afterwards, NPs were only displayed outside the ONL at the injection site (three days) or encapsulated by dislocated cells in the vitreous (five days). The table underlined the tendency already indicated by the pictures. After half a day 5/6 rat eyes showed positive findings. After day one only 4/6 could be identified as positive. After three days this decreased to only half of the analyzed samples showed presence of fluorescence and only 1/6 eyes was showing NPs under the fluorescence microscope five days post injection.

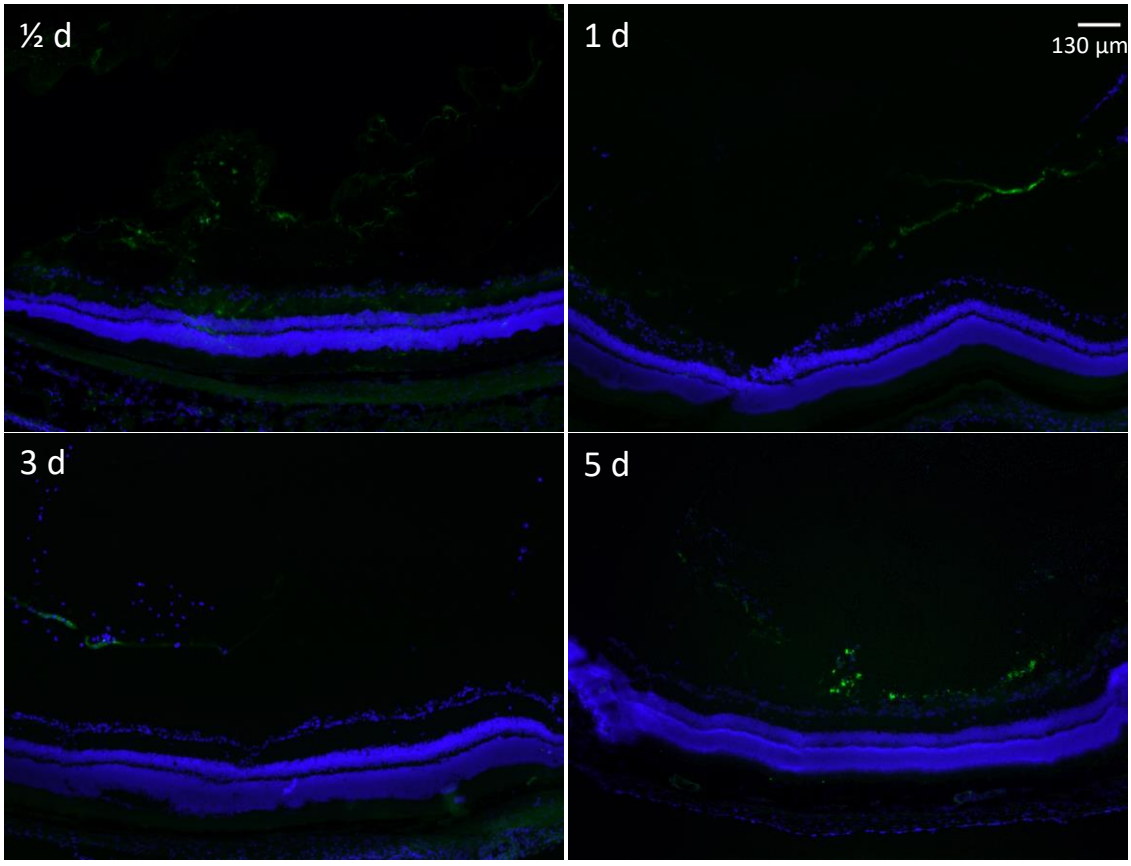

Time points (d)	Positive results
½	5/6
1	4/6
3	4/6
5	1/6

Figure 33 Representative fluorescent images of the retina of rat eyes injected with U6T-18 at different time points. Bottom: table of positive results found in the eyes at different time points. The pictures and the table exemplify the outstanding adhesion and retention of U6T-18 towards the retinal tissues.

With six modified bases, U6T-18 was the second NP investigated in an in-vivo setup (Figure 33). The experiment was performed as described for U4T-12.

The U6T-18 NPs showed a lot of similarities in the half day time point to the one of U4T-12. The filamentous arrangements in the vitreous appeared to be fainter but were also arranged in a reticular pattern. The faint formation surrounding these filaments was less bright in this picture, but still visible. The most remarkable difference was the NP stratum on the GCL, which was nowhere near as strong as for U4T-12. A couple of green spots indicated the presence of NPs

between the GCL and the INL. Here, fluorescence was present in the inward tissue from the retina on in the entire width of the displayed picture. The image obtained after one day showed a definable line of NP originating from the retina and continuing inwards into the vitreous body. However, no extensive diffusion from the vitreous toward the retina was visible. On the left side of the picture the NPs made contact with the retina in the GCL. At three days after injection, a line of NPs could be detected similar in appearance to the previous time point and measuring around 500 µm in length. The fluorescing NPs were less prominent than before and attached to dislocated cells in the vitreous. These cells were presumably disrupted due to the injection. Remarkably, in the image of five days, a thin layer of NPs was again established, covering approximately 1/3 of the displayed retina. The NPs were located towards the inside of the eye on the GCL. Local spots of comparatively strong fluorescence, but mostly less than 10 µm diameter were mainly in line with the described covering of NPs. One noticeable aggregation of NPs of 200 µm in the center of the image represented the thickest part of the observed stratum. Faint reticular filaments were visible in the upper left quadrant, similar to those displayed in the pictures of the early time points.

All in all U6T-18 displayed a consistent location of NPs in the GCL with dominant presence of filamentous structures of NPs in the vitreous for the half day time point. The one and three day images showed a definable line of green NPs spreading out parallel to the retina with mostly no contact to the different retinal layers. Remarkably, in the image of five days a covering was again visible, stretching out approximately over 1/3 of the displayed retina, incorporating spots of strong fluorescence of approximately 10 µm in size.

A declining trend in occurrence of positive findings was obvious (Figure 33). U6T-18 NPs were detected in 5/6 eyes after half a day and 4/6 positive after one and three days. Only 1/6 eyes was found to be positive five days after injection.

3.3. Injection of lipid-modified DNA NPs into periocular tissue of in-vivo rat eyes

3.3.1. Examination of adhesion sites and variations in adhesion duration of DNA NPs in an in-vivo setup

After proving the retention in the vitreous and adhesion potential of the lipid-DNA NPs after intravitreal injection in ex-vivo and in-vivo models, further experiments were undertaken to evaluate other possible administration sites for the treatment of retinal diseases. One promising approach was the injection of drugs into the periocular tissue. From here the medication could then diffuse into the ocular space to reach clinically relevant concentrations at the retinal tissue. In the previous section the different layers of the retina were already introduced. In the following the tissue outside the bulbus is going to be focused upon.

Because of the positive results obtained after intravitreal injection, the retention of the NPs in the periocular tissue was directly studied in-vivo using fluorescence microscopy. A typical example of microscopy imaging after periocular NP injection is given in Figure 34. After DAPI staining the typical layer-structure of the retina, choroid, sclera and connective tissue becomes visible and their location has been indicated as before. Additionally, the sclera and the connective tissue were labelled. The NPs that were applied using a subconjunctival injection route appear as green fluorescent moieties adhering towards the outside of the sclera and between the cells of the connective tissue.

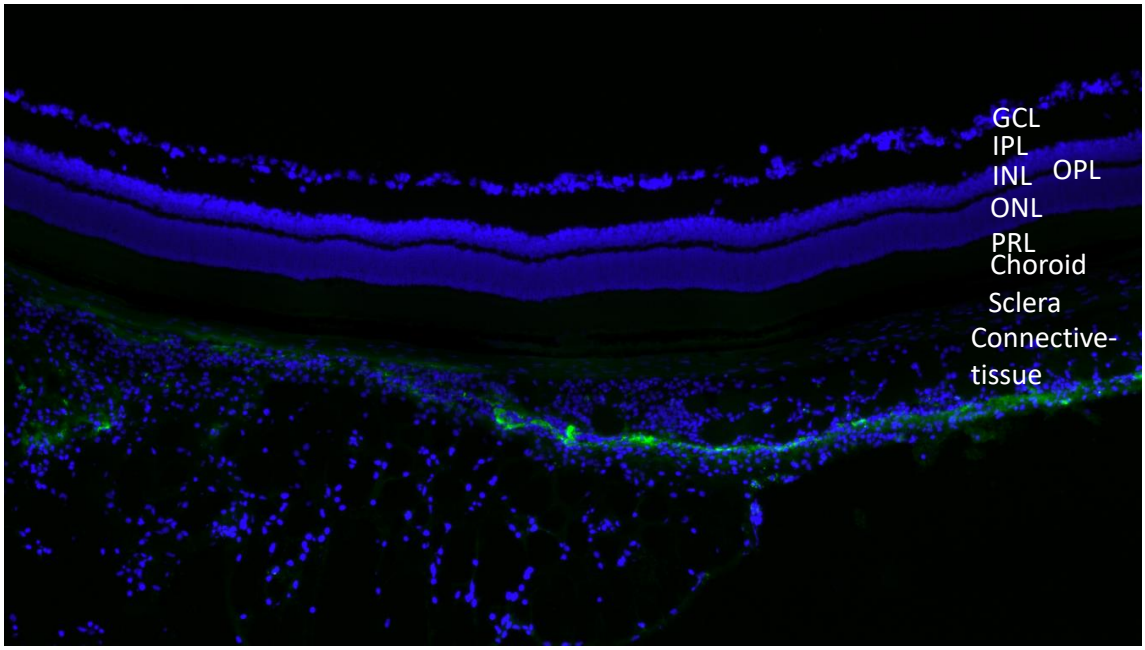

Figure 34 Fluorescent image of a rat eye 24 hours after in-vivo periocular injection of U4T-12 NPs showing the retina, sclera and connective tissue. Designation of different layers is displayed. Coming from the vitreous body and going out of the eye the found layers are: ganglion cell layer (GCL), inner plexiform layer (IPL), inner nuclear layer (INL), outer plexiform layer (ONL), outer nuclear layer (OPL), photoreceptor layer (PRL), choroid, sclera and the connective tissue.

From the intravitreal injection of the two selected NPs, U4T-12 has been identified as having the strongest adherence towards the ocular structures. Therefore this NP was selected for initial studies using subconjunctival injections. In this experiment the retention in the surrounding tissue was compared to the small molecular control Atto-488 and time points of 30 minutes, two hours and four hours were selected. Although these periods were significantly shorter than those chosen for intravitreal injection, they were selected to obtain preliminary information about the retention of U4T-12 in the periocular space. To this end rats were injected with 40 µL of 20 µM NP solution into the subconjunctival tissue. The animals were sacrificed after the designated time and the eyes including the surrounding tissue were enucleated, frozen and prepared as cryosections. Counterstaining with DAPI was performed and the presence of the fluorescently labelled NPs was studied by fluorescence microscopy (Figure 35).

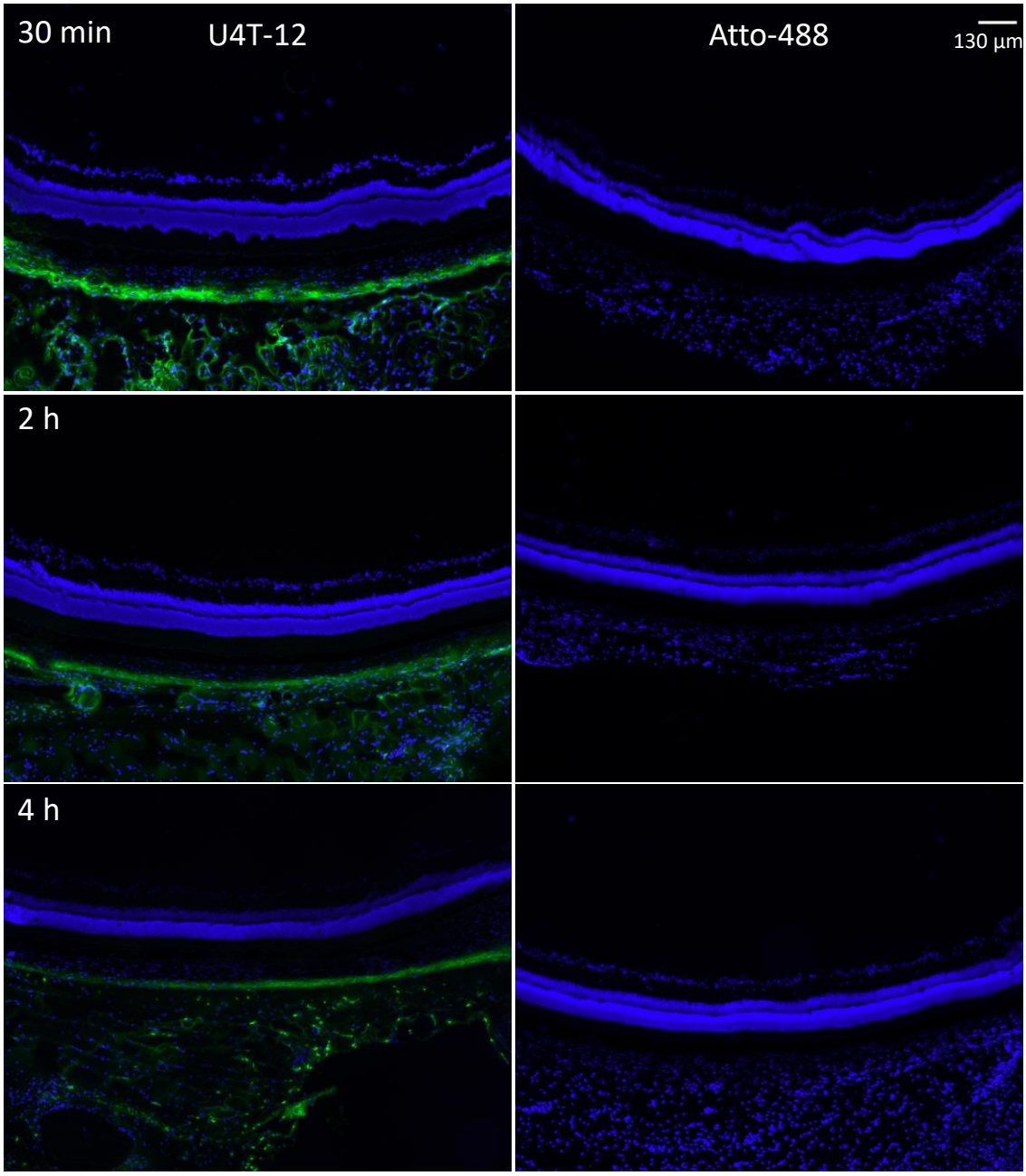

Time points	Positive U4T-12	Positive Atto-488
30 min	2/2	0/2
2 h	2/2	0/2
4 h	2/2	0/2

Figure 35 Representative fluorescent images of rat eyes after periocular in-vivo injection of U4T-12 NPs (left column) or Atto-488 control (right column). Visible are the retina, sclera and surrounding periocular connective tissue at different time points post injection. Below: table of time points and positive eyes found injected with the respective solutions. In stark contrast to the control dye, the animals treated with U4T-12 displayed a large amount of the NPs at a high intensity.

Already 30 minutes after subconjunctival application of Atto-488, the control did not provide any positive results regarding its adhesion towards the connective tissue outside the sclera. Also no other fluorescence was found throughout the cryosections of the samples which were injected with the control.

In stark contrast, the animals treated with U4T-12 displayed a large amount of the NPs at a high intensity. For all time points a similar distribution of the fluorescent NPs was apparent. The U4T-12 particles were mainly localized on the outside of the sclera and form a thick layer covering the complete scleral tissue. At 30 minutes post injection the stratum had a rather consistent thickness of ca. 100 µm. In contrast, the two later time points varied more in their average thickness. The two hours picture showed the same tissue covered but exhibited less intense fluorescence. Also, the NP stratum on the outside of the sclera was only about half compared to the 30 minutes time point. A similar observation could be made for the four hours time point, displaying a layer of approximately 40 µm thickness on the scleral surface. In all given pictures for U4T-12 fluorescence was spread in a honeycomb-like structure in the connective tissue. No explicit findings of fluorescence inside the sclera were apparent although the scleral tissue itself seemed to be infiltrated by the NPs, especially in the 30 minutes image. It must be noted here that this showed that the U4T-12 carrier did not cross the sclera and could therefore not be found in the inner tissues of the eye.

All six of the eyes injected with U4T-12 were found to be positive, showing strong and area wide green fluorescence. This supported the efficacy of the subconjunctival pathway, encouraging further experiments.

The high fluorescence intensity for these shorter time points indicated that the diffusion of the NPs was happening at a large time scale, which invited to perform the same studies with longer post injection periods. Therefore, U4T-12 and U6T-18 NPs were injected into conjunctival tissue and their adherence was evaluated after one and three days. For the fluorescent control only the one day time point was implemented, since all control injections so far had been negative. A representative picture for the control experiment is displayed in Figure 36.

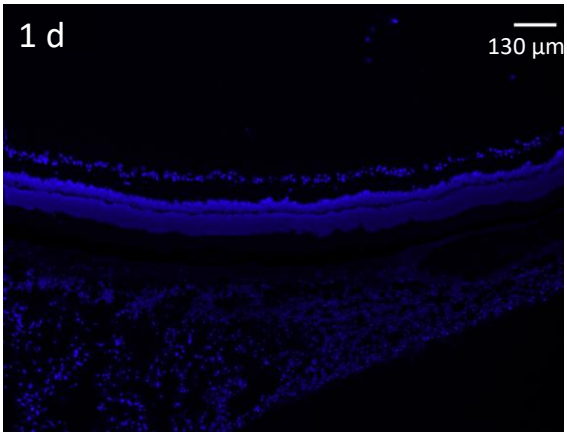

Figure 36 Representative fluorescent image of rat eyes after in-vivo periocular injection of Atto-488 at 1 day post injection.

As has been seen before in the ex vivo setups, also here the Atto-488 showed no sign of retention in the tissue of the injected eyes. Afterwards, both the U4T-12 and U6T-18 NPs were injected in the periocular tissue. Representative images for the given time points are found in Figure 37.

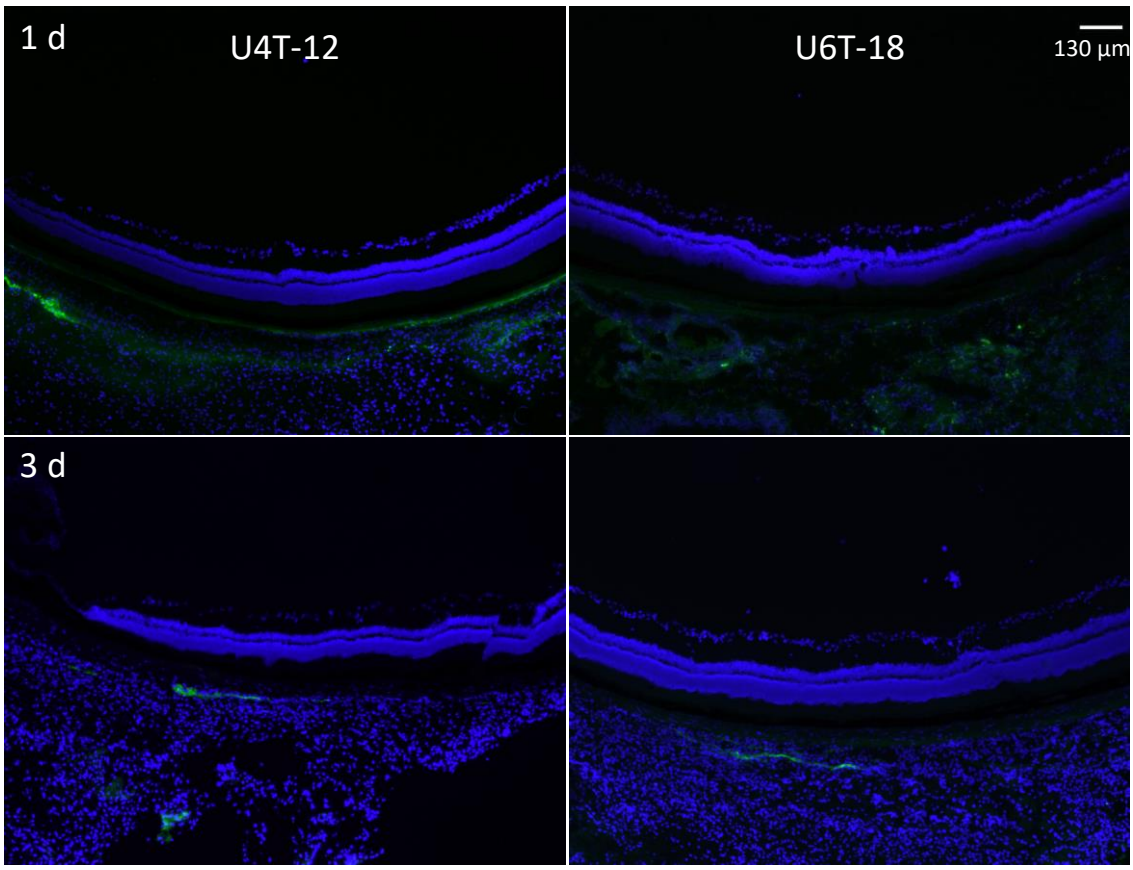

Time points	Positive U4T-12	Positive U6T-18	Positive Atto-488
1 d	5/6	5/6	0/2
3 d	6/6	5/6	-

Figure 37 Representative fluorescent images of rat eyes after in-vivo periocular injection of U4T-12 (left column) or U6T-18 (right column) NPs. Visible are the retina, sclera and surrounding periocular connective tissue at different time points post injection. Below: table of time points and positive eyes found injected with the respective solutions. Both U4T-12 and U6T-18 displayed efficient NP retention at the injection sites up to 3 days post injection.

At one day after injection in the periocular tissue the U4T-12 NPs were found as strong green fluorescence on the outside sclera and the connective tissue. The NP layer on the ocular surface displayed a continuous stratum throughout the tissue with a maximum thickness of approximately 10 µm. Accumulations of NPs could be found on the right and on the left side of the picture. The stronger, left one measured about 300 µm in width and 100 µm in thickness presenting intensive fluorescence. These results were similar to the findings made in the shorter observation periods albeit with weaker fluorescence. The correlating U6T-

18 one day image showed a less strong adherence of this specific NP. The NPs outside the sclera appeared faint and diffuse but were recognizable nevertheless. Due to the blurring boundaries measures could not be given. Additionally, dozens of smaller fluorescent spots were observed on the outside of the conjunctive subconjunctival tissue. The isolated sections appeared to be randomly spread between the cells. After three days the displayed fluorescence for both NPs looked very alike. No continuous layer of NPs was visible. For both images the green fluorescence only covered half of the pictured scleral surface with the fluorescent layers showing less than 10 µm in thickness. Only very hazy and faint areas of NPs without distinct spots of fluorescence were obvious.

In summary, the visible fluorescence decreased in strength and spatial distribution with longer time periods. For one day the images for both NPs presented near full coverage with strong local accumulation of fluorescence, especially for U4T-12 NPs. After three days of incubation the NP stratum only covered half of the pictured scleral surface with the fluorescent layers showing less than 10 µm in thickness. Nevertheless, one day of incubation for U4T-12 and both of the U6T-18 time points displayed 5/6 eyes to be positive. For U4T-12 even 6/6 eyes were detected with NPs in the subconjunctival tissue at three days post injection. However, for neither of the two NPs signs of fluorescence were found inside of the bulbus at any of the given time points.

4. Discussion

4.1. Intravitreal injection of lipid-modified DNA NPs into ex-vivo pig eyes

After presenting the evaluation of the performed experiments for NPs as a drug delivery platform in section 3, the diffusion behavior, retention in the vitreous body and adherence to tissue will be discussed and possible explanations for the found observations will be pointed out in the following discussion.

4.1.1. Examination of diffusion of DNA NPs within an ex-vivo vitreous body

To illustrate and highlight the differences in diffusion characteristics for the investigated NPs, the integrals obtained from section 3.1.1 were merged into a single graph. As before, the fluorescence intensity for each time point and every NP was first normalized to the solution value (Figure 38).

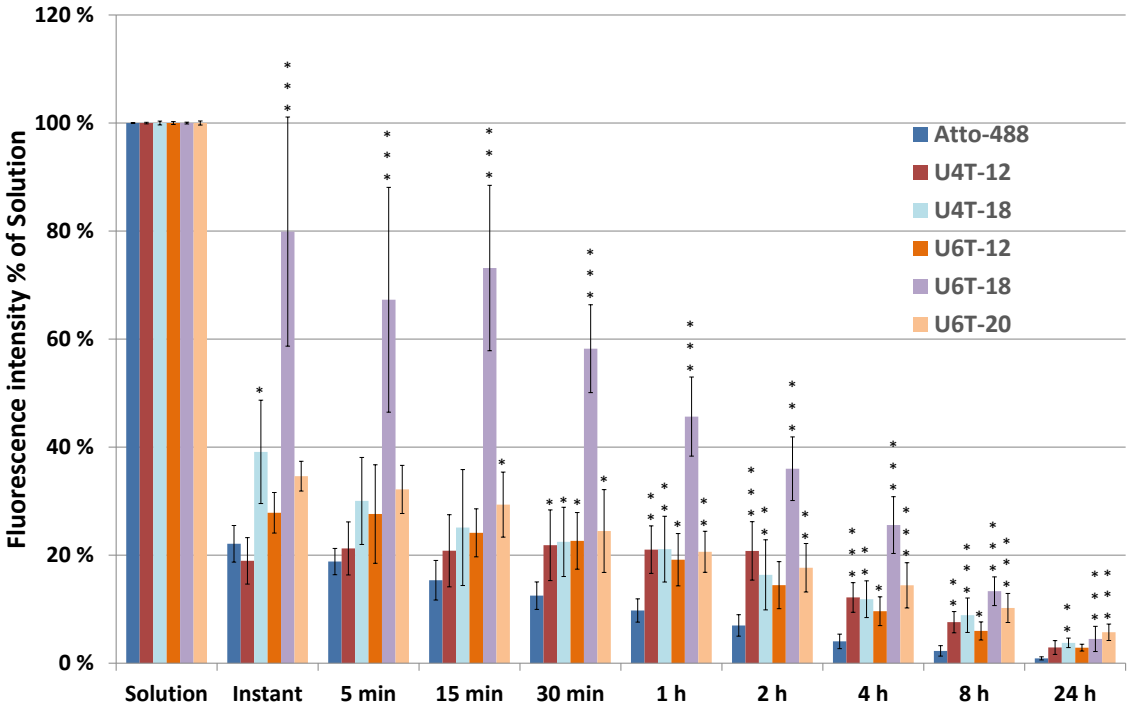

Figure 38 Integrated fluorescence intensity normalized to the solution measurement (y axis) at the different time points after injection (x axis) into the vitreous body for all investigated NPs in ex-vivo procine eyes (n=6-8), standard deviation added. In this case the U6T-18 NPs were particularly visible as they showed superior properties in regard to retention in the vitreous

The graph containing the combined integrals clearly highlights the differences in decrease of fluorescence intensities for the specific NPs, similar to what was already observed in the results section.

The first clear observation was that all of the NPs exhibited a sudden drop from solution to the instant measurements, which could presumably be explained by the dilution of the respective NP or control by the vitreous fluid. At this point all showed integrated fluorescence intensities lower than 50 % of the initial value, with the exception of U6T-18 which was found at 80 %, indicating that it diluted not as quickly within the vitreous fluid as the other NPs. Here, U4T-12 showed a lower percentage at the instant time point than the control which was detected to be at 22 %. After five minutes U4T-12 rose above the control value (19%) to 21 %. The NP showing remarkable performance in this figure is U6T-18. It had by far the highest fluorescence levels until eight hours after injection and displayed a steady decrease. After one hour of incubation the investigated U6T-18 level remained at approximately 46%, which was more than double of what the closest detected fluorescence for the other NPs displayed (21% for U4T-12, U4T-18 and U6T-20).

In the statistical analysis of the values normalized to “solution” U6T-18 exhibited a P value of ≤ 0.001 at all given time points. U4T-18 displayed significant values at the instant time point and 30 minutes after injection ($P \leq 0.05$), as well as after 1, 2, 4 and 24 hours ($P \leq 0.01$) and the highest P value after the eight hours measurement ($P \leq 0.001$). U6T-20 showed significant values at 15 and 30 minutes ($P \leq 0.05$), 1 and 2 hours ($P \leq 0.01$); as well as 4, 8 and 24 hours ($P \leq 0.001$) after injection. U4T-12 displayed a significant value at 30 minutes ($P \leq 0.05$), 1 and 8 hours ($P \leq 0.01$) and also 2 and 4 hours ($P \leq 0.001$) after injection. The NP with the lowest level of significance was U6T-12 with $P \leq 0.05$ at 30 minutes, 1, 4 and 8 hours.

Analyzing the NPs normalized to their respective solution value provided information about the detected fraction of NPs out of the total amount that was injected. Additionally, another normalization method was desirable where more focus rested on what the diffusion, distribution and retention of the NPs was like

after injection. Therefore, in the second method, the fluorescence of each NP has been incorporated and normalization to the respective instant measurement of the NP was performed.

The normalization of the measurements to the integrated fluorescence intensity right after injection (instant) was incorporated in Figure 39.

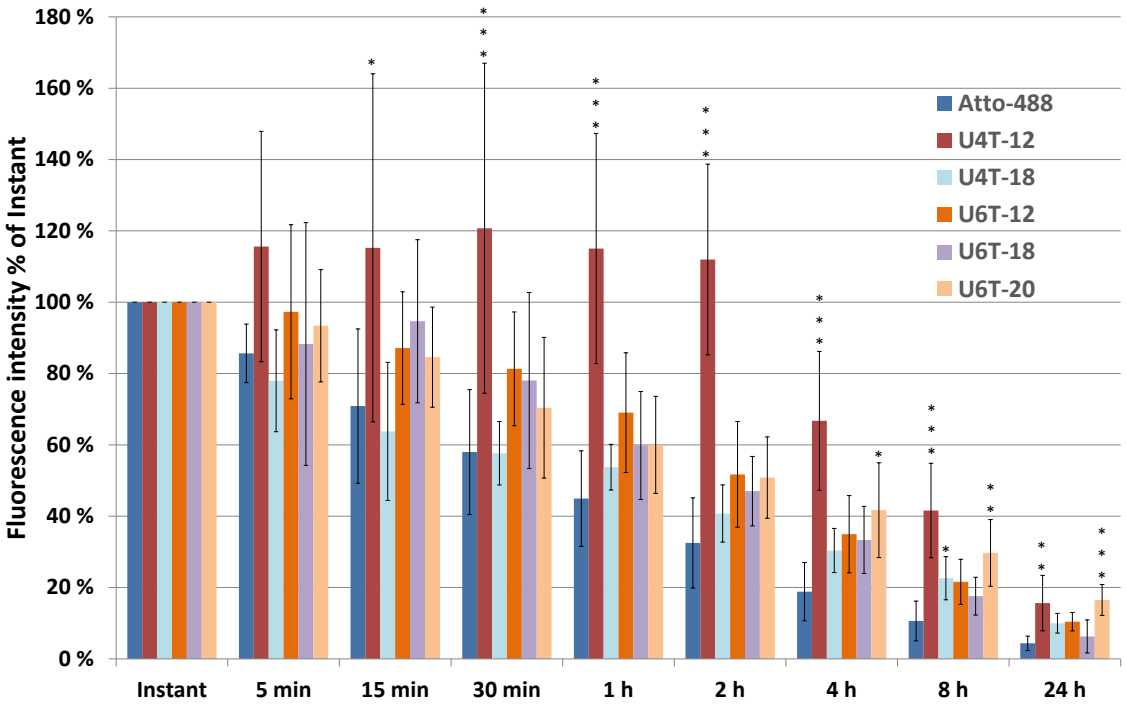

Figure 39 Integrated fluorescence intensity normalized to the instant measurement (y axis) at the different time points after injection (x axis) into the vitreous body for all investigated NPs in ex-vivo procine eyes (n=6-8), standard deviation added. Especially U4T-12 NPs displayed outstanding properties concerning their retention in the vitreous body.

Out of the investigated NPs only U4T-12 exhibited increased fluorescence intensity after the instant value, and had its maximum at 30 minutes after injection. This would have indicated a further increase in the amount of NP present in the vitreous body. As no further injections were applied, this cannot have been the case. However, there are several possible explanations for this observation which mainly relate to the optical axis of the measurements and the diffusion of NPs into it. For administration of the NPs, injections were performed at the limbus of the eye. Therefore, the ocular layers were penetrated and the NP solution was injected in the approximate center of the vitreous body. However, due to the anatomical structure of the vitreous, defined by a framework of

collagen fibers, an insertion channel might have remained after drawing back the needle. This could have offered an ideal opportunity for the NP to flow back out of the injection site and into the preformed channel. However, the fluorophotometer only has a limited optical axis in which the NPs are detectable. Therefore, directly after injection the detected signal would have been lower than it should have been. In the course of the experiment the NPs might have diffused back into the optical axis of the fluorophotometer and the measured fluorescence could have increased thereafter. The process described above might have resulted in a fluorescence maximum being later observed than instantly after injection. A second possible reason for the found increase is that injections could have been performed slightly outside the optical axis of the fluorophotometer. For measurement of the complete amount of injected NP, they would have first had to diffuse into the investigated tissues. This might have led to an increased fluorescent signal in the first measurements. Lastly, the observed phenomenon could also have been a combination of both explanations given above.

In contrast to U4T-12 which exhibited increasing fluorescence over the first 30 minutes, all other NPs showed a decreasing trend directly after injection. Strikingly, only U4T-18 displayed values below the ones of the control, five (78%) and 15 minutes (64%) after injection. Afterwards slower diffusion was observed, resulting in an integral that exceeded the Atto-488 value for the later time points. Nevertheless, when compared to the other NPs, U4T-18 exhibited the lowest average intensities over the course of the experiment.

The U6T-20 NPs showed a constant decrease in measured fluorescence intensity directly after injection and showed a similar profile as U6T-12 and U6T-18 NPs. It must be noted that already five minutes post injection the three NPs exhibited comparable values. At four hours, more pronounced differences were evident between the three vehicles. U6T-20 continued the steady decreasing trend found in earlier measurements, whereas the U6T-12 and U6T-18 fluorescence integrals suddenly dropped to only 35% and 35% of their original values. Therefore U6T-20 showed the second highest value of all NPs at four

hours post injection (42 %). With an observed value of 17 % it eventually became one of the two most abundantly present NPs after 24 hours incubation.

The NP showing the highest fluorescence at all time points was

U4T-12. It was the only NP that did not drop below its initially measured value until the four hours measurement. With that it stayed by far on the highest level amongst all NPs until the 24 hours measurement where it was second best with approximately 16 % of fluorescence remaining.

In the statistical analysis for instant normalization U4T-12 was the only NP displaying significance before four hours of measurement: 15 minutes ($P \leq 0.05$), 30 minutes, 1, 2, 4, 8 hours ($P \leq 0.001$) and 24 hours ($P \leq 0.01$). U6T-20 showed three significant time points which were 4 hours ($P \leq 0.05$), 8 hours ($P \leq 0.01$) and 24h ($P \leq 0.001$) after injection. Finally the value for the 8 hours' time point ($P \leq 0.05$) was the only significant one found for U4T-18.

In the fluorophotometric analysis two NPs showed superior performance in regard to their diffusion and half life time. Firstly, when normalized to the instant fluorescence, U4T-12 convinced with high values, a strong plateau phase and a late decrease in integrated fluorescence. This indicated strong retention of the NP leading to a prolonged half-life time in the vitreous body. When normalized to the solution measurement, strikingly U4T-12 showed weaker levels after injection (Figure 38). However, in the course of the graph U4T-12 constantly stayed at an approximate value of 20 % until after two hours, which was a time frame longer than for almost all other NPs except U6T-18. This consistency is what is desired in drug delivery to the posterior segment, which made U4T-12 one of the two selected NPs for further in-vivo investigations. The second NP which stands for superior performance is U6T-18. When normalized to the instant measured fluorescence, this NP already displayed great levels of intensity and a steady decrease over time. Compared to the solution measurement this NP was able to maintain the highest percentage of original fluorescence intensity of all the NPs by far. This indicated a strong retention in the vitreous body and a good half-life

time. Therefore, this NP was selected second as preferred candidate for further investigations.

4.1.2. Examination of adhesion sites and variations in adhesion duration of DNA NPs in an ex-vivo setup

After investigating the differences in diffusion for the different NPs, their adherence to ocular tissue and distribution was analyzed and compared by fluorescence microscopy. In order to summarize the previous observations of the fluorescence imaging Figure 40 displays the number of positive findings out of the total number of eyes that have been investigated for the specific time point.

	NP					
Point in time	**Atto-488**	**U4T-12**	**U4T-18**	**U6T-12**	**U6T-18**	**U6T-20**
5 min	0/3	3/3	2/3	2/3	2/3	2/3
15 min	0/3	3/3	3/3	2/3	3/3	2/3
30 min	0/3	2/3	2/3	3/3	3/3	2/3
1 h	0/3	3/3	2/3	3/3	3/3	3/3
2 h	0/3	3/3	3/3	3/3	3/3	3/3
Total	**0/15**	**14/15**	**12/15**	**13/15**	**14/15**	**12/15**

Figure 40 Number of positive eyes found out of total number of investigated eyes by fluorescence microscopy after intravitreal injection of NPs or control in ex-vivo porcine eyes. The number of positive findings out of all eyes examined for a NP is displayed at the bottom of the table. As is visible, the U4T-12 and U6T-18 NPs displayed the highest amount of positive eyes out of all tested eyes.

The first thing to notice is that for the control out of the 15 investigated eyes none were found positive. This strongly supports the efficacy of the investigated NPs. Although the results of the fluorophotometry clearly indicated presence of fluorescent dye directly after injection, no signs of fluorescence can be found in the pictures obtained by fluorescence microscopy. The explanation for this negative outcome could lie in the preparation of the cryosections. Before the evaluation under the microscope, each slide with the sections of the respective eye was fixated in methanol and washed six times with buffer. Due to the low adhesion capacity of the dye, it was expected that this leads to total clearance of the control from the ocular tissue. However, this also indicated the strong adhesion of the different NPs that were still to be found even after the same procedure was followed.

From the fluorescence images it was clear that U4T-12 NPs showed the strongest adhesion to the retina compared to the other investigated NPs. Fluorescence could be observed reaching through the GCL into the INL in the one hour and two hours images indicating strong adherence towards the retinal tissue. This was underlined by the 14/15 total positive eyes that have been found. Hence, it can be concluded that U4T-12 NPs presented exceptional properties regarding their adherence and distribution towards the retinal tissue.

Supporting the observation made in the fluorophotometric analysis, also in this experiment U4T-18 and U6T-20 showed inferior adhesion to the retinal tissue. Although the fluorescence of U4T-18 NPs could be found in the more basal parts of the retina such as the INL, the average fluorescence observed was much fainter than in U4T-12. Furthermore, NPs constructed of U6T-20 appeared less promising than all other investigated NPs due to weak fluorescence intensity and nearly non-existent coverage in the majority of the pictures. These two were the only NPs displaying a mere 12/15 positive eyes, which confirmed the earlier findings regarding their poor diffusion characteristics. Strikingly, these two NPs were the ones with the lowest percentage of lipid modified bases out of all investigated NPs. The U4T-18 and U6T-20 contained 22 % and 30 % of alkyl functionalized nucleotides, respectively. This could indicate that the ratio of the amount of lipid tails to the total amount of bases might have a profound influence on the diffusion behavior of the formed NPs.

The U6T-12 NPs displayed a total of 13/15 positive results. In total U6T-12 showed rather weak fluorescence mostly for the short incubation periods with incomplete covering of the retina. This was especially clear when compared to U4T-12 and U6T-18. Only for the two hours' time point complete covering of the displayed retina was detected. Also Figure 40 stresses that U6T-12 was not as promising regarding adhering properties as other NPs with 13/15 positive eyes.

Recapitulating the findings for U6T-18, one must note the high predominance of fluorescent NPs which was still to be found in the vitreous body even for the longer periods of incubation. This clearly underlined the excellent retention qualities of this NP. Similar as for U4T-12, also for this NP 14/15 eyes were

detected to be positive. However, the images showed that U6T-18 NPs also formed a constant coating displaying intense fluorescence on the GCL. This NP therefore seemed more favorable in regard to adherence properties than U4T-18, U6T-12 and U6T-20.

As found in fluorophotometry, the fluorescence imaging of U4T-12 and U6T-18 showed that these NPs provide the most promising properties out of all NPs studied after ex-vivo intravitreal injections. Not only did they both display excellent coverage of the retinal tissue but they were also found to be the only NPs displaying 14/15 positive eyes in the ex-vivo experiments. Remarkably, these two NPs have the same percentage of lipid modified DNA compared to their total base-length (33 %). This again indicates that the amount of modified nucleotides might play an important role for the adherence behavior of lipid modified DNA NPs. Due to their superior performance the U4T-12 and U6T18 NPs were chosen for further in-vivo experiments.

4.2. Intravitreal injection of lipid-modified DNA NPs into in-vivo rat eyes

4.2.1. Examination of diffusion of DNA NPs within an in-vivo vitreous body

In a first step the diffusion characteristics for two NPs and for the control were compared in-vivo by fluorophotometric measurement. Therefore U4T-12, U6T-18 and Atto-488 were measured pre injection and after time points of 0, 1, 3 and 5 days.

One will find that compared to the results of the fluorescent microscopy which are discussed in the next paragraph, the data generated from the fluorophotometric measurements appear rather deficient. This is mainly due to methodic difficulties originating from working with living animals. For accurate measurements the optical axis of the injected eyes needed to be aligned meticulously with the optical axis of the Fluorotron Master™. After anesthetizing the rats, the alignment of the bulbus varied for each respective measurement because between those the rats were awake and moving. Therefore, the entire rat needed to be positioned, depending on the axis of the respective eye, in a different way in front of the lens

of the Fluorotron Master™ every time before a measurement could be commenced. Unfortunately, the alignment turned out to be a bigger obstacle than originally anticipated although trying various alignment aids. The given anesthesia allowed only a limited timeframe for measurements until the rat would wake up and further experiments would be impossible. Multiple injections of anesthesia held the risk of inadvertently euthanizing the animals and therefore losing the possibility of measuring at the very moment and later time points altogether. Due to these difficulties the decision was made to keep the fluorophotometric measurements with living rats within a limited amount in order to consciously avoid unnecessary animal suffering. In conclusion this means that the little data in “Examination of diffusion of DNA NPs within an in-vivo vitreous body” (3.2.1) is rather due to difficulties in accurately aligning and measuring the fluorescence present in the respective eye than no fluorescence being present.

For the control and U4T-12 NPs only directly after injection measurable fluorescence levels were recorded, most likely due to the above mentioned difficulties. However, for U6T-18 NPs distinctly elevated levels of fluorescence were detected also the day after injection. For comparison the data obtained with the control has been incorporated in Figure 41, where the U6T-18 results are summarized.

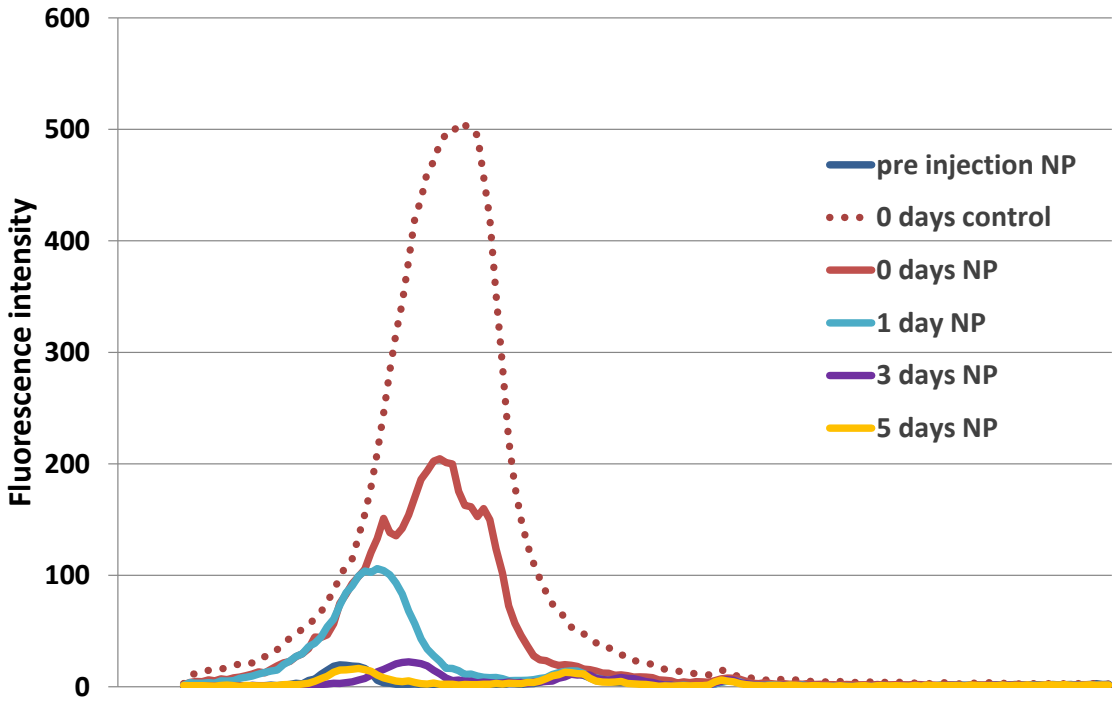

Figure 41 Fluorophotometric scan of the fluorescence intensity (y axis) inside the in-vivo rat eye after intravitreal injection of U6T-18 along the optical axis (x axis) over time. The "pre injection NP" measurement showed the native eye without any treatment. The "0 days control" measurement has been included to stress the differences in detected fluorescence right after injection between NP and control dye alone due to the chemical modification of the dye. No other control time points were added since only this one showed positive findings of fluorescence.

When comparing the U6T-18 NP with the control, two differences for the initial 0 day measurement were found. Firstly, the detected fluorescence intensity for U6T-18 NPs (200 RFU) was less than half the amount of Atto-488 (500 RFU). This was due to the differences in fluorescence intensity of the molecules that have been injected. As explained in section 3.1.1 chemical modification of the structure of the dye can lead to alteration in fluorescence intensity. Secondly the peak of the U6T-18 NPs showed two shoulder peaks of around 150 RFU. This could be interpreted as an embodiment of the retention properties of the injected NP because it did not spread out steadily and evenly but was held back at the injection site. In the progress of the measurements these retention properties of the NP were also responsible for maintaining detectable traces of fluorescence at the injection site up to three days post application whereas the control did not differ in the investigations after the "0 days" time point. These results, despite the methodical difficulties already indicated the promising properties of the NPs and invited to perform further in-vivo imaging.

4.2.2. Examination of adhesion sites and variations in adhesion duration of DNA NPs in an in-vivo setup

For the in-vivo examination of the adherence and distribution towards the retinal tissue a summary of the positive findings is displayed in Figure 42.

	NP		
Point in time	Atto-488	U4T-12	U6T-18
½ d	0/6	5/6	5/6
1 d	0/6	4/6	4/6
3 d	0/6	3/6	4/6
5 d	0/6	1/6	1/6
Total	0/24	13/24	14/24

Figure 42 Number of positive eyes found out of total number of investigated eyes by fluorescence microscopy after intravitreal injection of U4T-12, U6T-18 or control in in-vivo rats. The numbers of positive findings out of all eyes examined are displayed at the bottom of the table. Also here the U4T-12 and U6T-18 NPs displayed similarly superb results concerning the long-term adhesion and retention whereas the control did not exhibit any affinity to the retinal tissue.

As already expected, the eyes injected with the control dye did not provide any positive results regarding adhesion of the fluorescent dye towards the retinal tissue. Neither were any other signs of fluorescence found throughout the prepared cryosections, leading to no positive images out of the 24 tested eyes.

In contrast, U4T-12 and U6T-18 displayed consistent uptake of green in the retinal layers and the vitreous, especially for the shorter points in time. However, for both NPs the same tendency of strong decrease in positive findings with increased incubation time could be observed.

Interestingly, as seen before in the ex-vivo images also for the in-vivo experiments filamentous formations of NPs could be observed in the vitreous body. They were found for U4T-12 in the first two points in time and for U6T-18 at half a day and even five days. These formations were probably caused by adherence of the NPs towards the reticular framework of the vitreous composed of a network of type II collagen fibers. Interlaced into this 3D framework are glycosaminoglycans, hyaluronic acid and a variety of selected proteins. Further

research is needed for identification of the structure responsible for the observed NP retention.

In conclusion, both examined NPs showed adhesion towards the retinal tissue for a maximum of five days. In more than 50 % of the cases NPs were found to be present after three days of incubation in fluorescence imaging. Additionally, the fluorophotometric analyses of U6T-18 confirmed the presence of NPs in the ocular tissue after three days of incubation. This was a strong improvement compared to the retention of most drugs with low molecular weights, which have previously been shown to have an average half-life time of only several hours[39]. Nevertheless, also the lipid-modified DNA NPs observed are subject to ocular clearance through the retinal tissues via passive and active transport mechanisms such as circulation of the aqueous humor, which may lead to excretion through the channel of Schlemm. However, it is expected that the NPs are detectable for longer periods of time than five days, but different analysis methods will be needed for this. Here one for example can use LC-MS. The limiting factors in fluorescence imaging are restricted resolution and interference of the background fluorescence with fluorescence of NPs. Especially the latter one prevented more experiments with even longer times of incubation than for five days because with decreasing fluorescent intensity the NPs become harder to differentiate from the ocular tissue's auto fluorescence.

4.3. Injection of lipid-modified DNA NPs into periocular tissue of in-vivo rat eyes

4.3.1. Examination of adhesion sites and variations in adhesion duration of DNA NPs in an in-vivo setup

Finally, also subconjunctival injections were performed in an in-vivo rat eye model in order to evaluate the benefit of periocular injections compared to intravitreal drug application. As explained before, different time points were chosen in two different sets. Firstly, in a short period trial only U4T-12 and the control were included. Afterwards a second experiment was conducted in which U4T-12, U6T-18 and control were compared. A combined summary of both results is presented in Figure 43.

	NP		
Point in time	**Atto-488**	**U4T-12**	**U6T-18**
30 min	**0/2**	**2/2**	**-**
2 h	**0/2**	**2/2**	**-**
4 h	**0/2**	**2/2**	**-**
1 d	**0/2**	**5/6**	**5/6**
3 d	**-**	**6/6**	**5/6**

Figure 43 Number of positive fluorescence findings in the periocular tissue of the eyes out of total number of investigated eyes after in-vivo subconjunctival injection of U4T-12, U6T-18 or control and subsequent fluorescence imaging. The numbers of positive findings out of all eyes examined are displayed at the bottom of the table. Also here the control dye does not show any affinity to the tissue and cannot be detected already 30 minutes post injection.

For the first experiment relatively short time periods of 30 minutes, two hours and four hours were employed for U4T-12 NPs and the control. Here, similar distribution characteristics of the fluorescently labelled NPs were found in all of the investigated eyes. The NPs were only detectable on the outside of the bulbus, forming a thick fluorescent layer of variable size. The NPs covered the scleral tissue completely and were visible from one end of the pictured tissue to the other.

For the longer time points of one and three days the findings of NP-fluorescence decreased in strength and spatial distribution with increasing residence time. For one day the images for both NPs presented area-wide and strong local accumulation of NPs, especially for U4T-12. After three days the green NP stratum only covered half of the pictured scleral surface with the fluorescent layers being less than 10 µm thick. Nevertheless, the numbers of total positive findings were still impressive. Here, all of the performed NP experiments displayed 5/6 positive eyes per time point, except U4T-12 which even showed 6/6 eyes positive three days after injection.

In contrast, none of the eyes injected with the control via the subconjunctival route provided evidence of positive results neither for the short nor for the long time periods, which supported the superior properties of the NPs.

The performed experiments showed that up to three days the investigated NPs U4T-12 and U6T-18 provide excellent adhesion towards the periocular tissue. From fluorescence imaging it became clear that the NPs form a covering layer on the scleral surface. This is also an excellent starting situation for diffusion into the bulbus for small molecular medication bound to the NPs. Both the long lasting presence and the targeting of the sclera provide excellent properties for drug delivery depots composed of lipid modified DNA NPs. However, for neither of the two NPs signs of fluorescence were found inside of the bulbus at any of the given time points, employing the method of fluorescence imaging. For further investigation in efficacy different analysis methods are necessary in order to overcome the limitations in resolution and background fluorescence. Due to the latter one, imaging for longer incubation times in subconjunctival administration was not possible because in the generated pictures the faint NP fluorescence was almost entirely overshadowed with the blue stained nuclei of the periocular tissue. Additionally this could mean that due to limitations in resolution for this method dye-fluorescence inside the bulbus might potentially have remained undetectable even though being present. This indicates that other methods than fluorescence microscopy are needed to further analyze the actual residence time of the NPs in the periocular tissue. Although no signs of toxicity or inflammation could be observed in the injected animals, further studies to confirm the retinal safety of the employed NPs are necessary.

4.4. Comparison of DNA NPs to other drug delivery options for treatments of the posterior segment

After highlighting the current treatment options for the therapy of intraocular diseases in 1.3, it is evident that the employed methods are not very efficient and far from ideal. A summary of those options with their respective properties is presented in Figure 44.

Drug	Active agent	Application	Dosage	Pharmacokinetics	Biodegradable
Ranibizumab	Antibody Fragment	Intravitreal injection	0,5 mg	Half-life time: 7.19 days	Yes
Bevacizumab	Whole Antibody	Intravitreal injection	1,5 mg	Half-life time: 9.82 days	Yes
Triamcinolone	Triamcinolone	Intravitreal injection	4 mg	Half-life time: 18.6 days	Yes
Ozurdex®	Dexamethason	Intravitreal implant	0.7 mg	Duration of action: 1 month	Yes
Retisert®	Fluocinolone acetonide	Intravitreal implant	0.59 mg	Duration of action: 30 months	No
Iluvien®	Fluocinolone acetonide	Intravitreal implant	0.19 mg	Duration of action: 24 – 36 months	No
Vitrasert®	ganciclovir coated with polyvinyl alcohol	Intravitreal implant	4.5 mg	Duration of action: 5 – 8 months	No

Figure 44 Summary of the FDA approved medication for intravitreal application for diseases of the posterior segment of the eye. The respective active agent, the route of application, the dosage, the pharmacokinetics and the biodegradability are given for comparison reasons.

Anti-VEGF antibodies, like Bevacizumab, or antibody fragments such as Ranibizumab show intravitreal half-life times of approximately seven to ten days[54,55], which makes multiple injections unavoidable in most cases. With a half-life of 18.6 days[56], Triamcinolone maintains significantly longer in the vitreous than the previously mentioned active agents but still does not provide a time period long enough to prevent multiple injections for the diseases highlighted in 1.2. Although sufficiently high drug concentrations can be reached using intravitreal injections, frequent surgical procedures are still necessary which pose a large burden on the patient. A reduction of the injection frequency is highly desired in the field, something that might be possible using novel drug delivery platforms. A lower administration regimen can only be attained with prolonged retention of the drug in a controlled and sustained fashion. Intravitreal implants such as Retisert® and Iluvien® sufficiently release their active agents for an approximate period of 30 months[57,58], however, both of them are not biodegradable and therefore require surgery for implantation and explantation. Additionally, just like the Ganciclovir implant Vitrasert®, which displays an

intravitreal duration of action of only five to eight months[59], Retisert also requires suturing due to its larger size after implantation[60]. The biodegradable Ozurdex® sustained-release Dexamethasone implant only requires surgery once for implantation, but at the same time displays a much shorter duration of efficacy than its non-biodegradable equivalents. In-vitro and in-vivo rabbit eye experiments have shown that the drug release has effectually been completed after approximately one month post implementation[61]. At least for glucocorticoids, implants represent an option to prolong the duration of intravitreal drug release and therefore reducing interventions. Yet implants are not employed for other than anti-inflammatory drugs and still they require rather invasive implementation. Ideally, a drug delivery platform also possesses targeting mechanisms to specifically reach the tissues of interest and minimize side effects[62], which implants are not able to provide at this current stage. There is a vast variety of delivery platforms that have been investigated for their applicability in the field of ophthalmology. However, not all have proven as promising as they initially seemed. Below a selection of possible approaches has been highlighted. The ones displayed have been chosen in regard to relevance and innovative potential.

4.4.1. Nanoparticles

This work focuses on a special kind of DNA-Nanoparticles which were introduced in 1.4. This section elaborates on Nanoparticles in general and additionally other representative examples of submicron molecules which could provide progress in solving the problems encountered in the field of drug delivery. Subsequently they will be compared to our DNA-NPs. NPs may vary in size from 10 to 100 nm and could already be used as a launcher system for pharmaceuticals and as target-oriented transportation devices into diseased tissues[63]. In contrast to macroscopic objects, these sub-micron vehicles exhibit special properties due to their high surface area and the large influence of Brownian motion. NPs are providing a large potential by overcoming static diffusion barriers, which results in an increased ocular bioavailability. Additionally, they are also able to enhance the solubility of the loaded drug[64,65]. One of the major advantages of these

vehicles is that physiological barriers can be overcome and the guidance of the drug to intraocular compartments or even specific cells is possible through targeting mechanisms[66,67]. Polymeric nanoparticles loaded with drugs have the habit to reside in the target tissue for an extended period of time which generates a depot for the loaded medication. Drug release and degradation of the NP are highly dependent on the size, weight, morphology and the physical state of both NP and loaded drug[68]. Two prerequisites that such nanometer-sized vehicles need to fulfil are biodegradability and biocompatibility. Numerous polymeric NP prototypes claim to fulfil these requirements and are being tested in various projects[69,70]. Recently promising data has been acquired with a PLGA composition, when they were used to form NPs loaded with Dexamethasone[71]. Here, a rabbit eye model was employed to test the NP properties under in-vivo conditions. After intravitreal injection a sustained release of Dexamethasone was achieved for up to 50 days, while maintaining a nearly constant drug level for the first approximate 30 days. High concentrations of the released drug were found in the choroidea, retina and in the vitreous body. In contrast, the animal's blood plasma did not contain the active ingredient, which indicates systemic side effects can be minimized while at the same time obtaining a higher bioavailability. Remarkably, the sustained release lasted approximately 20 days longer when PLGA NPs were employed than observed in the above described Ozurdex® devices. It is possible that the properties resulting from the employed polymer nanoobjects influence the drug release and generate longer release periods. This could lead to fewer injections and would therefore be highly favorable. Another example is given by Jo et al, which use silica NPs that already function themselves as active agent[72]. They were tested in regard to their anti-angiogenetic impact on retinal neovascularization in oxygen induced mice and displayed a reduced angiogenesis whilst showing no signs of direct toxicity. Apparently the silica NPs cause a blockage of the VEGFR-2 pathway which in turn leads to the inhibition of neovascularization triggered by VEGF. This study illustrates that NPs could potentially function as an active agent while at the same time act as a carrier for drug delivery. Our DNA NPs hold the very elegant opportunity to be functionalized to form an oligonucleotide aptamer sequence in

order to target various different molecules via adaptive binding. These aptamers can theoretically be designed to bind VEGF and therefore block its further pathway. At the same time, they can be used as a delivery vehicle for a large variety of drugs employing one of various loading possibilities which where pointed out in 2.4.1. As can be seen by the examples given above, nanoscaled carrier platforms hold a variety of possible advantages for the field of ocular drug delivery. However, one should note that some portions of NPs may accumulate in liver, kidney and other organs[73], although the risk after ocular applications seems to be very low. The stability and toxicity of a lot of potential NP-structures still needs further research especially in regard to the treatment of retinal diseases. In this view their accumulation and long-term toxicity may cause serious obstacles. Therefore, biodegradable NP formulations would be highly preferable. As a promising alternative for the formation of NPs from synthetic polymers, such vehicles can be constructed from biopolymers such as DNA in our case. In the course of this work different NP formulations have been examined. In the long-term, the aim is to refine those structures to suit the demands of a novel drug delivery platform.

4.4.2. Microspheres

Another approach to enhance effectiveness of drug administration to the eye involves the use of microspheres. These are globular aggregates of molecules with dimensions between 1 and 1000 µm that consist of a polymeric matrix in which the desired drug is dispersed[74,75] (Figure 45). Often biodegradable polymers are used to ensure the degradation and clearance in the eye without the need of surgical removal. This is obviously an enormous advantage compared to non-degradable platforms. For the formation of such biodegradable microspheres, gelatin, albumin, polyanhydrides and polyesters are often used[76]. Here, polylactic-acids (PLA), polyglycolic-acids (PGA) and polylactic-co-glycolic-acids (PLGA) are most frequently employed[74]. For the preparation of microspheres various methods are available. They range from denaturation, cross linking of macromolecules in emulsion or interfacial polymerization to aerosol phase formation, spray drying and pH adjustment aggregation[77]. Evaporation of a solvent from an oil in oil or oil in water emulsion is most

commonly used for the enclosure of drugs in a polymeric matrix. Here, the preparation starts with the polymer in an organic solvent added with the required drug. Sonication is employed to guarantee a homogeneous suspension. A drug-polymer dispersion is used to form an emulsion before the evaporation of the organic solvent follows. Finally the obtained microspheres are washed with an inert solvent, then filtered to separate the differing sizes and dried[78]. With a complex synthesis like this, a lot of variables influence the amount of encapsulated drug in the microsphere, such as the physicochemical properties of the polymer and the drug, the used synthesis techniques and the evaporation rate of the solvent[79]. In this regard, DNA NPs have clear benefits when being formulated. The assembly procedure of the carrier consists of applying a simple heat gradient, which can be performed in virtually any lab. For production of polymeric microspheres however equipment allowing for interfacial polymerization, spray-drying or aerosol formation is required. The above mentioned preparation processes are rather complex and offer a lot of potential for variety in the amount of loaded drug, whereas for our DNA NPs, changes in the dosing regimen can be easily undertaken and controlled entirely in a few simple steps. Microspheres, consisting of the mentioned polymers are degraded in the aqueous environment into their components, which are eliminated from vitreous. Here, the speed of degradation depends on the polymer composition and their molecular weight, as well as the total surface area and porosity of the microsphere. The release of the drug is affected by the decomposition of the particles and additionally is dependent on diffusion of the compound through the polymer matrix and out of the pores of the particles[78]. Unfortunately, the polymer microspheres and especially their degradation products also hold the potential of causing severe side effects such as inflammation[80] or retinal detachment, which is induced by the fibroblast activity of certain polymers[81]. Another potential drawback is the reduced stability of macromolecules due to pH drops caused by the acidic degradation products of polymers such as PGLA[82]. In the contained environment of the eye, such a reduced pH can cause rapid degradation of the polymer and therefore fast release of the drug. This negates the purpose of the carrier and can result in unwanted side effects. In comparison to microspherical

approaches, DNA NPs hold a significant advantage concerning their degradation profile. As the carrier is designed out of solely DNA and lipid tails, they consist of body own molecules that can easily be degraded in physiologic enzymatic degradation processes. Therefore, no adverse effects such as inflammation or pH drops are to be expected. Additionally, the soft nature of the micellar constructs minimizes the risk for retinal detachment. In the current state microspheres still represent an interesting platform with a lot of potential, but due to the above-mentioned inconveniences in regards to assembly and side effects their relevance in today's treatment of retinal diseases remains virtually non-existent.

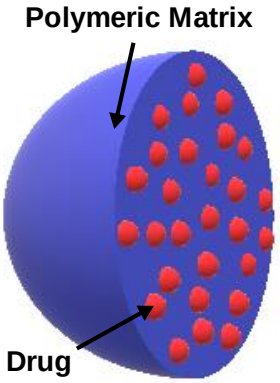

Figure 45 Structural model of a microsphere consisting of an active substance dispersed in a polymer matrix

4.4.3. Ocular Implants

Several devices which are microspheres in regard to their chemical structure have been approved for clinical use by the FDA and EMA and are employed as plugs, implants and discs[75]. A selection of them has already been introduced in 1.3.2. The implants Retisert® and Iluvien® consist of a polymer matrix of polyvinyl alcohol and silicone that control the sustained release of the corticosteroid Fluocinolone acetonide for up to 30 months[83,84]. Due to their non-biodegradability these devices require not only implantation but in the case of Retisert also explantation which is far from ideal. To date the only biodegradable implant employed in for ophthalmic clinical use is Ozurdex®, which has been on the market since June 2009[85]. This PLGA polymer matrix contains 700 µg Dexamethasone as an active agent[85] and is employed in cases of macula edema due to RVO, diabetes and noninfectious uveitis[86]. Although the drug release has

been shown to be completed after approximately one month[61], biodegradation requires an extra two months in rabbit and monkey eyes[87]. This results in a prolonged time window for possible adverse effects caused by degradation products whereas the active agent is only dispersed in one third of the time needed for biodegradation, hence in a relatively short period of efficacy versus a much longer period of possible adverse effects. This is not to be expected from our DNA NPs since their molecular formulation does not involve a complex matrix but rather a short and therefore easily degradable strand of ubiquitous DNA. Recently, also experiments were performed in which Ozurdex® was applied adjunct to anti VEGF treatments witch Ranibizumab in age-related macular degeneration. Here, no visual or anatomical benefits were observed after treatment with Dexamethasone in adjunct to Ranibizumab compared to the monotherapy with anti VEGF[88]. Up to date, no implants have found their way into the treatment of AMD and therefore the half-life time of a maximum ten days of Anti-VEGF antibodies or antibody fragments currently represent the limited option of intravitreal treatment. So far, no small molecule drug delivery therapy has been established for clinical use due to comparably short half-life times and disadvantageous side effect profiles. Here the time period of five days which was evident for our DNA NPs could open up new therapy options where implants are not available. In contrast to the above introduced implants, our NPs are able to be loaded with more than just a single drug, allowing treatment of multiple different diseases with the same carrier. If the sustained release of biodegradable microspheres or nanoparticles could be extended to a period close to the release properties of their non-degradable counterparts, this carrier type could potentially revolutionize ocular drug delivery to the posterior segment. So far, we were only able to trace DNA NP presence in the eye for a maximum of five days. However, these results were obtained via observation under the fluorescence microscope. LC-MS measurements may be able to detect longer lasting positive results in which case our lipid DNA NPs will be a serious alternative to biodegradable implants.

4.4.4. Liposomes

Another promising platform for drug delivery is provided by liposomal formulations. Liposomes are vesicles exhibiting an aqueous core and having a shell formed by a lipid bilayer[25] (Figure 46). In the interior water soluble drugs can be encapsulated. Therefore these vehicles might offer many advantages for intraocular drug delivery. It has already been shown in rat models that after injection of such liposomes they are retained in the ocular tissue for several weeks[89,90]. Here, the lower mobility of liposomes compared to the free drug allows an extended presence of encapsulated substances which results in an increased half life time of pharmaceuticals[91]. This reduces the necessary amount of injections, which in turn reduces the patient burden and the risk of complications. Our DNA NPs hold the option to bind medication using aptameric interactions, which offers a more versatile drug functionalization, compared to liposomal formulations. As almost any small molecule can be loaded using an aptamer, the carrier does not need to be adjusted to the lipophilic characteristics of the drug. By encapsulating labile molecules, liposomes are able to stabilize peptides[92] and oligonucleotides[93] and protect these from the harmful environment until they are delivered to the site of action. They can also serve to shield possible toxicity of the encapsulated cargo[94]. However, it must be noted that the toxicity of these carriers themselves strongly depends on their surface properties. For example, injections of cationic liposomes may lead to heavy inflammatory processes[95]. Another drawback of liposomes is their tendency to lead to blurry vision due to their larger size[94]. A simple benefit of the DNA-NPs is that no blurry vision after implementation of the nanocarriers is unlikely, as they have an approximate diameter of 12 nm and their solution is clear. For the formation of liposomal delivery vehicles, the phospholipids lecithin or phosphatidylcholine are most commonly used. However, addition of other molecules for their formation gives the potential to change the behavior of the liposomes depending on the respective demand. For example, cholesterol influences the viscosity of liposomal formulations when included in the shell. Thereby also control over the drug release is gained[96]. Furthermore, polyethylene glycol could be used to modify the mobility of these carriers within the vitreous body[97]. The different

composition possibilities of liposomes allow manifold modifications of the carrier to accommodate different drugs and regulate their release characteristics but at the same time this also heavily influences their surface properties and therefore their toxicity profile. In contrast, the NPs examined in this thesis are constituted out of a single amphiphilic oligonucleotide. Due to this and the excellent biodegradability, no large variation in their safety is to be expected upon loading of different medication. Besides all of the mentioned advantages of liposomal formulations, so far none have been released on the market for intravitreal application. The only example relevant to ophthalmology is Visudyne, which is employed for the treatment of predominantly subfoveal choroidal neovascularization, mainly in cases of AMD. However, this liposome containing solution is not applied intravitreally, but requires intravenous administration[94]. The liposomal structure is necessary to dissolve the hydrophobic active agent verteporin for injection purposes. After reaching the choroida and the neovascular vessels via systemic blood circulation, the drug may be activated using a non-thermal laser. This procedure results in selective occlusion of the targeted blood vessels, which in turn leads to a decrease in exudation and bleeding[98]. However, photodynamic treatment concepts involving medication like Visudyne have been reported to hold risks of immediate visual loss and adverse effects due to the occluding properties of the carrier[99] Moreover, the efficacy of photodynamic treatment in neovascular AMD is inferior to anti-VEGF therapy.

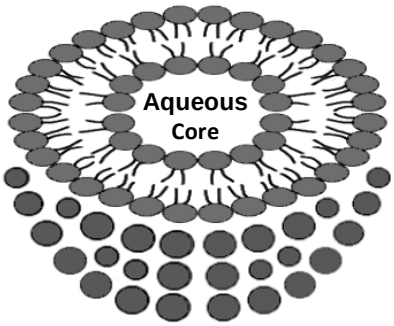

Figure 46 Example of liposome displaying a single phospholipid bilayer without any further structural modification

4.4.5. Dendrimers

Dendrimers are spherical multi-branched polymers of a size between 3-20 nm[100]. They consist of an inner “core” from which branching chains reach out to

peripheral multivalent moieties[101]. By chemical modification of a dendrimer's structure, the drug loading as well as the release can be adjusted[102]. Their chemical structure, size and therefore their physical properties can be designed on the molecular level[103]. The functional groups of dendrimers can be used for drug loading via lipophilic or ionic interactions and covalent bonds. However, only lower amounts of drugs can be incorporated compared to other carriers, such as liposomes, microspheres and nanocarriers[98]. This means that higher concentrations of dendrimers are needed to deliver the same amount of drug as a DNA NP at lower concentrations. Strikingly, only little work has been published regarding the toxicity of dendrimers, offering unsatisfactory results. To date, there is still only fragmentary in-vivo animal investigations and no published clinical data for the ocular use of dendrimers in humans[104]. Regarding treatments for diseases located in the posterior segment of the eye, dendrimers designed out of biodegradable polymers are highly desirable. Recently, there has been reported synthesis and characterization of biodegradable dendrimers composed out of biocompatible polyamides[105,106]. Although it has been proven in cytotoxicity studies that these dendrimers are non-toxic, they are not employed in tests for use in the posterior segment of the eye so far. As for non-biodegradable dendrimers, one of the species most commonly referred to is a polyamidoamin (PAMAM) dendrimer. Due to advantageous solubility and no immunogenicity[107] this formulation has been well characterized and closely investigated. Besides the fact that some PAMAM dendrimers are toxic in cells and animals[104], they have been employed for several studies including intravitreal injections into the posterior segment of the eye[108,109]. Guo et al. were able to proof that cyanine dye-conjugated OH-PAMAM dendrimers remained in the rat eye vitreous for up to two days, originally applied for the reason of targeting ischemia lesions. Also regarding retention, our DNA NPs display more promising results, lasting in the eye for up to five days. Similar to the earlier introduced microspheres, dendrimers are primarily the subject of research. They have not found their way into clinical treatment of retinal diseases yet most likely due to insufficient loading and more importantly unsatisfactory toxicity results.

4.5. Prospects for further research

On one hand special attributes of NPs due to sub-micron properties hold a lot of potential for medical treatment in the future. On the other the effects of our body are yet inadequately understood. Long time toxicity analysis with special focus on the effect of the Brownian motion and diffusion barriers are necessary. NP molecules have been known to cause immune reactions when brought into the human body[110]. Research shows that nanomaterials can stimulate and/or suppress the immune responses, and that their compatibility with the immune system is largely determined by their surface properties. NP size, composition, surface chemistry, surface charge, hydrophobicity, shape, administration routes and protein binding tendency seem to be the main factors that contribute to the interactions of NPs with the immune system[111-113]. It is important to understand the immunological effect that the DNA NPs could have on the human body. Due to the very short sequences of the DNA-strands that were employed in our manufactured NPs immunological interactions are unlikely, but nevertheless need to be ruled out entirely. After confirming the safety of the NPs, the loading with medication needs to be commenced. Here, several options exist, as outlined in section 1.4. Upon conformation of the functionalization of the carrier, several in-vivo pharmacokinetic studies employing LC-MS studies should be performed to analyze the half-life time of the applied drug in different structures of the ocular cavity. Finally, the efficacy of the delivered pharmaceutical agents should be confirmed in a diseased animal model. Here, the beneficial delivery properties of the NP platform hopefully should result in prolonged effects of the drug or open the possibility of attaining a lower dosing regimen.

5. Conclusion

The tissue in the posterior segment of the eye remains a difficult target site in regard to ocular drug delivery. Therefore diseases, such as AMD, DME and RVO are difficult to treat and therapy is associated with numerous side effects. Currently, intravitreal injections or topical drug application result in only a limited duration time of the active agent in the eye and therefore lack efficiency. A novel method of drug delivery is desirable in order to enhance the performance of local treatments and reduce side effects as much as possible. Here, the application of NPs consisting of DNA micelles offers a promising platform for future drug delivery. In this thesis it was shown that these lipid-modified DNA NPs meet the criteria needed for drug delivery to the posterior segment. Firstly, the efficient retention of the NPs in the vitreous body of ex-vivo porcine eyes was demonstrated, promising prolonged drug release in the ocular space. Secondly, these novel vehicles also showed excellent adhesion towards the retinal tissue, which was also verified in ex-vivo animal models. These targeting properties could lead to increased efficacy of the employed drugs and therefore offer the possibility to reduce the necessary drug concentrations. Both of these important properties were observed in several of the NPs that were tested. In particular the U4T-12 and U6T-18 NPs displayed superior characteristics in the ex-vivo setup (the “U” followed by a number stands for the amount of lipid modified deoxyuridine bases, which are located at the 5’-end of the NP base sequence; the second number in this code indicates the total amount of nucleotides in the NP) and were therefore employed in further in-vivo investigations. Efficient retention in the vitreous body was evident up to three days and the presence of the NPs could be confirmed in treated eyes up to five days in in-vivo experiments. To explore the use of alternative application routes, both prioritized NPs were also applied in living rats via subconjunctival injections. Here, the results indicate even more promising properties regarding the retention in the analyzed tissues. The NPs were notably accumulating on the scleral surface of the eyes. To conclude, we have shown here that the use of our NPs could lead to sufficient intraocular drug concentration for several days, preventing unneeded intravitreal injections and establishing this route of admission for small molecule active agents. These

promising results invite to conduct further research regarding the efficacy of delivered medication and establish DNA based NPs as a drug delivery platform for the posterior segment.

6. Zusammenfassung

Drug Delivery in die Region des hinteren Augensegments stellt die Augenheilkunde vor eklatante Schwierigkeiten. Krankheitsbilder wie die altersbedingte Makuladegeneration, das diabetische Makulaödem und der retinale Venenverschluss sind immer noch schwer behandelbar und die Therapien meist mit Nebenwirkungen verbunden. Derzeitige Therapieoptionen, wie beispielsweise intravitreale Injektionen oder die topische Anwendung der Wirkstoffe führen zu sehr kurzweiliger Präsenz der Medikation im Auge und somit nur zu unzufriedenstellender Effektivität. Wünschenswert wäre eine Verlängerung der Wirksamkeit lokaler Behandlungen und eine Minimierung der Nebenwirkungen. Nanopartikel, aufgebaut aus DNA-Mizellen bieten hier eine vielversprechende Plattformtechnologie. Die erfolgreiche Retention des Nanopartikels im Glaskörper eines ex-vivo Schweineaugenmodells wurde demonstriert, was eine verlängerte Wirkstofffreigabe verspricht. Weiterhin zeigt die neue Plattformtechnik exzellente Bindungseigenschaften für das retinale Gewebe, ebenfalls im ex-vivo Modell verifiziert. Sowohl die längere Retention als auch die Adhäsion zur Retina wurde bei verschiedenen getesteten Nanopartikeln beobachtet. Besonders fielen hierbei U4T-12 und U6T-18 durch überlegene Eigenschaften in den ex-vivo Experimenten auf (das „U“ mit nachfolgender Ziffer steht für die Anzahl an lipidmodifizierten Desoxyuridinbasen, welche am 5‘-Terminus „T“ der Nukleotidabfolge des DNA Nanopartikels angeordnet sind; die zweite Zahl im Bezeichnungscode steht für die Gesamtzahl an Nukleotiden des Nanopartikel), was sie für nachfolgende in-vivo Untersuchungen qualifizierte. Bis zu drei Tage nach der Applikation zeigte sich effektive Retention und bis zu fünf Tage danach waren Nanopartikel nachweisbar. Zur Untersuchung verschiedener Applikationsmethoden wurden beide priorisierten Nanopartikel auch in das periokuläre Gewebe lebender Ratten mittels subkonjunktivaler Injektion eingebracht. Die Retention war hier noch deutlicher in Form von Ansammlungen

auf der Außenseite der Sklera zu beobachten. Zusammenfassend waren wir in der Lage zu zeigen, dass an Nanopartikel gebundene Medikamentendepots zu suffizienten intraokularen Wirkstoffkonzentrationen für mehrere Tage führen können um somit ggf. intravitreale Injektionen zu minimieren oder bei kleineren Wirkstoffmolekülen überhaupt erst zu ermöglichen. Diese vielversprechenden Ergebnisse laden zu weiteren Untersuchungen ein um die lipid-modifizierten DNA Nanopartikel als *Drug Delivery* System für das hintere Segment des Auges zu etablieren.

7. Acknowlegements

This whole project was only made possible by Prof. Dr. Martin Spitzer who supported me with trust and confidence from the beginning on. Endless key advices to this thesis have followed from his pen and added a lot of quality. I don't think I know any promotors who reply to e-mails as fast as you do. Also, I don't think there are many promotors who actually invest their own time to push a project as much as you do. Thank you for the possibility of working for your team and the manifold options of training. It has been an outstanding experience and always a pleasure for me.

I would like to express special thanks to Jan Willem de Vries for his extraordinary guidance. The first time we sat together in order to discuss what I had been doing so far, I had to discard all of my results, which was exceptionally painful. Over the course of time we had quite a lot of these sessions, similar to this first one. Therefore I can say I have suffered a bit, but in return I was taught so much more, which I am very thankful for. Jan always took the time to patiently explain the circumstances and reasons of all various variables whilst also giving me enough room to try out different setups in the course of this thesis. I was supported with genuine trust as well as with an open ear whenever it was necessary. I don't think many other students can rock up at their supervisor's house on a Sunday afternoon with questions regarding statistics and formatting and even get invited for coffee in return. However, I can't remember a time working with you in the lab which didn't result in jokes and great conversations besides being very productive

nevertheless. The time under your guidance in the lab has been exceptionally instructive and educative, also away from scientific paths or matters, and I want to thank you for leading me to a story of success.

The next person who deserves special acknowledgements for great supervision is Sven Schnichels. Cryocutting never went by faster as when philosophizing with you about Tarantino's best movies. Seemingly invincible problems with the fluorescence microscope were solved within minutes with your very competent help. Hours have been spent between us trying to find the best route of evaluation for various experiments which eventually ended in novel approaches and fruitful decisions. I want to thank you for your patience, your steady hand during injections and your trust, all without which this thesis would not have been possible.

Special thanks deserve Jose Hurst and Agnieszka Gruszka-de Vries for their numerous introductions into all different topics, endless advices on possible improvements and for their inspiring presence in my time in the lab. Process would have been made much slower in my work without you two and much less joyful.

Due to Karin my work on the cryomachine was sped up by at least several days. With Felix's help I was able to master the art of measuring multiple eyes at once, over 24 hours behind the fluorophotometer. Without Johanna's advice I would have been unable to find several utilities for my work, probably until today. Thank you all so much!

An meine Lieben,

Mama, ich danke dir für die Zuversicht zu jeder Zeit, deine Inspiration und für die kompromisslose Unterstützung. Papa, ich danke dir für die unendlichen Stunden am Telefon, für die kostbaren Ratschläge und deine Gewissenhaftigkeit. Jonas & Bennet, ich danke euch für die Ehrlichkeit, die Freude an den kleinen Dingen und das Gefühl einer von drei Brüdern zu sein. Weiterhin möchte ich meinem erweiterten Verwandtenkreis danken, der großartiger Weise so groß ist, dass alle

namentlich zu nennen die Rahmen dieser Danksagung sprengen würden - Danke.

Schlussendlich möchte ich Lisa Pohl danken. Ohne dich wäre diese Arbeit nicht zu Stande gekommen. Danke fürs Aufbauen, danke fürs Durchhalten und danke für die Kraft es zu Ende zu bringen. Danke für Alles.

I am sure to have forgotten somebody in these acknowledgements. Please be aware that this has happened without purpose and that I am honestly sorry about it. Thanks, all of you for making this piece of work possible.

8. Declaration of Authorship

I, David Simmang, hereby declare, that this thesis submitted is composed by me of my own unaided work. All direct or indirect sources of work of others used are acknowledged as references. The given results were not previously presented to another examination board and have not been published before. However, manuscripts containing the presented data are currently in preparation and will be submitted to peer-reviewed journals in the near future.

Date: 18.11.2019

Signature: 

9. References

1. Sachsenweger, M., Klauß, V., Nasemann, J. & Ugi, I. Augenheilkunde. Vol. 2 (eds. Bob, A. & Bob, K.) 248-248 (Georg Thieme Stuttgart, 2002).
2. Klein, R., Klein, B.E. & Linton, K.L. Prevalence of age-related maculopathy. The Beaver Dam Eye Study. *Ophthalmology* **99**, 933-943 (1992).
3. Rein, D.B.*, et al.* Forecasting age-related macular degeneration through the year 2050: the potential impact of new treatments. *Arch Ophthalmol* **127**, 533-540 (2009).
4. Klein, R., Klein, B.E., Linton, K.L. & De Mets, D.L. The Beaver Dam Eye Study: visual acuity. *Ophthalmology* **98**, 1310-1315 (1991).
5. Leibowitz, H.M.*, et al.* The Framingham Eye Study monograph: An ophthalmological and epidemiological study of cataract, glaucoma, diabetic retinopathy, macular degeneration, and visual acuity in a general population of 2631 adults, 1973-1975. *Surv Ophthalmol* **24**, 335-610 (1980).
6. Fisher, D.E.*, et al.* Incidence of Age-Related Macular Degeneration in a Multi-Ethnic United States Population: The Multi-Ethnic Study of Atherosclerosis. *Ophthalmology* **123**, 1297-1308 (2016).
7. Kellner, U. & Wachtlin, J. Retina, Diagnostik und Therapie der Erkrankungen des hinteren Augenabschnitts. Vol. 1 (ed. Kellner, U.) 129-145 (Georg Thieme, Stuttgart, 2008).
8. Martin, D.F.*, et al.* Ranibizumab and bevacizumab for neovascular age-related macular degeneration. *N Engl J Med* **364**, 1897-1908 (2011).
9. Brown, D.M.*, et al.* Ranibizumab versus verteporfin photodynamic therapy for neovascular age-related macular degeneration: Two-year results of the ANCHOR study. *Ophthalmology* **116**, 57-65 e55 (2009).
10. Rosenfeld, P.J.*, et al.* Ranibizumab for neovascular age-related macular degeneration. *N Engl J Med* **355**, 1419-1431 (2006).
11. Varma, R.*, et al.* Biologic risk factors associated with diabetic retinopathy: the Los Angeles Latino Eye Study. *Ophthalmology* **114**, 1332-1340 (2007).
12. Dedov, I.*, et al.* Prevalence of diabetic retinopathy and cataract in adult patients with type 1 and type 2 diabetes in Russia. *Rev Diabet Stud* **6**, 124-129 (2009).
13. Provided by Prof. Dr. Martin Spitzer, Images of the Universitäts-Augenklinik Tübingen.
14. Aiello, L.P.*, et al.* Vascular endothelial growth factor in ocular fluid of patients with diabetic retinopathy and other retinal disorders. *N Engl J Med* **331**, 1480-1487 (1994).
15. Beck, R.W.*, et al.* Three-year follow-up of a randomized trial comparing focal/grid photocoagulation and intravitreal triamcinolone for diabetic macular edema. *Arch Ophthalmol* **127**, 245-251 (2009).
16. Brown, D.M.*, et al.* Long-term outcomes of ranibizumab therapy for diabetic macular edema: the 36-month results from two phase III trials: RISE and RIDE. *Ophthalmology* **120**, 2013-2022 (2013).
17. Nguyen, Q.D.*, et al.* Primary End Point (Six Months) Results of the Ranibizumab for Edema of the mAcula in diabetes (READ-2) study. *Ophthalmology* **116**, 2175-2181 e2171 (2009).
18. Do, D.V.*, et al.* One-year outcomes of the da Vinci Study of VEGF Trap-Eye in eyes with diabetic macular edema. *Ophthalmology* **119**, 1658-1665 (2012).
19. Cugati, S., Wang, J.J., Rochtchina, E. & Mitchell, P. Ten-year incidence of retinal vein occlusion in an older population: the Blue Mountains Eye Study. *Arch Ophthalmol* **124**, 726-732 (2006).

20. Green, W.R., Chan, C.C., Hutchins, G.M. & Terry, J.M. Central retinal vein occlusion: a prospective histopathologic study of 29 eyes in 28 cases. *Retina* **1**, 27-55 (1981).
21. Ciftci, S.*, et al.* Intravitreal bevacizumab combined with panretinal photocoagulation in the treatment of open angle neovascular glaucoma. *Eur J Ophthalmol* **19**, 1028-1033 (2009).
22. Spaide, R.F.*, et al.* Prospective study of intravitreal ranibizumab as a treatment for decreased visual acuity secondary to central retinal vein occlusion. *Am J Ophthalmol* **147**, 298-306 (2009).
23. Kondo, M.*, et al.* Intravitreal injection of bevacizumab for macular edema secondary to branch retinal vein occlusion:results after 12 months and multiple regression analysis. *Retina* **29**, 1242-1248 (2009).
24. Urtti, A. Challenges and obstacles of ocular pharmacokinetics and drug delivery. *Adv Drug Deliv Rev* **58**, 1131-1135 (2006).
25. Gaudana, R., Jwala, J., Boddu, S.H. & Mitra, A.K. Recent perspectives in ocular drug delivery. *Pharm Res* **26**, 1197-1216 (2009).
26. Ranta, V.P.*, et al.* Barrier analysis of periocular drug delivery to the posterior segment. *J Control Release* **148**, 42-48 (2010).
27. Maurice, D.M. Drug delivery to the posterior segment from drops. *Surv Ophthalmol* **47**, 41-52 (2002).
28. Rossetti, L., Chaudhuri, J. & Dickersin, K. Medical prophylaxis and treatment of cystoid macular edema after cataract surgery. The results of a meta-analysis. *Ophthalmology* **105**, 397-405 (1998).
29. Hiratani, H. & Alvarez-Lorenzo, C. Timolol uptake and release by imprinted soft contact lenses made of N,N-diethylacrylamide and methacrylic acid. *J Control Release* **83**, 223-230 (2002).
30. Alvarez-Lorenzo, C., Yanez, F., Barreiro-Iglesias, R. & Concheiro, A. Imprinted soft contact lenses as norfloxacin delivery systems. *J Control Release* **113**, 236-244 (2006).
31. Danion, A., Arsenault, I. & Vermette, P. Antibacterial activity of contact lenses bearing surface-immobilized layers of intact liposomes loaded with levofloxacin. *J Pharm Sci* **96**, 2350-2363 (2007).
32. Endophthalmitis-Vitrectomy-Study-Group. Results of the Endophthalmitis Vitrectomy Study. A randomized trial of immediate vitrectomy and of intravenous antibiotics for the treatment of postoperative bacterial endophthalmitis. Endophthalmitis Vitrectomy Study Group. *Arch Ophthalmol* **113**, 1479-1496 (1995).
33. Young, S., Larkin, G., Branley, M. & Lightman, S. Safety and efficacy of intravitreal triamcinolone for cystoid macular oedema in uveitis. *Clin Experiment Ophthalmol* **29**, 2-6 (2001).
34. Smith, J.R.*, et al.* Role of intravitreal methotrexate in the management of primary central nervous system lymphoma with ocular involvement. *Ophthalmology* **109**, 1709-1716 (2002).
35. Wu, H. & Chen, T.C. The effects of intravitreal ophthalmic medications on intraocular pressure. *Semin Ophthalmol* **24**, 100-105 (2009).
36. Eyetech-Study-Group. Anti-vascular endothelial growth factor therapy for subfoveal choroidal neovascularization secondary to age-related macular degeneration: phase II study results. *Ophthalmology* **110**, 979-986 (2003).
37. Meyer, C.H., Krohne, T.U. & Holz, F.G. Intraocular pharmacokinetics after a single intravitreal injection of 1.5 mg versus 3.0 mg of bevacizumab in humans. *Retina* **31**, 1877-1884 (2011).

38. Durairaj, C., Shah, J.C., Senapati, S. & Kompella, U.B. Prediction of vitreal half-life based on drug physicochemical properties: quantitative structure-pharmacokinetic relationships (QSPKR). *Pharm Res* **26**, 1236-1260 (2009).
39. Bochot, A., Couvreur, P. & Fattal, E. Intravitreal administration of antisense oligonucleotides: potential of liposomal delivery. *Prog Retin Eye Res* **19**, 131-147 (2000).
40. Ozkiris, A. & Erkilic, K. Complications of intravitreal injection of triamcinolone acetonide. *Can J Ophthalmol* **40**, 63-68 (2005).
41. Rhee, D.J*., et al.* Intraocular pressure alterations following intravitreal triamcinolone acetonide. *Br J Ophthalmol* **90**, 999-1003 (2006).
42. Jonas, J.B. Intravitreal triamcinolone acetonide: a change in a paradigm. *Ophthalmic Res* **38**, 218-245 (2006).
43. Thompson, J.T. Cataract formation and other complications of intravitreal triamcinolone for macular edema. *Am J Ophthalmol* **141**, 629-637 (2006).
44. Gragoudas, E.S., Adamis, A.P., Cunningham, E.T., Jr., Feinsod, M. & Guyer, D.R. Pegaptanib for neovascular age-related macular degeneration. *N Engl J Med* **351**, 2805-2816 (2004).
45. Choonara, Y.E., Pillay, V., Danckwerts, M.P., Carmichael, T.R. & du Toit, L.C. A review of implantable intravitreal drug delivery technologies for the treatment of posterior segment eye diseases. *J Pharm Sci* **99**, 2219-2239 (2010).
46. Bourges, J.L*., et al.* Intraocular implants for extended drug delivery: therapeutic applications. *Adv Drug Deliv Rev* **58**, 1182-1202 (2006).
47. Aukunuru, J.V*., et al.* A biodegradable injectable implant sustains systemic and ocular delivery of an aldose reductase inhibitor and ameliorates biochemical changes in a galactose-fed rat model for diabetic complications. *Pharm Res* **19**, 278-285 (2002).
48. Raghava, S., Hammond, M. & Kompella, U.B. Periocular routes for retinal drug delivery. *Expert Opin Drug Deliv* **1**, 99-114 (2004).
49. Ayalasomayajula, S.P. & Kompella, U.B. Retinal delivery of celecoxib is several-fold higher following subconjunctival administration compared to systemic administration. *Pharm Res* **21**, 1797-1804 (2004).
50. Ahmed, I. & Patton, T.F. Importance of the noncorneal absorption route in topical ophthalmic drug delivery. *Invest Ophthalmol Vis Sci* **26**, 584-587 (1985).
51. Prausnitz, M.R. & Noonan, J.S. Permeability of cornea, sclera, and conjunctiva: a literature analysis for drug delivery to the eye. *J Pharm Sci* **87**, 1479-1488 (1998).
52. Vries, J.W.d. DNA Nanoparticles as Ocular Drug Delivery Plaform. 128-128 (University of Groningen, 2015).
53. Kwak, M*., et al.* Virus-like particles templated by DNA micelles: a general method for loading virus nanocarriers. *J Am Chem Soc* **132**, 7834-7835 (2010).
54. Krohne, T.U., Eter, N., Holz, F.G. & Meyer, C.H. Intraocular pharmacokinetics of bevacizumab after a single intravitreal injection in humans. *Am J Ophthalmol* **146**, 508-512 (2008).
55. Krohne, T.U., Liu, Z., Holz, F.G. & Meyer, C.H. Intraocular pharmacokinetics of ranibizumab following a single intravitreal injection in humans. *Am J Ophthalmol* **154**, 682-686 e682 (2012).
56. Beer, P.M*., et al.* Intraocular concentration and pharmacokinetics of triamcinolone acetonide after a single intravitreal injection. *Ophthalmology* **110**, 681-686 (2003).
57. Bertens, C.J.F., Gijs, M., van den Biggelaar, F. & Nuijts, R. Topical drug delivery devices: A review. *Exp Eye Res* **168**, 149-160 (2018).
58. Campochiaro, P.A*., et al.* Sustained delivery fluocinolone acetonide vitreous inserts provide benefit for at least 3 years in patients with diabetic macular edema. *Ophthalmology* **119**, 2125-2132 (2012).

59. Kompella, U.B., Kadam, R.S. & Lee, V.H. Recent advances in ophthalmic drug delivery. *Ther Deliv* **1**, 435-456 (2010).
60. Nentwich, M.M. & Ulbig, M.W. The therapeutic potential of intraocular depot steroid systems: developments aimed at prolonging duration of efficacy. *Dtsch Arztebl Int* **109**, 584-590 (2012).
61. Bhagat, R., Zhang, J., Farooq, S. & Li, X.Y. Comparison of the release profile and pharmacokinetics of intact and fragmented dexamethasone intravitreal implants in rabbit eyes. *J Ocul Pharmacol Ther* **30**, 854-858 (2014).
62. Liu, S., Jones, L. & Gu, F.X. Nanomaterials for ocular drug delivery. *Macromol Biosci* **12**, 608-620 (2012).
63. Kellner, U. & Wachtlin, J. Retina, Diagnostik und Therapie der Erkrankungen des hinteren Augenabschnitts. Vol. 1 (ed. Kellner, U.) 88-92 (Georg Thieme, Stuttgart, 2008).
64. Earla, R.*, et al.* Development and validation of a fast and sensitive bioanalytical method for the quantitative determination of glucocorticoids-quantitative measurement of dexamethasone in rabbit ocular matrices by liquid chromatography tandem mass spectrometry. *J Pharm Biomed Anal* **52**, 525-533 (2010).
65. Boddu, S.H., Gunda, S., Earla, R. & Mitra, A.K. Ocular microdialysis: a continuous sampling technique to study pharmacokinetics and pharmacodynamics in the eye. *Bioanalysis* **2**, 487-507 (2010).
66. Hamidi, M., Azadi, A. & Rafiei, P. Hydrogel nanoparticles in drug delivery. *Adv Drug Deliv Rev* **60**, 1638-1649 (2008).
67. Sahoo, S.K., Dilnawaz, F. & Krishnakumar, S. Nanotechnology in ocular drug delivery. *Drug Discov Today* **13**, 144-151 (2008).
68. Nagarwal, R.C., Kant, S., Singh, P.N., Maiti, P. & Pandit, J.K. Polymeric nanoparticulate system: a potential approach for ocular drug delivery. *J Control Release* **136**, 2-13 (2009).
69. Ludwig, A. The use of mucoadhesive polymers in ocular drug delivery. *Adv Drug Deliv Rev* **57**, 1595-1639 (2005).
70. Nemoto, E., Ueda, H., Akimoto, M., Natsume, H. & Morimoto, Y. Ability of poly-L-arginine to enhance drug absorption into aqueous humor and vitreous body after instillation in rabbits. *Biol Pharm Bull* **30**, 1768-1772 (2007).
71. Zhang, L., Li, Y., Zhang, C., Wang, Y. & Song, C. Pharmacokinetics and tolerance study of intravitreal injection of dexamethasone-loaded nanoparticles in rabbits. *Int J Nanomedicine* **4**, 175-183 (2009).
72. Jo, D.H., Kim, J.H., Yu, Y.S. & Lee, T.G. Antiangiogenic effect of silicate nanoparticle on retinal neovascularization induced by vascular endothelial growth factor. *Nanomedicine* **8**, 784-791 (2012).
73. Kunzmann, A.*, et al.* Toxicology of engineered nanomaterials: focus on biocompatibility, biodistribution and biodegradation. *Biochim Biophys Acta* **1810**, 361-373 (2011).
74. Herrero-Vanrell, R., Bravo-Osuna, I., Andres-Guerrero, V., Vicario-de-la-Torre, M. & Molina-Martinez, I.T. The potential of using biodegradable microspheres in retinal diseases and other intraocular pathologies. *Prog Retin Eye Res* **42**, 27-43 (2014).
75. Yasukawa, T.*, et al.* Drug delivery systems for vitreoretinal diseases. *Prog Retin Eye Res* **23**, 253-281 (2004).
76. Colthurst, M.J., Williams, R.L., Hiscott, P.S. & Grierson, I. Biomaterials used in the posterior segment of the eye. *Biomaterials* **21**, 649-665 (2000).
77. Jalil, R. & Nixon, J.R. Biodegradable poly(lactic acid) and poly(lactide-co-glycolide) microcapsules: problems associated with preparative techniques and release properties. *J Microencapsul* **7**, 297-325 (1990).
78. Herrero-Vanrell, R. & Refojo, M.F. Biodegradable microspheres for vitreoretinal drug delivery. *Adv Drug Deliv Rev* **52**, 5-16 (2001).

79. Torres, A.I., Boisdron-Celle, M. & Benoit, J.P. Formulation of BCNU-loaded microspheres: influence of drug stability and solubility on the design of the microencapsulation procedure. *J Microencapsul* **13**, 41-51 (1996).
80. Visscher, G.E.*, et al.* Biodegradation of and tissue reaction to 50:50 poly(DL-lactide-co-glycolide) microcapsules. *J Biomed Mater Res* **19**, 349-365 (1985).
81. Rincon, A.C.*, et al.* Biocompatibility of elastin-like polymer poly(VPAVG) microparticles: in vitro and in vivo studies. *J Biomed Mater Res A* **78**, 343-351 (2006).
82. Brunner, A., Mader, K. & Gopferich, A. pH and osmotic pressure inside biodegradable microspheres during erosion. *Pharm Res* **16**, 847-853 (1999).
83. Eljarrat-Binstock, E., Pe'er, J. & Domb, A.J. New techniques for drug delivery to the posterior eye segment. *Pharm Res* **27**, 530-543 (2010).
84. Campochiaro, P.A.*, et al.* Sustained ocular delivery of fluocinolone acetonide by an intravitreal insert. *Ophthalmology* **117**, 1393-1399 e1393 (2010).
85. Amsden, B.G. & Marecak, D. Long-Term Sustained Release from a Biodegradable Photo-Cross-Linked Network for Intraocular Corticosteroid Delivery. *Mol Pharm* (2016).
86. Lee, S.S., Hughes, P., Ross, A.D. & Robinson, M.R. Biodegradable implants for sustained drug release in the eye. *Pharm Res* **27**, 2043-2053 (2010).
87. Australian_Government. Australian Public Assessment Report for Dexamethasone. 1−68 (2011).
88. Chaudhary, V.*, et al.* Ozurdex in age-related macular degeneration as adjunct to ranibizumab (The OARA Study). *Can J Ophthalmol* **51**, 302-305 (2016).
89. Camelo, S.*, et al.* Ocular and systemic bio-distribution of rhodamine-conjugated liposomes loaded with VIP injected into the vitreous of Lewis rats. *Mol Vis* **13**, 2263-2274 (2007).
90. Zhang, R.*, et al.* Treatment of experimental autoimmune uveoretinitis with intravitreal injection of tacrolimus (FK506) encapsulated in liposomes. *Invest Ophthalmol Vis Sci* **51**, 3575-3582 (2010).
91. Ebrahim, S., Peyman, G.A. & Lee, P.J. Applications of liposomes in ophthalmology. *Surv Ophthalmol* **50**, 167-182 (2005).
92. Lajavardi, L.*, et al.* Downregulation of endotoxin-induced uveitis by intravitreal injection of vasoactive intestinal Peptide encapsulated in liposomes. *Invest Ophthalmol Vis Sci* **48**, 3230-3238 (2007).
93. Bochot, A.*, et al.* Intravitreal delivery of oligonucleotides by sterically stabilized liposomes. *Invest Ophthalmol Vis Sci* **43**, 253-259 (2002).
94. Bochot, A. & Fattal, E. Liposomes for intravitreal drug delivery: a state of the art. *J Control Release* **161**, 628-634 (2012).
95. Omri, S.*, et al.* Microglia/macrophages migrate through retinal epithelium barrier by a transcellular route in diabetic retinopathy: role of PKCzeta in the Goto Kakizaki rat model. *Am J Pathol* **179**, 942-953 (2011).
96. Barza, M., Stuart, M. & Szoka, F., Jr. Effect of size and lipid composition on the pharmacokinetics of intravitreal liposomes. *Invest Ophthalmol Vis Sci* **28**, 893-900 (1987).
97. Sanders, N.N., Peeters, L., Lentacker, I., Demeester, J. & De Smedt, S.C. Wanted and unwanted properties of surface PEGylated nucleic acid nanoparticles in ocular gene transfer. *J Control Release* **122**, 226-235 (2007).
98. Honda, M.*, et al.* Liposomes and nanotechnology in drug development: focus on ocular targets. *Int J Nanomedicine* **8**, 495-503 (2013).
99. Kawczyk-Krupka, A.*, et al.* Vascular-targeted photodynamic therapy in the treatment of neovascular age-related macular degeneration: Clinical perspectives. *Photodiagnosis Photodyn Ther* **12**, 161-175 (2015).

100. Xu, Q., Kambhampati, S.P. & Kannan, R.M. Nanotechnology approaches for ocular drug delivery. *Middle East Afr J Ophthalmol* **20**, 26-37 (2013).
101. Chaplot, S.P. & Rupenthal, I.D. Dendrimers for gene delivery--a potential approach for ocular therapy? *J Pharm Pharmacol* **66**, 542-556 (2014).
102. Wu, L.P., Ficker, M., Christensen, J.B., Trohopoulos, P.N. & Moghimi, S.M. Dendrimers in Medicine: Therapeutic Concepts and Pharmaceutical Challenges. *Bioconjug Chem* **26**, 1198-1211 (2015).
103. Kannan, R.M., Nance, E., Kannan, S. & Tomalia, D.A. Emerging concepts in dendrimer-based nanomedicine: from design principles to clinical applications. *J Intern Med* **276**, 579-617 (2014).
104. Rodriguez Villanueva, J., Navarro, M.G. & Rodriguez Villanueva, L. Dendrimers as a promising tool in ocular therapeutics: Latest advances and perspectives. *Int J Pharm* **511**, 359-366 (2016).
105. Carnahan, M.A. & Grinstaff, M.W. Synthesis and characterization of polyether-ester dendrimers from glycerol and lactic acid. *J Am Chem Soc* **123**, 2905-2906 (2001).
106. Carnahan, M.A., Middleton, C., Kim, J., Kim, T. & Grinstaff, M.W. Hybrid dendritic-linear polyester-ethers for in situ photopolymerization. *J Am Chem Soc* **124**, 5291-5293 (2002).
107. Malik, N.*, et al.* Dendrimers: relationship between structure and biocompatibility in vitro, and preliminary studies on the biodistribution of 125I-labelled polyamidoamine dendrimers in vivo. *J Control Release* **65**, 133-148 (2000).
108. Kambhampati, S.P.*, et al.* Systemic and Intravitreal Delivery of Dendrimers to Activated Microglia/Macrophage in Ischemia/Reperfusion Mouse Retina. *Invest Ophthalmol Vis Sci* **56**, 4413-4424 (2015).
109. Guo, Y.*, et al.* Dendrimers Target the Ischemic Lesion in Rodent and Primate Models of Nonarteritic Anterior Ischemic Optic Neuropathy. *PLoS One* **11**, e0154437 (2016).
110. Najafi-Hajivar, S.*, et al.* Overview on experimental models of interactions between nanoparticles and the immune system. *Biomed Pharmacother* **83**, 1365-1378 (2016).
111. Dobrovolskaia, M.A. & McNeil, S.E. Immunological properties of engineered nanomaterials. *Nat Nanotechnol* **2**, 469-478 (2007).
112. Albanese, A., Tang, P.S. & Chan, W.C. The effect of nanoparticle size, shape, and surface chemistry on biological systems. *Annu Rev Biomed Eng* **14**, 1-16 (2012).
113. Shima, F., Akagi, T., Uto, T. & Akashi, M. Manipulating the antigen-specific immune response by the hydrophobicity of amphiphilic poly(gamma-glutamic acid) nanoparticles. *Biomaterials* **34**, 9709-9716 (2013).